Characterization and Improvement of a Nicotine-Degrading Flavoenzyme

by

Mark Dulchavsky

A dissertation submitted in partial fulfillment
of the requirements for the degree of
Doctor of Philosophy
(Cellular and Molecular Biology)
in the University of Michigan
2022

Doctoral Committee:

Professor James Bardwell, Chair
Associate Professor Peter Freddolino
Assistant Professor Tobias Giessen
Associate Professor Jayakrishnan Nandakumar
Associate Professor Patrick O'Brien

Mark Dulchavsky

markdul@umich.edu

ORCID iD: 0000-0002-5253-8924

Acknowledgements

It takes a lab to raise a PhD student, and I would first like to thank James Bardwell for welcoming me to his group. Jim has an extremely positive attitude toward the research and students within his lab that I have always appreciated. He has provided me with a lot of space to grow, but always had helpful advice when I needed it. Anyone who knows Jim is aware of his immaculate fish tanks, whose blue glow gently lights the hallway into the lab. I have often had the pleasure to run into Jim at all hours of the day and night, seven days a week, as he is performing the ritual tasks necessary to keep those tanks alive and functioning. I don't know how he does it, but I always enjoyed the conversations occasioned by these meetings.

I would also like to extend thanks to my labmates, now friends, who have assisted me along the way. Rishav Mitra provided continuous advice throughout my time in the lab (some of it was even helpful!) and was instrumental in helping me with the NMR experiments shown in Chapter 3. Kevin Wu always had a moment to talk and is the supportive confidant of many in our lab. He also solved the structures for my crystals, a job he never asked for, but has never complained about (at least not to me). Ben Meinen is always good for a laugh, and I have been happy to remain in contact with him as he does his protein design work on the east coast. My undergraduates Joshua Li and Xiaomeng Liu were extremely helpful, their efforts on the many steady-state kinetic experiments contained in this document allowed me to maintain at least some sanity.

Special thanks go to Carina Ade, a hardworking graduate student with whom I worked directly on an acid tolerant enzyme. It was a lot of fun! Our other researchers Veronika, Xiexiong, Ee Lin, Hannah, Bikash, Changhan, and Hyun-hee constitute the fabric of our lab, and every one of them has made this place a cheerful and supportive environment for me. I would be remiss to not also mention Traci Banjanin, Ken Wan, Chris Sinkler, and May Tsoi, without whom our lab would not function, thank you for your hard work.

I would like to extend thanks to all members of Ursula Jakob's lab, but especially: Ursula herself, who is a wellspring of valuable feedback. Kathrin Ulrich, my desk-neighbor, with whom I have shared the excitement of her burgeoning career and our shared interests. Ellen Quarles, though our worm-song project never took off, it was a fun and interesting diversion.

My committee has always shown genuine interest in the work that I've done; Pat O'Brien, Peter Freddolino, JK Nandakumar, and Tobi Giessen have all provided helpful comments that gave me new direction and fueled my scientific interest. I also had a great time teaching with Pat, we ended up staying after class to talk about science almost every session.

I owe much to the efforts of Frederick Stull, who began the work that we extend in this thesis. He and his lab contributed greatly to this project, and to my growth as a scientist. Thanks Ricky!

I extend deep gratitude to all my friends. You are too numerous to mention here, but I have appreciated every moment of the dinners, concerts, dungeons and dragons, music, tubing sessions, weekend trips, near-death experiences, late night walks by the river, grotto hangouts, questionable advice, tomato planting, rock skipping; and most

importantly, ordinary conversations that have helped to sustain me for the last years. You know who you are, please keep doing what you do.

Finally, I would like to extend my thanks to my family. I was lucky to be raised in a household full of creative people, in which my interests were always encouraged. The magnitude of this gift is something I appreciate daily.

Table of Contents

List of Tables

List of Figures

Abstract

Nicotine oxidoreductase (NicA2) is a flavin-dependent enzyme that has the ability to catalyze oxidation of nicotine to N-methylmyosmine. Though nicotine is a psychoactive substance with high addictive potential, N-methylmyosmine is not. Due to its ability to catalyze the breakdown of nicotine, NicA2 has been studied as a therapeutic to aid in the cessation of smoking. When NicA2 is injected intravenously or into the peritoneum of rats it reduces brain and bloodstream levels of nicotine, eases withdrawal symptoms, and cuts compulsive nicotine intake. The results of these preclinical studies are promising, but there is a major barrier to the use of this enzyme as a therapeutic in humans— the very high dose of enzyme that is required to achieve a positive response. This is likely due to the poor catalytic activity of NicA2 when only oxygen is supplied as an electron acceptor, as it can only degrade nicotine slowly under ambient conditions.

My research uncovered that the reason for NicA2's poor activity is a slow step in its reactive cycle, oxidation of flavin by dioxygen (O_2). In the organism from which the *nica2* gene was isolated, *Pseudomonas putida* S16, I discovered an alternative electron acceptor: a cytochrome c now named CycN. We have characterized the kinetic mechanism of the interaction between NicA2 and CycN and find that CycN oxidizes NicA2's flavin at a rate ~10,000 times faster than O_2 does. Additionally, I found that the *cycN* gene is required for the growth of *P. putida* S16 using nicotine as its carbon source. These data strongly support that CycN is the in vivo electron acceptor for NicA2.

Though this cytochrome c allows NicA2 to achieve rapid turnover, is unlikely to be useful as an aid to smoking cessation. In order to make NicA2 a more effective therapeutic, the most direct approach is instead to increase its rate of reaction with O_2, an oxidative substrate that is readily available in the bloodstream. This approach, however, is challenging: the molecular features that enable oxygen reactivity in flavoenzymes are enigmatic, and it has proven to be difficult to evolve NicA2 to be O_2 reactive using rational substitutions based on our current understanding of flavoenzyme oxidation. I used directed evolution as an alternative approach, in part because it does not rely on a detailed mechanistic understanding of O_2 activation.

I randomly introduced mutations along the *nicA2* gene and selected for variants that enable *Pseudomonas putida* S16 to grow aerobically on nicotine in the absence of CycN. This enabled me to isolate variant NicA2 proteins that have up to a 200-fold improvement in their ability to use oxygen as an electron acceptor. The mutations that enable this activity cluster within a solvent accessible tunnel that reaches into the active site of NicA2 and appear to modulate the accessibility of O_2 to flavin. These improved variants are likely to be more effective as an aid to smoking cessation than wild type NicA2, as they should require a much lower dose to achieve the desired goal of nicotine degradation in the bloodstream.

Chapter 1
Introduction

1.1 Background

Nicotine dependence is a notoriously difficult habit to kick, with < 5% of quit attempts in the absence of medical management ending in success[1,2]. Medical management most commonly consists of nicotine replacement therapy, nicotine receptor partial agonists, or a norepinephrine-dopamine reuptake inhibitor; but these therapeutic options are estimated to increase the chance of a successful quit attempt less than 4-fold[3]. Given that nicotine dependence is projected to be responsible for 1/10 deaths worldwide for the foreseeable future, this is clearly lower than is desired[4]. A novel approach to aid in the cessation of smoking has recently been explored in several preclinical studies conducted in rats: administration of a nicotine degrading enzyme, nicotine oxidoreductase (NicA2), to directly remove nicotine from the bloodstream. Initial responses have been promising, rats administered with NicA2 demonstrate milder withdrawal symptoms as well as reduced compulsive intake of nicotine[5–7].

A major caveat of these studies, however, is the high dose of enzyme required to achieve these desirable effects, 10-70 mg kg^{-1}. This would translate to roughly a gram of enzyme to treat a human— an unrealistically high amount for an enzyme-based treatment. The reason such a dose is required is most likely the observed low catalytic rate of the enzyme, which has been measured in solution at 0.006 s^{-1} [7,8]. Ideally NicA2

would degrade most of the nicotine absorbed when smoking before it is able to reach the tissues upon which it acts. There are only about 7 seconds of “dead time” after inhaling nicotine before it reaches the brain[9]. Given the slow catalytic rate of NicA2, an extremely large dose is necessary to enact degradation of this much nicotine in this short time frame. We decided to explore the reasons behind the poor activity of NicA2, and investigate how it may be improved in order to make it an effective therapeutic at a lower dose.

NicA2 belongs to a subfamily of enzymes called flavin amine oxidases that falls within the broader class of flavoenzymes. This broader class is so named because these enzymes use flavin mononucleotide (FMN) or flavin adenine dinucleotide (FAD) as a prosthetic group (**Figure 1**). In general, flavoenzymes accomplish their chemistry by undergoing cycles of reduction and oxidation. For this reason, it is common to think of their chemical mechanism in distinct steps known as half-reactions. Conveniently, reduction and oxidation of flavoenzymes can be studied independently by controlling the access of the enzyme to its reductive or oxidative substrates. Flavin amine oxidases, like NicA2, catalyze reactions by first accepting electrons from an amine-containing substrate, resulting in their bound FAD becoming a reduced hydroquinone (**Figure 2a**)[10]. After this reductive step, the enzymes’ bound flavin cofactor must be oxidized before it can undergo another round of catalysis. Molecular oxygen, O_2, is a widely available oxidant that serves as electron acceptor for the oxidation of essentially all flavin amine oxidases[11].

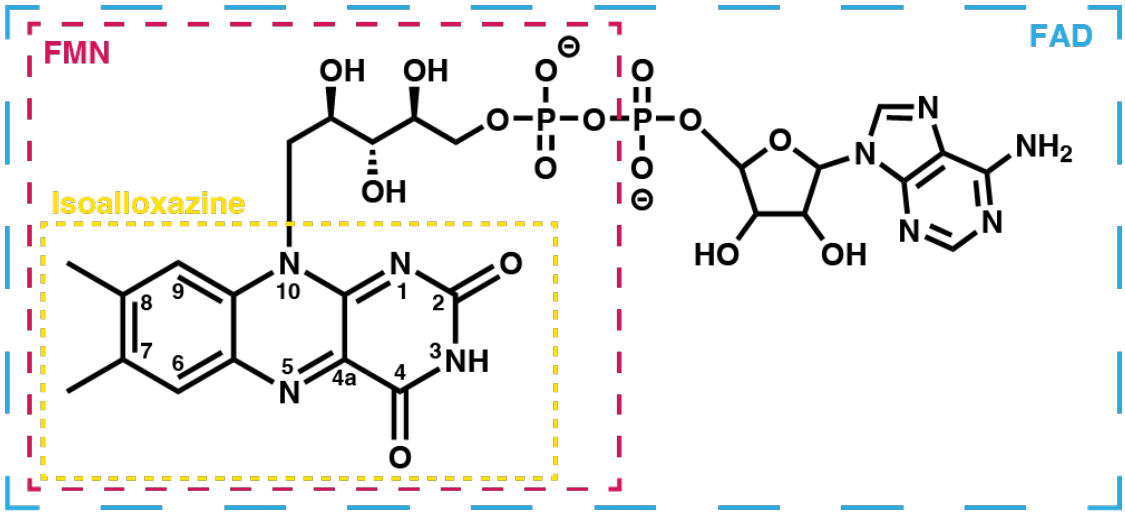

Figure 1. Flavin structures.

FMN, flavin mononucleotide; FAD, flavin adenine dinucleotide. Note the numbering scheme of the isoalloxazine ring.

A convenient quality of flavoenzymes is the intrinsic absorbent and fluorescent properties of isoalloxazine. These enzymes demonstrate a visible yellow color when bound by oxidized flavin, and this color changes based on the flavin's oxidation state. A characteristic spectral trace can be found for these various oxidation states, allowing for clear interpretation of redox status of the enzyme with a spectrophotometer or sometimes even by eye (**Figure 2b**). The flavin cofactor is essential for catalytic activity of flavoenzymes, and so absorbance of flavin is routinely used to determine the active concentration of enzyme within a preparation. Free FAD and FMN also demonstrate fluorescence, which is usually quenched upon being bound to an enzyme.

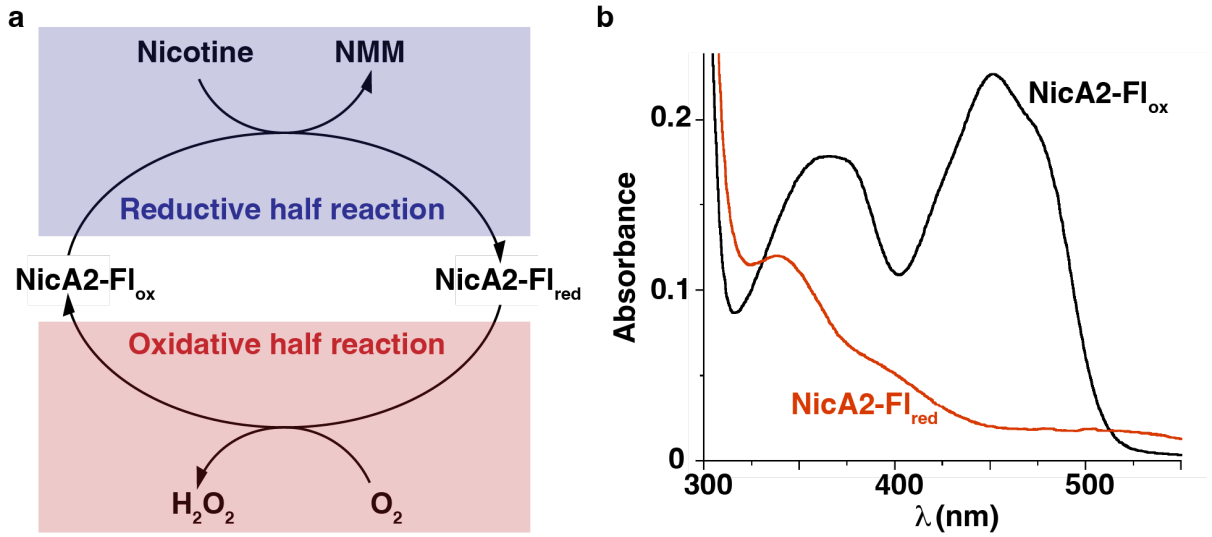

Figure 2. Flavin dependent enzymes undergo cycles of reduction and oxidation.

a, This schematic depicts the reactive cycle for NicA2 for oxygen-dependent turnover. **b,** The absorbance of NicA2's FAD prosthetic group in both an oxidized and reduced state.

An important question regarding flavoenzymes is the scope and control of their reactions with O_2 [12]. Due to the high redox potential of the O_2/H_2O_2 couple versus that of flavins, all reduced flavins are thermodynamically poised to be oxidized by O_2 [13]. In the case of flavin-containing oxidases, O_2 is a ready reactant, with rate constants for oxidation typically falling between 10^3-10^6 $M^{-1}s^{-1}$ [14]. Conversely, flavin-containing dehydrogenases do not facilitate a reaction between their bound flavins and O_2, irrespective of the thermodynamic driving force, having rate constants for oxidation that can approach zero. This implies there are molecular features in some flavoenzymes that act to slow the reaction with O_2[12]. Despite roughly one hundred years of study[15], the molecular rules that govern oxidase activity for a given flavoenzyme have remained obscure[14,16,17]. The behavior of NicA2 is particularly perplexing because, defying the trend within its enzyme family, it reacts poorly with O_2 as an oxidant and it is better classified as a dehydrogenase[18,19].

One aim of this thesis is to understand the molecular basis of the oxidase/dehydrogenase divide within flavin amine oxidases using NicA2 as a model protein. My characterization of NicA2 led to the discovery of a cytochrome c I termed CycN, that I then showed serves as NicA2's physiologic oxidative partner both in vivo and in vitro. Using a genetic selection designed to enhance the oxidase activity of NicA2, I isolated variants of the enzyme with increased catalytic rates. NicA2 appears to have evolved to acquire dehydrogenase-like activity despite its annotation as an oxidase[18,20]. By discovering mutations that can change the fundamental redox chemistry of NicA2 my work opens an avenue for directed evolution of flavoenzymes to catalyze oxidation/reduction reactions that might deviate substantially from their natural function.

1.2 *Pseudomonas putida* S16 and other nicotine degrading organisms

1.2.1 Isolation

The group of Wang et al. first isolated *Pseudomonas putida* S16, the microorganism containing the gene for NicA2, from the soil of a tobacco field in Shandong, China[21]. They found that *P. putida* S16 was able to grow readily using nicotine as sole carbon and nitrogen source with a doubling time of ~90 minutes and they characterized the pathway by which nicotine is degraded in this microorganism[22,23]. Other nicotine degrading organisms have subsequently been isolated from tobacco-growing fields[24], tobacco waste extract[25,26], nicotine contaminated water[27], and pesticide manufacturing waste[28].

1.2.2 Nicotine degradation pathways

Nicotine degradation in these microorganisms is achieved primarily through two pathways: the pyridine pathway, where the first catalyzed step is the hydroxylation of the pyridyl ring of nicotine; and the pyrrolidine pathway, wherein the pyrrolidine ring of nicotine is oxidized (**Figure 3**)[29]. Organisms that use variant pathways have also been isolated and they were found to have a mixture of nicotine degrading enzymes homologous to those from both the pyridine and pyrrolidine pathways[29]. The pyridine pathway has been most extensively characterized in *Arthrobacter nicotinovorans*[30,31]. A heterotrimeric enzyme, nicotine dehydrogenase, first catalyzes the hydroxylation of nicotine to form 6-hydroxynicotine whose pyrrolidine ring then gets oxidized in a reaction catalyzed by L-6-hydroxynicotine oxidase (LHNO). These first two steps of the pyridine degradation pathway are detailed in **Figure 3a**. However, the pyrrolidine pathway is of greater relevance to this thesis and thus will be discussed in more detail. There is a clear similarity between the reactions catalyzed by LHNO and NicA2, their substrates differ by only a carbonyl group. Curiously, LHNO is readily oxidized by O_2 whereas NicA2 is not[32].

Extensive mapping of the pyrrolidine degradation pathway in *Pseudomonas putida* S16 came from systematic knockout studies[23,33]. Knockout of either *nicA2*, *pnao*, or other downstream genes in the pyrrolidine pathway abolished the strain's ability to grow using nicotine as a carbon source, implicating these genes in nicotine metabolism. Purified NicA2 was found to bind FAD and react with nicotine to produce N-methylmyosmine, demonstrating that NicA2 catalyzes the first dedicated step in the pyrrolidine pathway for this organism[23]. Following its initial oxidation by NicA2, nicotine is further degraded along a metabolic pathway (described in **Figure 3b)**, which ends with production of fumarate that is funneled into central metabolism.

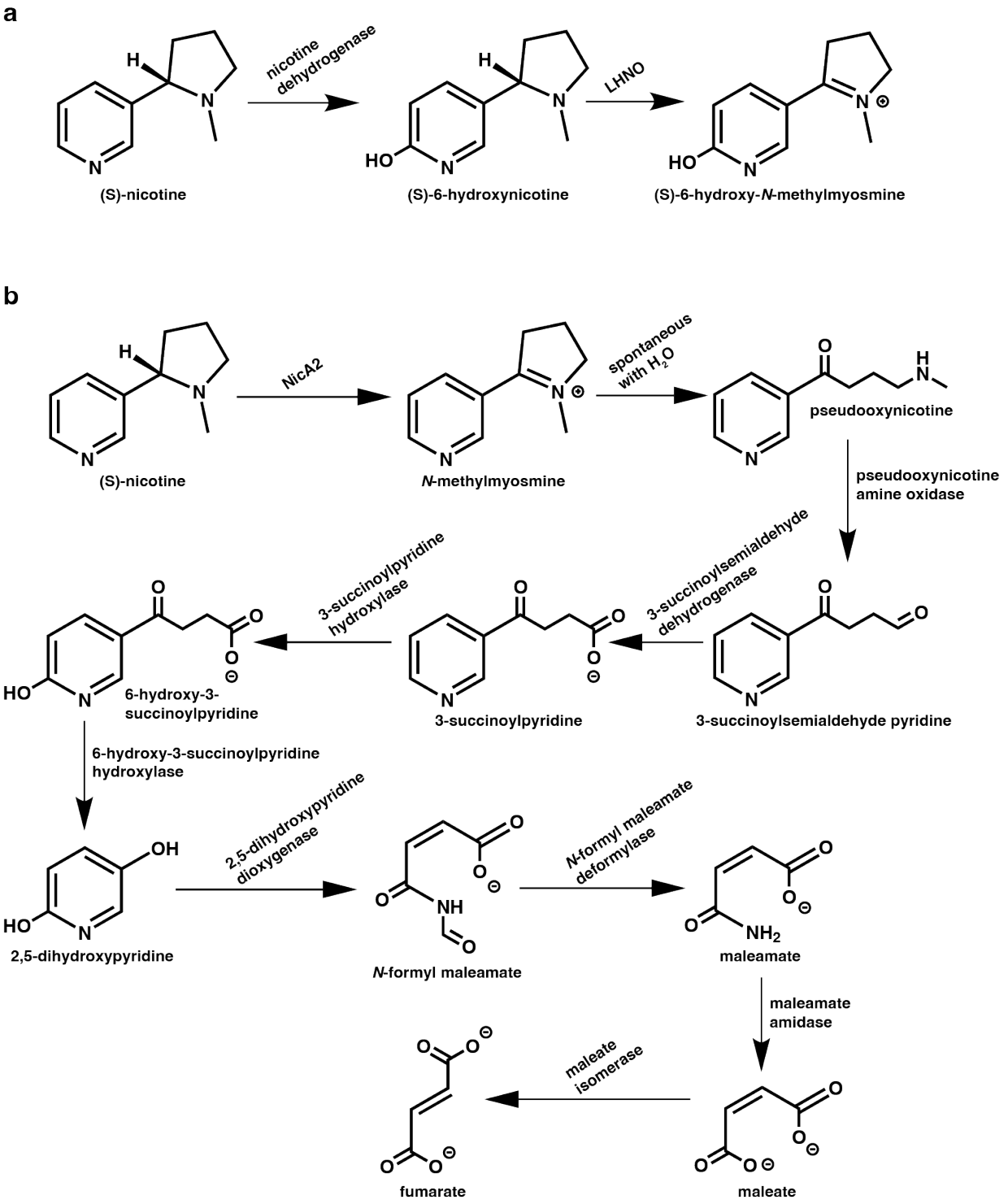

Figure 3. Nicotine degradation pathways.

a, The first two enzyme catalyzed steps of nicotine degradation in the pyridine pathway. LHNO, L-6-hydroxynicotine oxidase. **b,** The pyrrolidine nicotine degradation pathway as it exists in *Pseudomonas putida* S16. Note the similarity between the reactions catalyzed by NicA2 and LHNO.

1.3 Nicotine oxidoreductase (NicA2)

1.3.1 Mechanism and kinetic studies

Nicotine oxidoreductase has been the subject of several previous studies, including that of Xue et al. who first determined the kinetic properties of the enzyme in their evaluation of the possible application of NicA2 as a therapeutic intervention to aid in the cessation of smoking[7]. When NicA2 oxidizes nicotine, the direct product of the reaction is N-methylmyosmine, which spontaneously hydrolyzes in the presence of water to form pseudooxynicotine. These two products interconvert at neutral pH, forming a roughly 50:50 mixture[34]. Using a mass spectrometry linked assay, the authors determined that NicA2 had a k_{cat} of 0.007 s^{-1} and a K_M of 45 nM for nicotine degradation using O_2 as an electron acceptor. This k_{cat} is remarkably low, other members of the amine oxidase family typically turn over their substrates 1000-10,000x more rapidity[32,35,36].

If NicA2 catalyzes the degradation of nicotine at such a slow rate, how can *Pseudomonas putida* S16 rapidly grow using nicotine as its sole carbon and nitrogen source? NicA2 is essential for growth on nicotine, implying that there are no parallel pathways capable of degrading nicotine fast enough to allow growth. It is thus difficult to imagine how the microorganism can rapidly grow on the small supply of carbon liberated by NicA2's poor activity. This logical question led us to hypothesize that there must be an alternative electron acceptor in *Pseudomonas putida* S16 with which NicA2 is capable of rapidly catabolizing nicotine— thereby sustaining the growth of the microorganism documented in earlier studies. This is further explored in Chapter 2 of this thesis.

Tararina et al. solved a crystal structure of FAD bound to NicA2[37]. It was found that NicA2 has a flavin-containing amine oxidase fold similar to monoamine oxidase N (RMSD

of 2.1 Å), LHNO (RMSD of 2.6 Å), and monoamine oxidase B (RMSD of 2.9 Å)[37]. One unique feature of NicA2 is the lack of a hydrophobic cage enclosing the isoalloxazine of FAD, which is normally found in flavin amine oxidases[38,39]. Usually isoalloxazine is flanked by Tyr and Trp residues in other flavin-dependent oxidases, but NicA2 instead has an Asn residue adjacent to the head of FAD, similar to some dehydrogenase flavoenzymes[40]. This was seen as a clue that poor oxygen reactivity may be the cause of NicA2's low k_{cat}, and Tararina et al. suggest that some molecule other than O_2 may be this enzyme's physiological electron acceptor.

The presumed mechanism for flavin amine oxidases is a catalytic cycle of reduction and oxidation reactions performed using its FAD prosthetic group (**Figure 2a**). Due to the presence of oxygen in the environment, the flavins within amine oxidases are generally found to be oxidized under ambient conditions. In their catalytic cycle, amine containing substrates are oxidized by a direct hydride transfer to this oxidized FAD, thereby reducing it to the hydroquinone $FADH_2$ form (**Figure 4**). For the catalytic cycle to continue, $FADH_2$ must then be oxidized. In the case of the flavin amine oxidase family, $FADH_2$ is canonically oxidized by O_2, yielding FAD and H_2O_2 or superoxide[11].

NicA2 also appears to facilitate reduction of its bound FAD by direct hydride transfer from nicotine, resulting in the oxidized product N-methylmyosmine[41]. Under steady-state aerobic conditions, the enzyme produces an equimolar amount of H_2O_2 as nicotine is consumed, indicating that it can be oxidized by O_2. It does not appear to make a significant amount of superoxide[8]. Due to the large difference in reduction potential between $FADH_2$ and O_2 essentially all flavoenzymes should spontaneously oxidize with

O_2 to some degree[12]. Producing hydrogen peroxide is a general feature of flavoenzyme oxidases, whereas dehydrogenases tend to produce a fraction of superoxide[13].

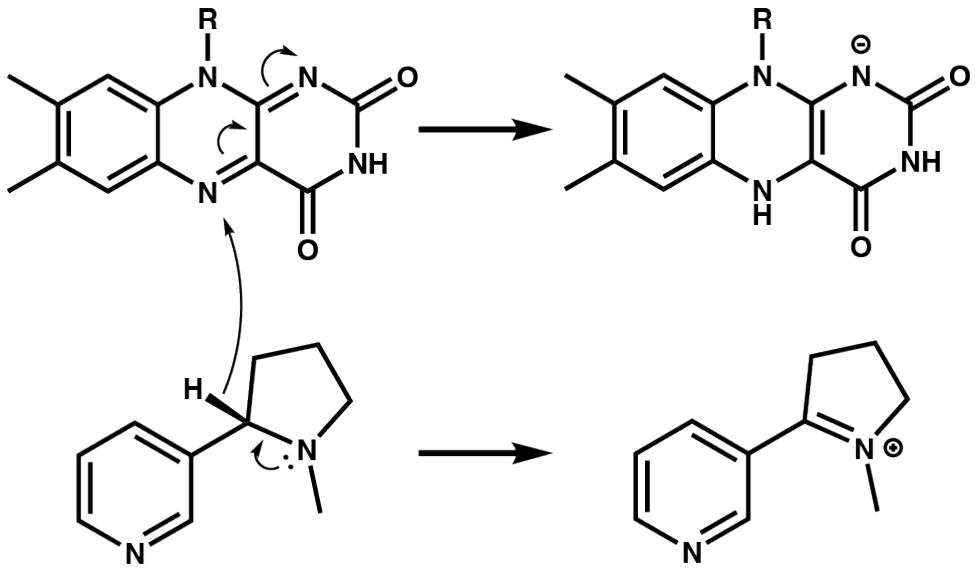

Figure 4. Schematic depicting hydride transfer from nicotine to NicA2-bound FAD

1.3.2 The structure of NicA2

The crystal structure of NicA2 shows similarity to other flavin amine oxidases (**Figure 5**)[37]. In general, the flavin amine oxidase family demonstrate a high degree of sequence and structural conservation within their shared flavin binding domains, but understandably show greater divergence between their substrate specificity domains.

Figure 5. Alignment of NicA2 against other flavin amine oxidases.

NicA2 (PDB 5TTJ)[37] is shown in green, human monoamine oxidase A (PDB 2BXR)[42] in orange, and human monoamine oxidase B (PDB 2VRL)[43] in magenta. Bound flavin adenine dinucleotides are rendered in yellow. The structure is oriented such that the flavin-binding domain is toward the bottom of the figure, and the substrate specificity domain the top of the figure.

In the nicotine bound structure of NicA2, nicotine is positioned toward the *Re*-face of FAD with its reactive hydrogen in a position suitable for hydride transfer (**Figure 6**)[8]. The specificity for nicotine binding appears to be mediated primarily by four hydrophobic residues W108, L217, W364, and W427; with possible stabilizing hydrogen bonds coming from T381 and Y218. LHNO, which catalyzes a similar reaction with NicA2 but is readily

oxidized by O_2, also orients its substrate 6-hydroxynicotine with hydrophobic residues and accommodates its substrate's carboxyl group with an additional stabilizing hydrogen bond from N166. Also visible in active site of NicA2 is the unusual N462 residue that substitutes the hydrophobic cage typical for amine oxidases, which can be compared to the more typical Y407 residue that makes this cage in LHNO.

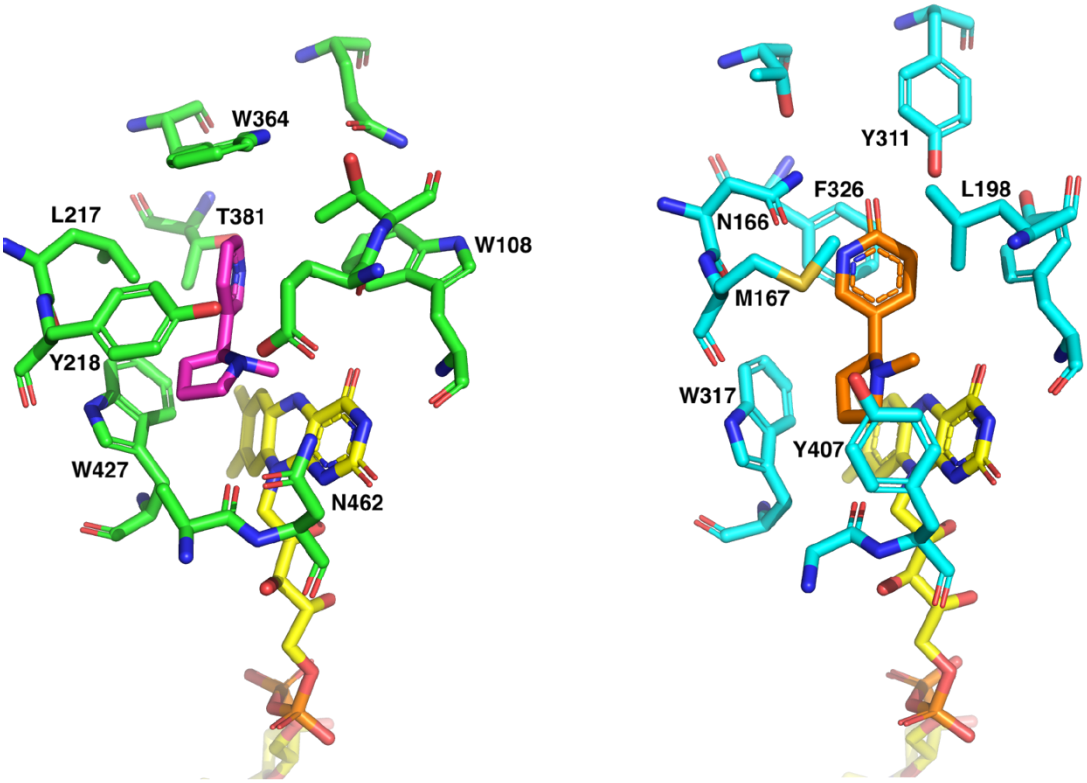

Figure 6. Active sites of LHNO and NicA2.

NicA2 (6C71)[8] is rendered in green, with its substrate nicotine in magenta. LHNO (3NG7)[44] is rendered in cyan, with its substrate 6-hydroxy-nicotine in orange. LHNO contains a typical hydrophobic cage residue in Y407; NicA2 has the unusual N462 substitution.

Binding of a substrate or product to a protein often results in conformational changes in the protein either by induced fit or conformational selection. A 4 Å shift in the substrate specificity domain is evident upon overlay of the nicotine bound structure with that of the unbound enzyme (**Figure 7**). This conformational shift results in the active site becoming less solvent exposed. This may assist in excluding oxygen from the active site

during the oxidative phase of NicA2's reactive cycle when nicotine or product is expected to be bound[8].

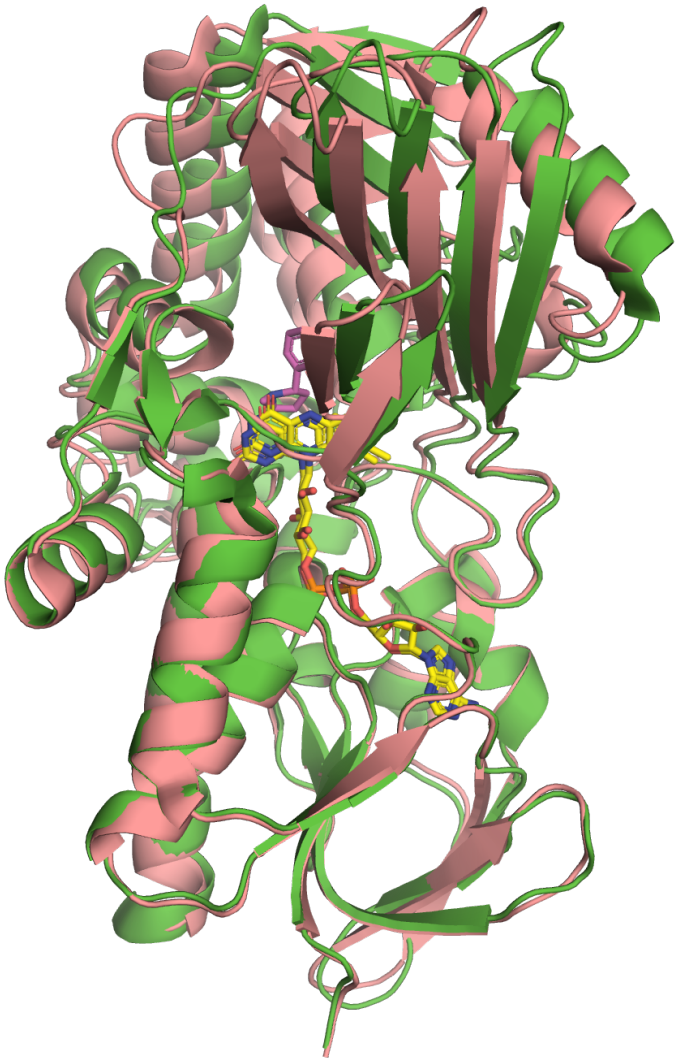

Figure 7. Overlaid structures of NicA2 bound and unbound by nicotine.

Apo NicA2 (PDB 5TTJ)[37] is rendered in green. NicA2 bound by nicotine (PDB 6C71)[8] is rendered in salmon. FAD is rendered in yellow, and nicotine rendered in magenta. Structures were aligned to their flavin binding domain (bottom half of the image), with a visible conformational change in the substrate specificity domain (upper half of the image).

1.3.3 Mutagenesis studies of NicA2 and other nicotine degrading enzymes

The very low turnover rate of NicA2 presents a barrier for its use as a therapeutic, so there have been several attempts to increase its catalytic rate. Comparison of NicA2 with *bona fide* oxidases in the same enzyme family inspired mutagenesis of residues that are generally conserved in the flavin amine oxidase family but are altered in NicA2. The aforementioned N462 position of NicA2, which is usually a conserved hydrophobic residue such as Tyr or Trp in other oxidases, has been substituted with several different residues in an effort to increase the oxidase activity of NicA2. Single substitutions N462Y and W427Y had relatively minor effects, increasing the k_{cat} by 6.5 and 2.8-fold respectively, but combining the two mutations intended to reconstruct the "hydrophobic cage" typically seen in most flavin amine oxidases did result in a larger ~12-fold increase of k_{cat} in the N462Y/W427 double mutant. Unfortunately, this came at the expense of K_M which increased from 0.11 μM to 2.5 μM[18]. Other substitutions of N462 show a similar trend, increasing both the k_{cat} and K_M. Though all possible substitutions were not attempted, it seems unlikely that this position alone controls oxygen reactivity of the bound flavin.

Another study conducted site saturation mutagenesis of 22 active site residues, and then screened the activity level of these variants using a novel peroxidase linked assay[6]. Proteins with improved k_{cat} values were further characterized. This study design provided the throughput necessary to test the hypothesis that these sites individually are sufficient to control oxygen reactivity. However, this study did not isolate any single mutants that had a substantially improved catalytic rate. This implies that that multiple residues may need to be targeted to switch NicA2's activity from a dehydrogenase to an

oxidase. Overall, these mutagenesis studies demonstrate that there is no “magic bullet” for engineering increased oxygen reactivity of NicA2.

A summary of the steady-state kinetic parameters determined for NicA2 variants generated in these studies is included in **Table 1**.

Table 1: NicA2 variants characterized from previous publications.

NicA2 variant	k_{cat} (s^{-1})	K_M (μM)	k_{cat}/K_M (s^{-1} M^{-1})
wild-type[8]	0.006	0.114	5.4×10^4
T381V[8]	0.011	0.317	3.5×10^4
T250V/T381V[8]	0.0259	2.52	1×10^4
N462V[18]	0.035	2.7	1.3×10^4
N462Y/W427Y[18]	0.093	5.9	1.6×10^4
N462H[18]	0.02	0.2	1×10^5
A107R[6]	0.159	0.83	1.9×10^5
A107T[6]	0.05	0.285	1.8×10^5
A107G[6]	0.053	0.335	1.6×10^5
F104T[6]	0.055	0.33	1.7×10^5
F104I[6]	0.039	0.24	1.6×10^5
F104R[6]	0.041	0.27	1.5×10^5
F104S[6]	0.031	0.25	1.2×10^5
G106A[6]	0.031	0.28	1.1×10^5
F355H[6]	0.029	0.22	1.3×10^5
A426C[6]	0.03	0.23	1.3×10^5
W103G/R253H/D130A[45]	0.014	Not determined	Not determined

NicA2 oxidizes nicotine, and LHNO oxidizes a substrate that differs by only a single carbonyl group, 6-hydroxynicotine. It was therefore expected that changing the substrate specificity of LHNO towards nicotine might be trivial, and so attempts have also been made to convert LHNO into an efficient nicotine degrading enzyme. Contrary to NicA2, LHNO enzymes react rapidly with their native substrate, 6-hydroxynicotine, using O_2 as an electron acceptor: ~60 s^{-1} as documented in one study[46]. LHNO is thus a true oxidase, and it has a similar reductive half-reaction when compared to NicA2[32]. Likely because of their natural ability to use oxygen as an electron acceptor, two LHNO enzymes actually manage to achieve a higher k_{cat} (0.1 s^{-1} and 0.9 s^{-1}) in degrading nicotine, a non-natural substrate, than NicA2 does [45,46]. However, their use as a smoking cessation therapy is greatly limited by their very high K_M for nicotine: between 1-10 mM, far higher than the nicotine concentration in the bloodstream of smokers which maximally reaches ~200 nM[47]. NicA2 has a K_M near this range, roughly 100 nM as determined by multiple studies[7,8]. LHNO from *Arthrobacter nicotinovorans* has a k_{cat} for nicotine degradation of 0.1 s^{-1} and a K_M for nicotine of 13 mM[46]. This enzyme was rationally engineered, introducing 3 simultaneous mutations to change its active site so that it should resemble NicA2. This resulted in a roughly two-fold increase in the specificity constant for LHNO's reaction with nicotine, however, this did not succeed in improving the K_M for the reaction which remained at 10 mM or larger for all mutations tested.

A similar attempt at active site engineering was made with LHNO from *Shinella sp.* HZN7. This enzyme was thought to be a more suitable starting point, as its k_{cat} for nicotine was 0.9 s^{-1} and it has somewhat lower K_M than the *A. nicotinovorans* enzyme,

around 1 mM, though this value is clearly still unacceptably high[45]. Rational substitutions in the active site of this enzyme managed to decrease the K_M slightly to 0.6 mM, while maintaining a k_{cat} of 0.6 s^{-1} [45]. Unfortunately, these kinetic parameters predict that at a bloodstream nicotine concentration of 200 nM this mutant would have a turnover rate of only 0.0002 s^{-1}– 10-fold lower than the already poor rate seen with wild-type NicA2.

1.4 Oxygen reactivity in flavoenzymes

The title of a review on this subject, "The enigmatic reaction of flavins with oxygen," well summarizes how much there is to learn in this area[16]. $FADH_2$ free in solution can be oxidized by O_2 with a bimolecular rate constant of 250 $M^{-1}s^{-1}$ [13]. When $FADH_2$ is bound to an enzyme, the oxidation rate may be enormously depressed or accelerated to between 2 and 10^6 M^{-1} s^{-1} [12]. Although not entirely understood, the structural features of flavoproteins that allow for this vast range in oxidation rate have been investigated, and a few guiding principles have been elucidated.

One way by which flavoenzymes may modulate oxidation of $FADH_2$ is by changing the accessibility of the protein interior to O_2. This makes intuitive sense, given that O_2 must be in the proximity of N5 or C4a of flavin for oxidation to occur. Dissolved oxygen is thought to infiltrate enzymes through either "breathing" motions intrinsic to the dynamics of the protein, or by predefined oxygen channels which have been uncovered in some flavoenzyme oxidases[48–53]. It has been shown that obstruction or modification of these channels can lead to a decrease of oxidase activity, which supports a direct role of channels in bringing O_2 to the active site[48,49,53]. It is not necessarily the case that access

is sufficient, however. There are examples of distinct flavoenzymes with a similar degree of exposure of their cofactor to solvent, one of which reacts readily with O_2 while the other does not[12]. Additionally it appears the properly positioned hydrophobic residues are essential for guiding and positioning O_2 properly for oxidation[16,54].

The rate limiting step for oxidation of flavoenzymes by O_2 is formation of an obligate superoxide-flavin semiquinone intermediate[12,55]. Ground-state oxygen is a triplet, and spin inversion is required before O_2 can interact with singlet $FADH_2$. This is thought to occur via two consecutive one electron transfers from $FADH_2$ to O_2. The first transfer necessitates formation of the caged radical pair superoxide-flavin semiquinone intermediate; after which it may collapse into a C4a hydroperoxide or into H_2O_2 (**Figure 8**)[13]. In order for this reaction to occur rapidly, it is therefore critical to generate a suitable environment near $FADH_2$ that can stabilize the superoxide-semiquinone intermediate. It is generally accepted that at least some positively charged feature is required for the activation of O_2, and for some flavoenzymes stabilization of this intermediate is achieved with a structural feature similar to an oxyanion hole[54,56].

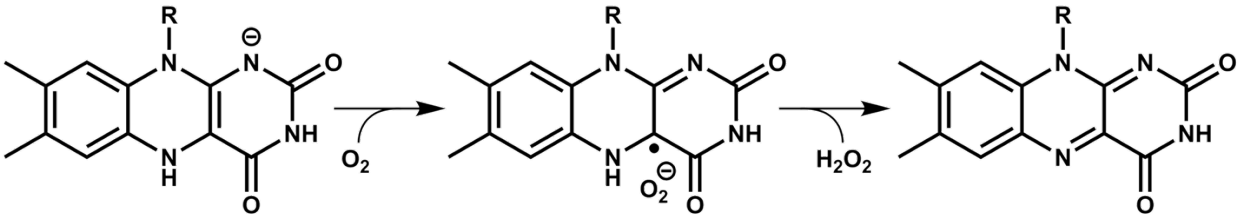

Figure 8. Schematic depicting formation of the superoxide-semiquinone intermediate during oxidation by O_2.

Two literature examples of converting dehydrogenase flavoenzymes into robust oxidases stand out[57,58]. In both cases, it appears that there was a steric clash from a residue of the protein which obstructed an O_2 activation site near N5 of FAD. By mutating the blocking residue into a smaller amino acid, a switch to oxidase activity was achieved. This result supports the requirements of positive charge in the activation of O_2 and stabilization of the flavin-semiquinone superoxide intermediate[54]. However, this does not provide a general route for engineering flavin-dependent enzymes to react with O_2; since not all members of this family contain preformed oxygen activation sites.

Conversely, destruction of oxidase activity is comparatively trivial, and has been accomplished many times[59–62]. Removal of the positive charge necessary to facilitate the caged radical intermediate, blocking of O_2 channels, or modification of the active site residues which cage the flavin have all proven to be sufficient to ameliorate oxygen reactivity[59–62].

Shifting the discussion of NicA2 within this context, it is observed that NicA2 contains a conserved lysine (K340) which has been demonstrated to be important for oxidation in other flavin amine oxidases (**Figure 9**)[59,60]. This lysine appears to provide the positive charge necessary to stabilize the formation of superoxide. In structures of other members of NicA2's protein family, the position of a crystallographic water molecule near N5 of flavin is considered to mark the location where O_2 would react. NicA2 also demonstrates this bound water molecule in a similar location, and there is no obvious steric block from the protein for the positioning of an oxygen next to N5 of the flavin and this lysine. Thus, it appears that NicA2 contains a similar oxygen activation site to other flavin amine oxidase enzymes.

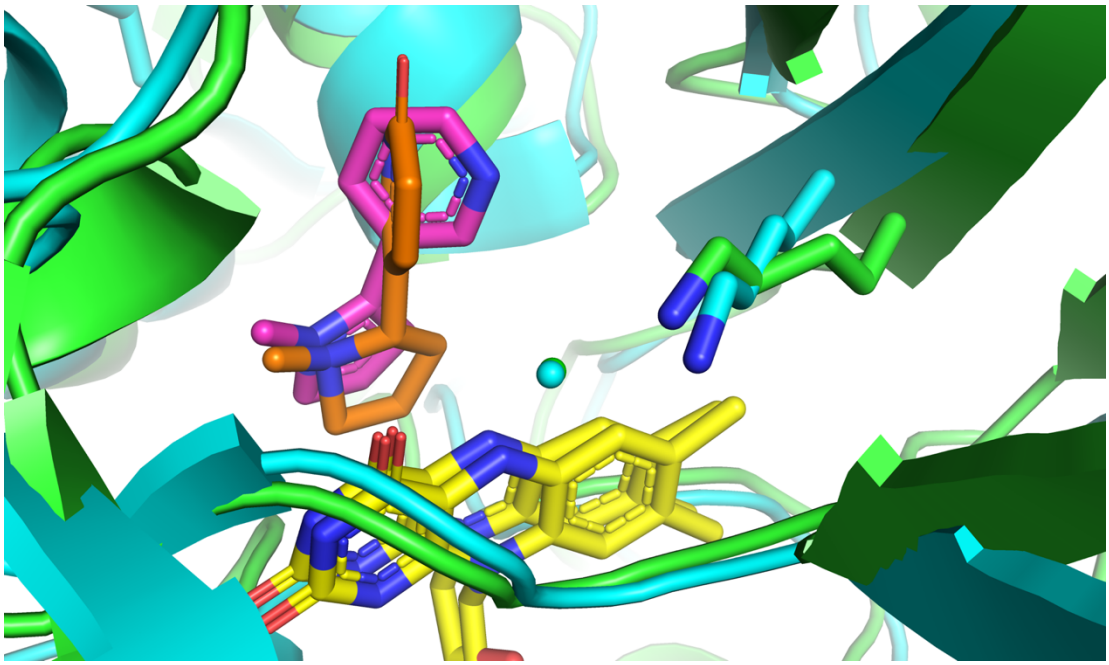

Figure 9. Position of a conserved lysine is maintained in NicA2.

NicA2 (PDB 6C71)[8] is rendered in green, nicotine bound in the active site in magenta. LHNO from *A. nicotinovorans* (PDB 3NG7)[44] is rendered in cyan, 6-hydroxynicotine in orange. The conserved lysine (K340 in NicA2, K287 in LHNO) is shown on the *Si*-flavin side. Note the highly overlapping water molecules rendered as spheres between N5 of FAD and lysine in the same colors as their respective proteins.

NicA2 has an active site that is solvent accessible in the crystal structure of the enzyme unbound by nicotine. In the nicotine-bound structure, there is an apparent closure of otherwise accessible solvent tunnels (**Figure 7**). It may be the case that O_2 diffusion follows along these same channels. It is interesting that several of the most activating mutations identified in previous studies cluster in this region (mutations of F104, G106, and A107); however, targeted mutagenesis with the goal of further opening this channel and decreasing steric hinderance to oxygen binding (W103G/R253H/D130A) did not significantly increase the catalytic activity of NicA2[45].

In summary, it is necessary to achieve both access of O_2 and also maintain an environment conducive to O_2 activation in order to achieve robust oxidation rates in flavoenzymes. NicA2 appears to have both features, like other *bona fide* oxidases. It is

therefore surprising that NicA2 does not react readily using O_2 as an oxidative substrate, and worthy of study because it may control oxygen reactivity by a different mechanism.

1.5 Thesis overview

The poor oxidase activity of NicA2 is a major barrier to its use as a therapeutic to aid in the cessation of smoking. I have devised powerful genetic selection to increase NicA2 oxidase activity to isolate improved activity variants of NicA2. These variants are better able to use O_2 as an oxidative substrate. This has provided a rare opportunity to study the development of enzymatic oxygen reactivity.

In order to gain a full understanding of NicA2's dehydrogenase and oxidase activities, I first characterized the reaction between NicA2 and its physiologic electron acceptor, the cytochrome c that we named CycN. This cytochrome c allows oxidation of NicA2 at a rate much greater than that of O_2, and is critical for NicA2's in vivo function. I then leveraged this discovery to create a genetic selection for the oxidase activity of NicA2 and used it to isolate variants that can oxidize using O_2 at a rate up to 200-fold greater than that of the wild-type enzyme. The mutations that enable oxidase activity localize to a putative oxygen tunnel in NicA2, changing the local dynamics of this tunnel and reducing solvent accessibility in the catalytically relevant product-bound form of the enzyme. These higher activity variants of NicA2 may be more useful than the wild-type enzyme as an aid to the cessation of smoking, as they should require a lower effective dose than the wild-type enzyme does. My work opens the possibility to realize the ultimate goal of developing a therapeutic that can help tackle the blight of smoking addiction that affects millions worldwide. Furthermore, the successful use of directed evolution in the development of

potent enzyme-based therapeutics may inspire future discovery of strategies to ameliorate other diseases addressable by catalytic proteins.

Chapter 2

A Cytochrome C is the Natural Electron Acceptor for Nicotine Oxidoreductase†

†The contents of this chapter were published in, and adapted from, Nature Chemical Biology: Dulchavsky M, Clark CT, Bardwell JCA, Stull F. A cytochrome c is the natural electron acceptor for nicotine oxidoreductase. *Nat Chem Biol*. 2021;17(3):344-350. Nature Chemical Biology permits the reproduction of articles by the author for the purpose of an academic thesis. I performed the aerobic in vitro and in vivo experiments in this chapter. Christopher T. Clark performed the anaerobic and stopped-flow experiments in the lab of Frederick Stull. Ben A. Meinen performed the analytical ultracentrifugation experiments.

2.1 Background

Flavin-dependent enzymes most often utilize their flavin adenine dinucleotide (FAD) or flavin mononucleotide cofactors to conduct reduction-oxidation chemistry. These enzymes are able to pass electrons between their cofactor and substrate in one or two-electron transfer reactions[63]. Some flavoenzymes, termed oxidases, rapidly deliver electrons to molecular oxygen (O_2), creating reactive oxygen species such as superoxide or hydrogen peroxide as a byproduct. Other flavoenzymes are more discerning, instead donating electrons to specific protein or small molecule substrates. These are defined as dehydrogenases and generally do not react rapidly with O_2. However, some degree of oxygen reactivity is inevitable in most flavin-dependent enzymes that form the flavin hydroquinone state due to the ~1 V reduction potential difference between flavins and O_2. Flavin-containing amine oxidases (pfam:01593)[64] are rapidly re-oxidized by O_2 after accepting electrons from their amine-containing substrates. This rapid re-oxidation is

evident, at least *in vitro*, for nearly all previously characterized members of this enzyme family[11,65,66]. Nicotine oxidoreductase (NicA2), however, appears to defy this convention, reacting with oxygen very slowly.

NicA2 is a FAD-dependent enzyme that catalyzes the oxidation of nicotine into N-methylmyosmine[22]. It was isolated from *Pseudomonas putida* S16, an unusual microorganism that can achieve robust growth using nicotine as its sole carbon and nitrogen source[23]. NicA2 catalyzes the first step in the catabolic pathway, which eventually results in the production of fumarate for primary metabolism[29]. NicA2's FAD cofactor accepts a hydride from nicotine, converting it into N-methylmyosmine in the enzyme's biologically-important reductive half-reaction[8]. N-methylmyosmine then undergoes spontaneous hydrolysis to pseudooxynicotine, which is non-toxic and non-addictive in animal models[7]. Because of this, NicA2 has recently received attention as a potential therapeutic for treating nicotine dependence[5–7,67]. Two recent studies revealed that injection of NicA2 into nicotine-dependent rats largely eliminated nicotine from the blood, reversed symptoms of nicotine withdrawal, dramatically reduced compulsive nicotine consumption and susceptibility to relapse[5,67].

NicA2 receives two electrons from nicotine. In order to function as a catalyst, the two electrons retained on NicA2's FAD from nicotine oxidation must be transferred to an electron acceptor. Given NicA2's homology to flavin-dependent amine oxidases that transfer their electrons directly to O_2, studies to date have assumed that O_2 directly accepts the electrons from NicA2's reduced FAD[6,8]. However, NicA2 has a turnover number of 0.007 s^{-1} when using O_2 as a terminal electron acceptor [7,37,68], an abysmally low number when compared with other flavin-containing amine oxidases which have

turnover numbers of ~10-100 s^{-1} [32,35,36]. NicA2's poor activity as an oxidase is an obstacle in developing this enzyme for nicotine cessation therapy. The low catalytic activity of the enzyme requires prohibitively large doses of NicA2, up to 70 mg kg^{-1}, to achieve symptomatic relief of nicotine-dependent behavior in rats[5]. Tararina et al. suggested that NicA2 may use a more effective electron acceptor, but did not propose any specific candidates[37].

Here, we demonstrate that a novel cytochrome c protein, dubbed CycN, is responsible for accepting electrons from reduced NicA2 *in vivo*, not O_2. Our results open a new avenue for using NicA2 in treating nicotine dependence and suggest that other flavin-dependent amine oxidases may also use alternative physiologic electron acceptors.

2.2 Results

2.2.1 NicA2 reacts poorly with O_2

The flavin cofactor contained in the nicotine-degrading enzyme NicA2 provides a convenient spectrophotometric readout for NicA2's oxidation status[63]. In the absence of nicotine, NicA2 has an absorbance spectrum typical for oxidized FAD (**Fig. 10a**). Upon the addition of nicotine to NicA2, however, a clear reduction of FAD to the two-electron reduced hydroquinone ($FADH_2$) was seen. NicA2's flavin remained in the $FADH_2$ state for several minutes before slowly re-oxidizing directly to oxidized FAD. This slow re-oxidation of NicA2 in the presence of oxygen suggests that flavin re-oxidation may be rate limiting during O_2-dependent turnover.

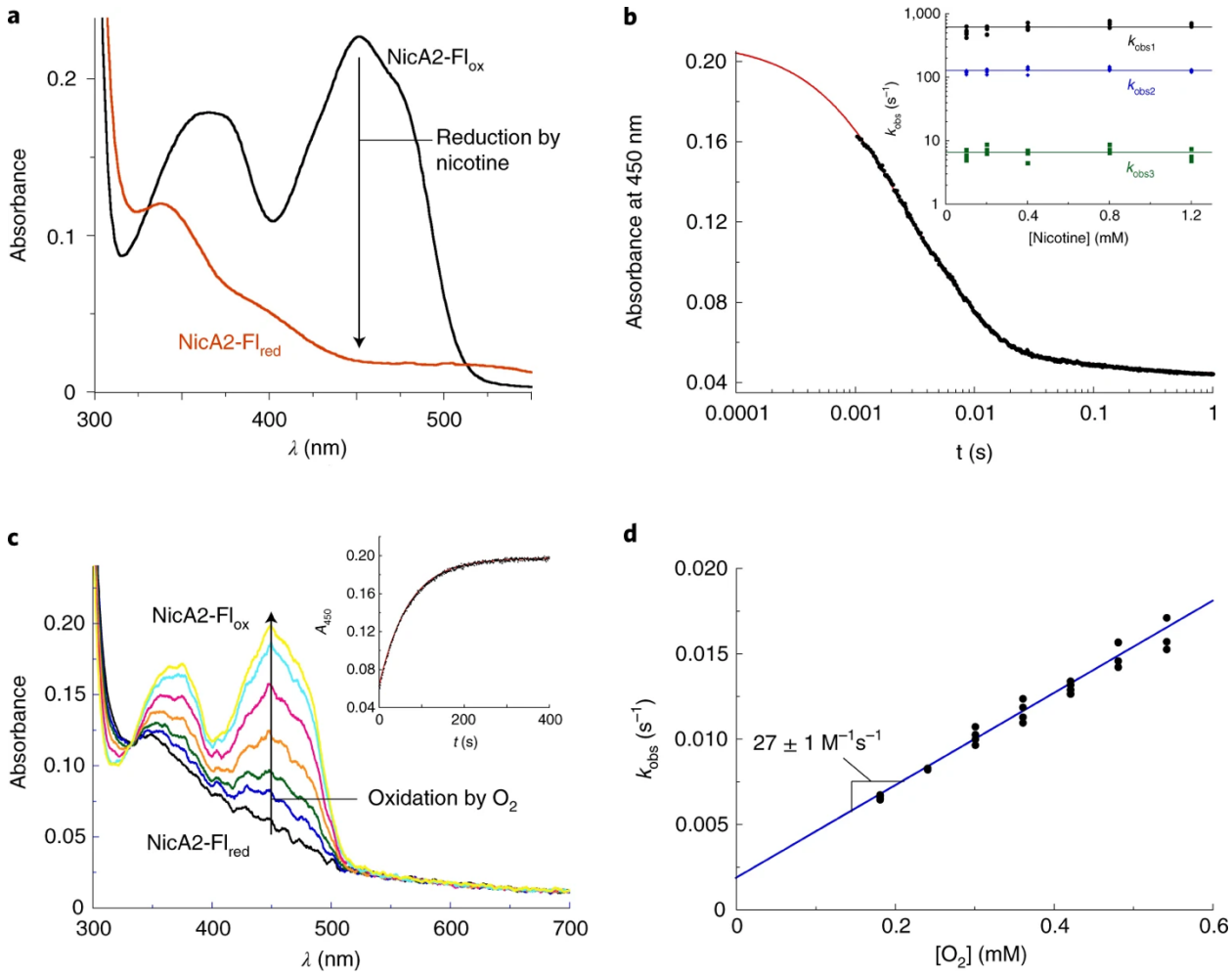

Figure 10. NicA2 is rapidly reduced by nicotine, but slowly re-oxidizes with O_2.

a, NicA2 under ambient conditions was monitored by UV-VIS spectrophotometry in the region of FAD absorbance. Upon addition of nicotine, rapid and complete reduction of FAD was observed and sustained for several minutes. NicA2-Fl$_{ox}$, NicA2 containing oxidized FAD; NicA2-Fl$_{red}$, NicA2 containing $FADH_2$. **b**, Oxidized NicA2 was combined with varying concentrations of nicotine and the change in absorbance at 450 nm was monitored by anaerobic stopped-flow spectrophotometry. Note the logarithmic timescale. The resulting traces required three exponentials to fit properly. Inset: plotting the k_{obs} values of the three phases against the concentration of nicotine shows concentration independence. **c**, NicA2 was reduced by sodium dithionite titration under anaerobic conditions, then mixed with various concentrations of O_2 and monitored for the change in FAD absorbance by stopped-flow spectrophotometry. Inset: a representative trace showing re-oxidation of NicA2's FAD by 540 μM O_2 at 450 nm. See **Figure 14** for traces at other O_2 concentrations. These traces were well fit with a single exponential. **d**, The k_{obs} values derived from fitting re-oxidation traces were plotted against the O_2 concentration, demonstrating linear dependence. These experiments were independently repeated twice with similar results. Values reported are the mean ± s.e.m. of the fit.

Like most flavin-dependent enzymes, the catalytic cycle of NicA2 can be divided into two half-reactions. In the reductive half-reaction, NicA2 containing oxidized FAD (NicA2-

Fl_{ox}) is reduced by reacting with nicotine to form N-methylmyosine. In the oxidative half-reaction, NicA2 containing $FADH_2$ (NicA2-Fl_{red}) is oxidized by reacting with O_2. To quantitatively determine the extent to which NicA2-Fl_{red} oxidation by O_2 limits the consumption of nicotine by NicA2, we examined each half-reaction separately by performing stopped-flow experiments. Reduction of anaerobic NicA2-Fl_{ox} by nicotine in the reductive half-reaction was extremely rapid (**Fig. 10b**). The observed rate constant (k_{obs}) for each of the three phases observed did not change with increasing nicotine concentrations (**Fig. 10b inset**), suggesting that all three events occur after the bimolecular step in which nicotine first binds to NicA2-Fl_{ox}. The first two phases (k_{obs} of ~620 s^{-1} and ~130 s^{-1}) contribute 95% of the signal change at 450 nm and have approximately the same amplitudes; the UV-VIS spectra observed at the end of these two phases suggest that both correspond to FAD reduction by nicotine (**Figure 11a**). That there are two phases may indicate that the two active sites of the NicA2 dimer may be reduced by nicotine with discrete rate constants (**Figure 12**). The change in UV-VIS spectrum for the final phase (k_{obs} of ~6.6 s^{-1}) is consistent with a ligand exchange event following FAD reduction by nicotine. This phase may represent exchange of N-methylmyosmine product with the available excess nicotine. Traces at all nicotine concentrations extrapolated back to the absorbance of NicA2-Fl_{ox} at time zero (**Figure 11b**). Notably, the reductive half-reaction is completed within 1 s. That k_{obs} for all three phases did not increase as the nicotine concentration was raised indicates that

nicotineconcentrations used were saturating and suggests that nicotine binds rapidly prior to FAD reduction.

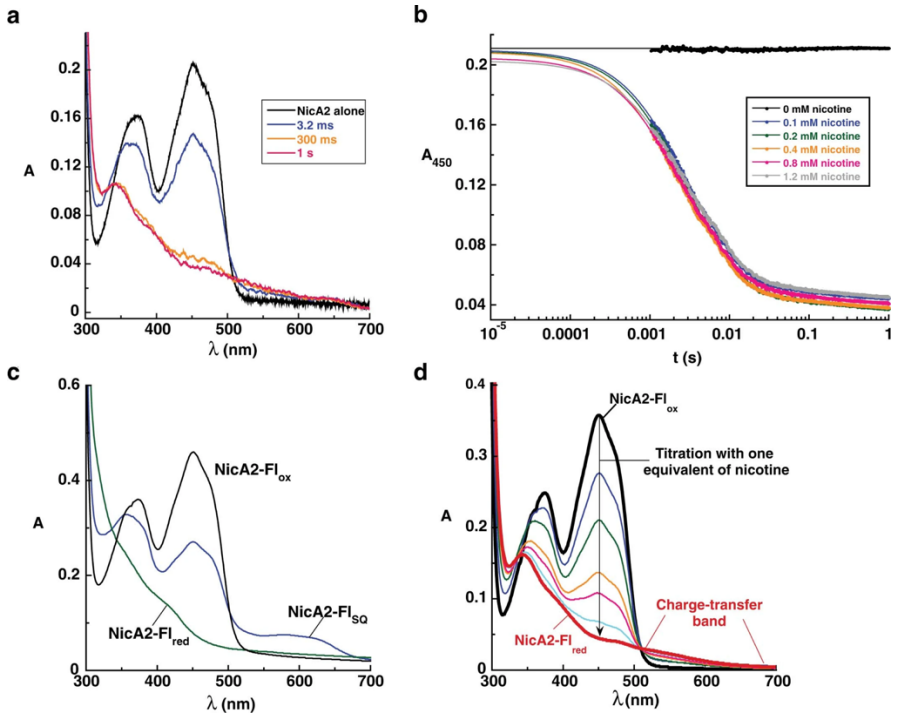

Figure 11. Reduction of NicA2 by nicotine, absorbance traces and intermediates.
a, Oxidized NicA2 was rapidly mixed with 0.2 mM nicotine and absorption of its flavin cofactor monitored using a CCD detector. The two intermediates detectable in reaction traces at 450 nm were maximally populated at 3.2 and 300 ms, and the absorbance spectra at these two points is shown. **b,** Absorbance trace overlay at 450 nm from stopped-flow experiments where NicA2 was reduced by rapid mixing with various concentrations of nicotine. Traces at all nicotine concentrations extrapolated back to the absorbance of NicA2-Fl_{ox} at time zero, indicating that no observable kinetic events were missed within the dead time of the stopped-flow instrument. Note the logarithmic timescale. **c,** Partial reduction of oxidized NicA2 with sodium dithionite produced a species with an increased absorbance from 525–650 nm. The spectrum of the titration point with the highest absorbance in this region is most consistent with a mixed population of oxidized flavin, flavin hydroquinone, and neutral flavin semiquinone[69]. Further titration with sodium dithionite resulted in complete reduction to the hydroquinone ($FADH_2$) state. NicA2-Fl_{ox}, NicA2 containing oxidized FAD; NicA2-Fl_{red}, NicA2 containing $FADH_2$; NicA2-Fl_{SQ}, NicA2 containing flavin semiquinone. **d,** NicA2-Fl_{ox} was reduced by titration of one molar equivalent of nicotine, resulting in reduction of the flavin cofactor as monitored by absorbance. Additionally, a charge transfer band developed in the region of 500-700nm over the course of the titration, likely indicating that at least some amount of N-methylmyosmine product remains bound to NicA2 after reduction of its flavin.

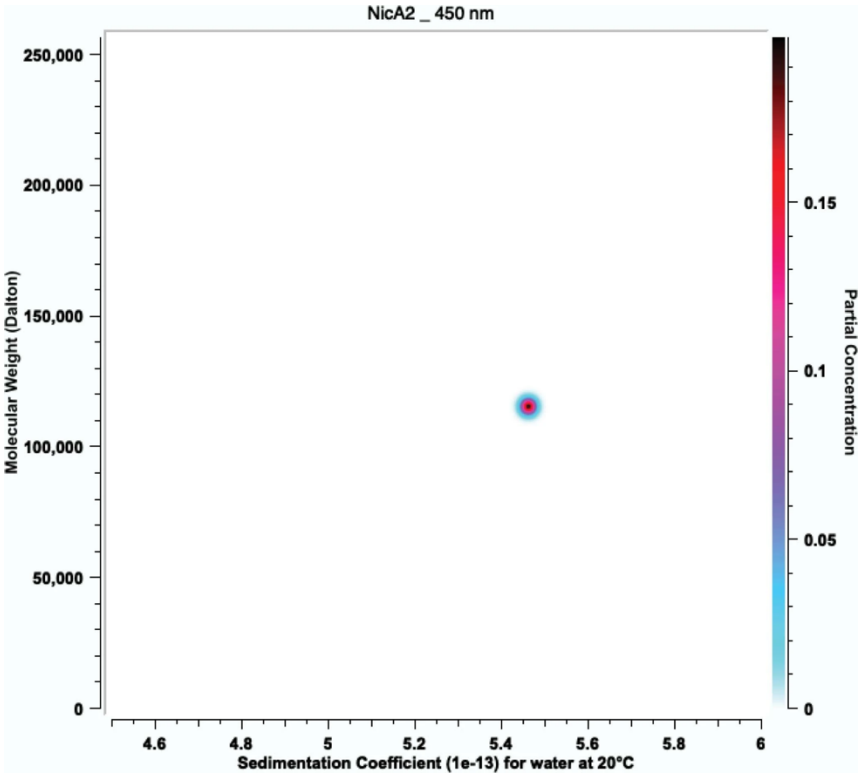

Figure 12. NicA2 is a dimer in solution.

Previous work has described NicA2 as a monomer using size exclusion chromatography[37,68]. To determine the quaternary structure of NicA2 in our buffer conditions, a solution of NicA2 at 20 μM (monomer concentration) was subjected to analysis by sedimentation velocity AUC at a rotor speed of 44,000 rpm while monitoring 450 nm. Data were analyzed using UltraScan 4, version 4.0. One species predominated in solution, with a sedimentation coefficient of ~5.45 and an apparent molecular weight of ~115 kDa. The expected molecular weight for the NicA2 monomer is 53.13 kDa, indicating that NicA2 is a homodimer in solution under these conditions. This experiment was independently repeated twice with similar results.

To further assess the possibility of rapid substrate binding, we measured binding kinetics using the non-catalytic nicotine analog myosmine. Myosmine binding was completed within the 1 ms dead time of the instrument at all myosmine concentrations (**Figure 13**), indicating that myosmine binds to NicA2-Fl_{ox} with a k_{obs} significantly greater than the rate constant for FAD reduction by nicotine.

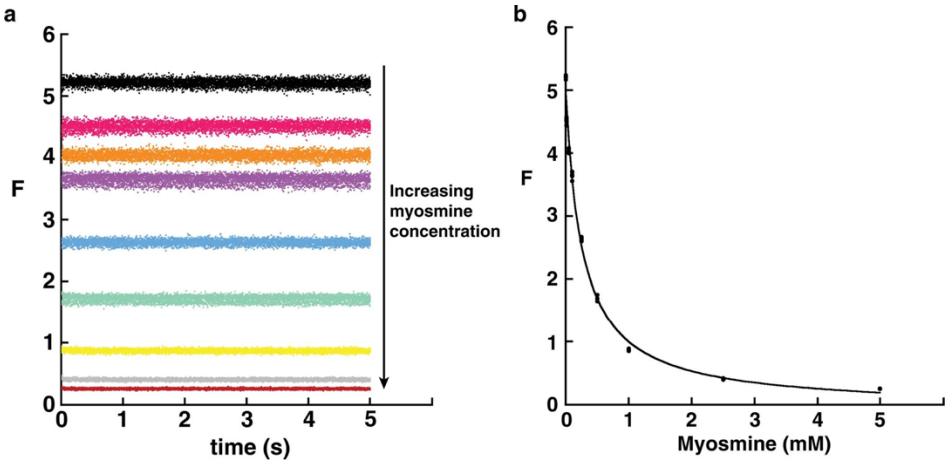

Figure 13. NicA2 rapidly binds myosmine.

a, Tryptophan fluorescence was used to quantify binding of myosmine as previously performed[8]. Traces from a stopped-flow experiment where oxidized NicA2 was mixed with varying concentrations of myosmine demonstrate a rapid binding event, occurring within the dead time (1 ms) of the instrument. **b,** Averaged fluorescence values of 5 traces per myosmine concentration were fit to determine the K_d for myosmine binding at 268 ± 3 μM (s.e.m.).

We next monitored the reaction of NicA2-Fl_{red} with O_2 in the oxidative half-reaction. NicA2-Fl_{red} was prepared by titrating NicA2-Fl_{ox} with one equivalent of dithionite. The use of dithionite as a reductant enabled us to study the oxidative half-reaction in the absence of nicotine reaction products. During the dithionite titration, NicA2's FAD first populated a form with a UV-VIS spectrum resembling a neutral flavin semiquinone[69] before reaching the fully reduced $FADH_2$ state (**Figure 11c**). This suggests that NicA2 is capable of stabilizing a one-electron reduced flavin. Once fully reduced, NicA2-Fl_{red} was then mixed with buffer equilibrated with various O_2/N_2 ratios to re-oxidize NicA2's flavin. Flavin re-oxidation by O_2 was dramatically slower than the reductive half-reaction with nicotine, taking ~400 s for re-oxidation at 540 μM O_2 (**Figure 14a**). NicA2-Fl_{red} oxidized directly into NicA2-Fl_{ox} (**Fig. 10c**). Kinetic traces at 450 nm could be fit with a single exponential and the k_{obs} for this phase increased linearly with O_2 concentration (**Fig. 10c inset and 10d**), indicating that O_2 directly oxidizes NicA2-Fl_{red} into NicA2-Fl_{ox} in a bimolecular

reaction. Linear fitting of k_{obs} against [O_2] yielded a bimolecular rate constant for flavin oxidation (k_{ox}^{O2}) of 27 ± 1 $M^{-1}s^{-1}$. We also measured k_{ox}^{O2} for NicA2 reduced with one equivalent of nicotine instead of dithionite to test if the presence of the N-methylmyosmine product affects NicA2-Fl_{red} oxidation by O_2. Titrating NicA2-Fl_{ox} with one equivalent of nicotine produced a charge-transfer band from 500-700 nm as the FAD was reduced, indicating that the N-methylmyosmine product stays bound to NicA2-Fl_{red} after reduction (**Figure 11d**). N-methylmyosmine-bound NicA2-Fl_{red} was oxidized even slower by O_2 than NicA2-Fl_{red} in the absence of N-methylmyosmine (**Figure 14b,c**), with a k_{ox}^{O2} value of 5 ± 1 $M^{-1}s^{-1}$ (**Figure 14d**). Our data indicate that O_2 is a poor electron acceptor for NicA2-Fl_{red}, particularly when compared to the k_{ox}^{O2} values of 10^5–10^6 $M^{-1}s^{-1}$ seen for most flavin-containing amine oxidases[70].

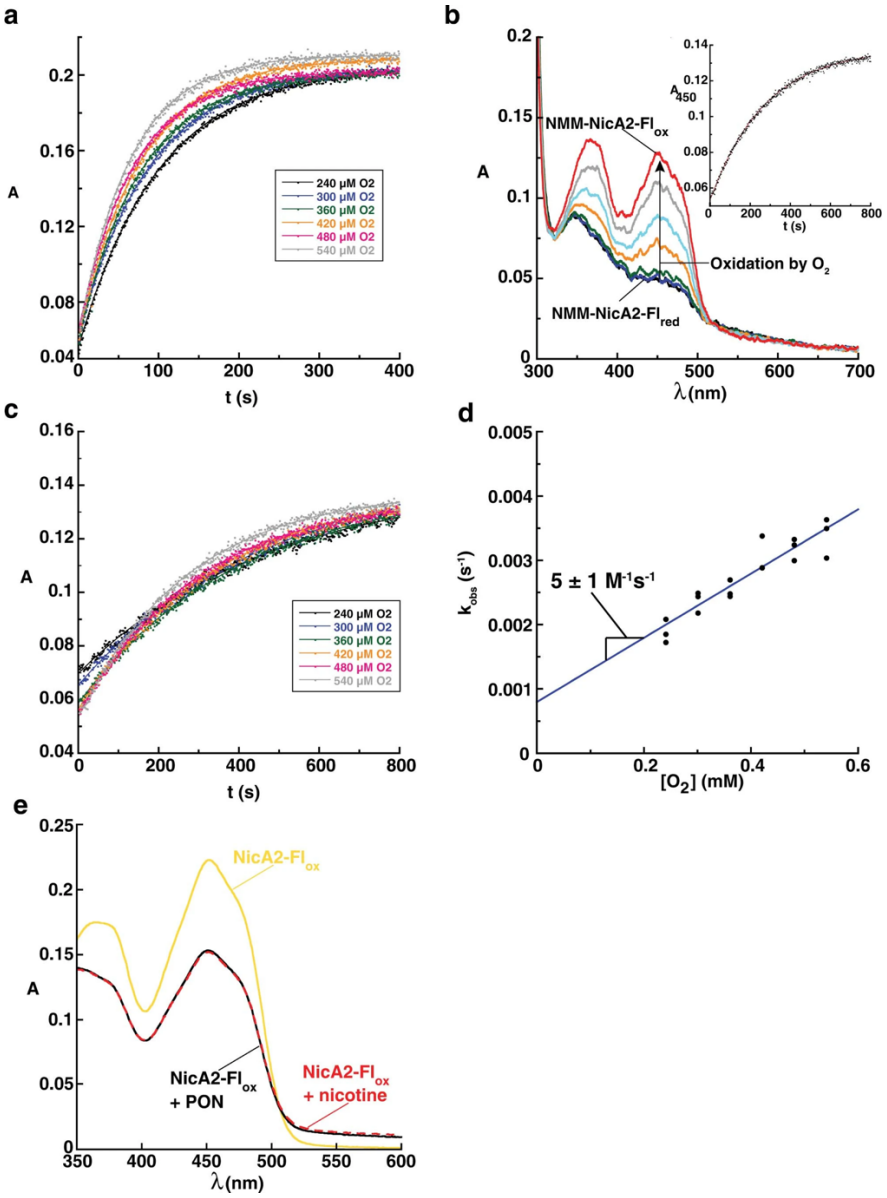

Figure 14. NicA2 is slowly re-oxidized by O_2 in the presence and absence of N-methyl-myosmine. **a,** Absorbance traces from stopped-flow experiments where NicA2, first reduced with dithionite, was then rapidly mixed with variable concentrations of O_2. **b,** NicA2 was reduced with an equimolar amount of nicotine, and then rapidly mixed with O_2 in a stopped-flow experiment which was monitored via the CCD detector. Inset: following the absorbance at 450nm over time in this experiment, re-oxidation was very slow, similar to the behavior of dithionite reduced NicA2. NMM-NicA2-Fl_{ox}, N-methylmyosmine bound NicA2 containing oxidized flavin; NMM-NicA2-Fl_{red}, N-methylmyosmine bound NicA2 containing reduced flavin. **c**, Absorbance traces from stopped-flow experiments where NicA2, first reduced with nicotine, resulting in NMM-NicA2-Fl_{red}, was then rapidly mixed with variable concentrations of O_2. **d,** k_{obs} values for the re-oxidation of NMM-bound NicA2 were plotted against the concentration of O_2, demonstrating linear dependence. **e,** The absorbance spectrum of NicA2-Fl_{ox} (yellow) was compared in two conditions. In one case (red dashed line), nicotine was added to 40 µM end concentration, and the reaction allowed to proceed for 30 minutes until complete re-oxidation of the flavin. In the other case (black solid line) pseudooxynicotine was added to an end concentration of 40 µM and the spectrum taken immediately. NicA2-Fl_{ox}, NicA2 containing oxidized flavin; PON, pseudooxynicotine. These experiments were independently repeated twice with similar results. Values reported are the mean ± s.e.m. of the fit.

2.2.2 ***Identification of NicA2's physiologic electron acceptor***

P. putida S16 is able to grow with a doubling time of about 90 min using nicotine as its sole carbon and nitrogen source[23]. At the established *in vitro* catalytic rate of NicA2 using O_2[7], it is impossible to accumulate enough biomass from nicotine to sustain this doubling time. Even if 5% of *P. putida* S16's biomass was made up of NicA2 enzyme, we calculate that this enzyme must have a catalytic rate of at least 1 s^{-1} *in vivo* to support a 90 min doubling time (see Methods). This implies that NicA2 uses a different electron acceptor *in vivo*.

The genome of *P. putida* S16 indicates a poorly annotated open reading frame (PPS_RS28240) just downstream of *nicA2* (**Figure 15a**)[22,23,33]. Both *nicA2* and this open reading frame possess signal sequences for periplasmic localization (SignalP 5.0[71]). A BLAST search of the downstream open reading frame revealed homology to cytochrome c proteins, and we therefore designate this gene as *cycN*. Cytochrome c proteins are small electron carrier proteins that mediate electron transfer reactions, such as those between complex III and complex IV of the aerobic electron transport chain[72]. This, and the fact that *cycN* forms an operon with *nicA2* led us to hypothesize that CycN plays a similar role for NicA2, shuttling electrons between NicA2 and the electron transport chain.

2.2.3 P. putida S16 ∆cycN is unable to grow on nicotine

To test if CycN is NicA2's physiological electron acceptor, an in-frame deletion of *cycN* was assessed for its ability to grow on nicotine[73]. Both the ∆*cycN* and wild-type (WT) strains grew well on rich media. When plated onto media where nicotine is the sole carbon

and nitrogen source, the Δ*cycN* strain showed a growth defect (**Figure 15b**). While WT *P. putida* S16 formed large, easily visible colonies within two days, the Δ*cycN* strain grew poorly. Presumably this is because in the absence of CycN, NicA2 is forced to use other electron acceptors such as O_2, causing poor growth. The nicotine growth phenotype of the Δ*cycN* strain was complemented by plasmid-based expression of *cycN* (**Figure 15b**), confirming that the growth deficiency is due to the loss of *cycN*. *In vivo* nicotine consumption experiments demonstrate that *cycN* is also necessary for NicA2's ability to degrade nicotine (**Figure 15c,d**). The NicA2 protein level is similar in WT and Δ*cycN* strains; however, while the WT strain consumed all the nicotine in the culture, the Δ*cycN* strain showed trivial nicotine consumption. This indicates that NicA2's activity is dramatically reduced in the absence of CycN, in agreement with CycN being NicA2's physiological electron acceptor. That nicotine is not degraded in Δ*cycN* strains makes it unlikely that any alternative oxidants make a physiologically significant contribution toward re-oxidation of NicA2 *in vivo*.

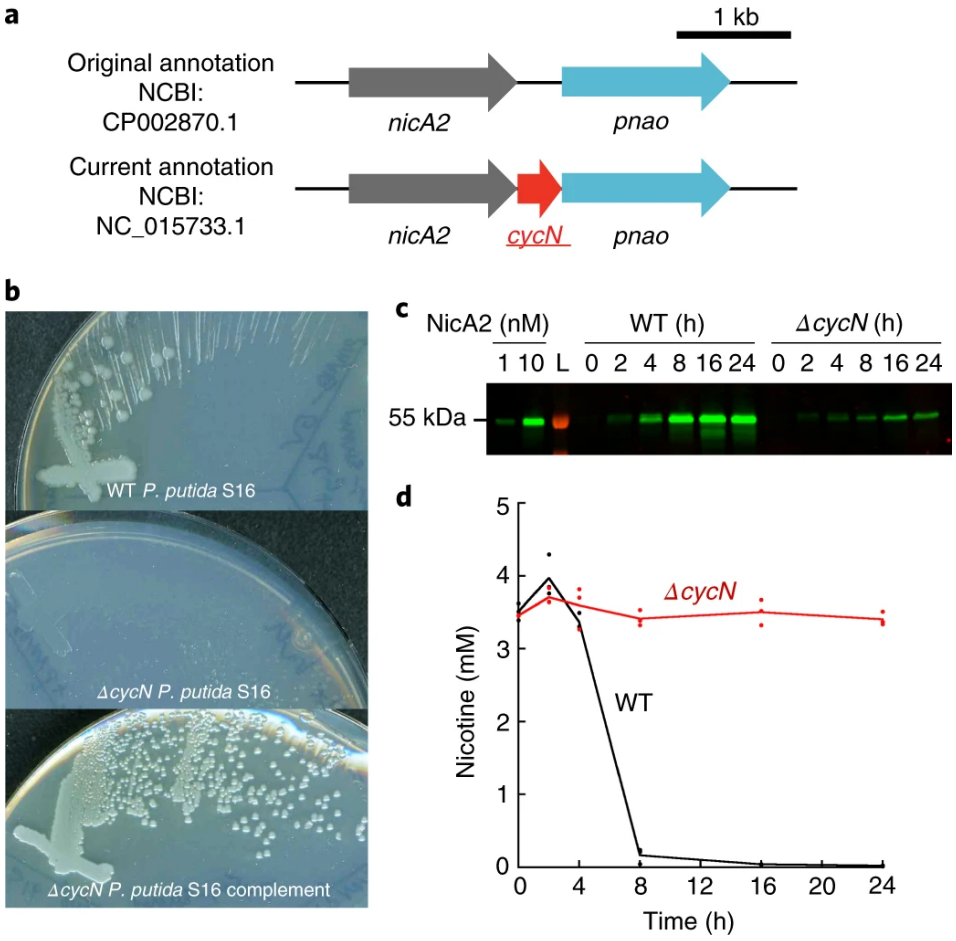

Figure 15. A cycN knockout is unable to grow on or degrade nicotine.

a, **Top,** The gene annotations when the genome of *P. putida* S16 was originally sequenced[33]. **Bottom**, The updated gene annotations currently available from NCBI show an uncharacterized cytochrome c gene WP_080563818.1 between nicA2 (PPS_RS28245) and pnao (PPS_RS21095), which we termed cycN (PPS_RS28240). **b**, Single colonies of *P. putida* S16 were streaked onto M9 salts agar supplemented with nicotine and imaged after two days of growth at 30 °C. The WT strain showed robust growth, whereas the ΔcycN strain grew poorly. Plasmid-based expression of cycN complemented the knockout. **c**, Quantitative western blots against NicA2 (green) in *P. putida* S16 lysates show expression of NicA2 as induced by nicotine in both the WT and ΔcycN strains over time. Purified NicA2 of known concentration was included as a loading control. **d**, Nicotine concentration as determined from cell culture by HPLC demonstrates decreasing concentration of nicotine over time in the WT strain, with no decrease in a ΔcycN strain. These experiments were independently repeated twice with similar results.

2.2.4 CycN is reduced by NicA2

Flavin-dependent dehydrogenases are known to transfer their electrons to a variety of small molecules and protein clients, including cytochrome c proteins[74,75]. To further probe the relationship between NicA2 and CycN, we recombinantly expressed and purified both

proteins from *Escherichia coli* to characterize their *in vitro* electron transfer activities. We used the spectral differences in the redox status for heme in cytochrome c[76] as a readout to determine if NicA2 can transfer electrons from nicotine to CycN. Upon incubation of oxidized CycN with excess nicotine and a catalytic amount of NicA2, a characteristic shift of the Soret-banding pattern occurred indicating that CycN had become reduced (**Figure 16**). This reduction in CycN required both nicotine and NicA2. NicA2 also produces H_2O_2 when aerobically degrading nicotine in the absence of CycN, but not when CycN is provided (**Figure 17a**).

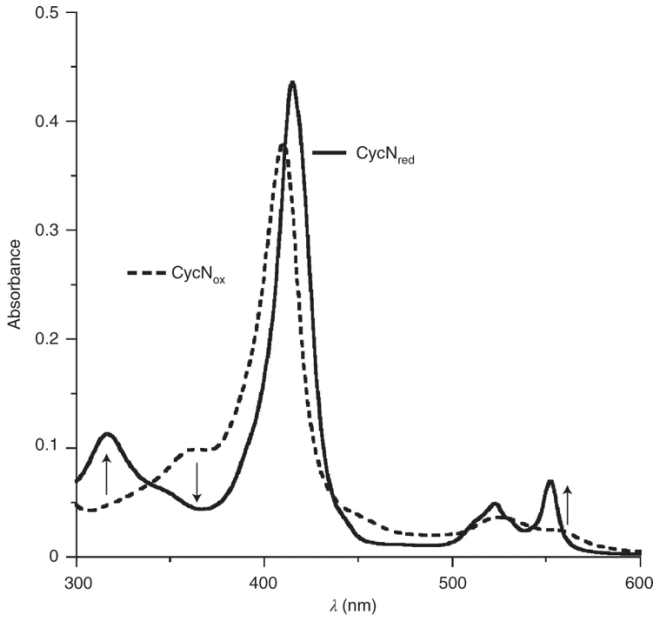

Figure 16. CycN is reduced by NicA2.

Oxidized CycN (dashed line) under ambient conditions was monitored by UV-VIS spectrophotometry. Upon addition of 30 nM NicA2 and 100 μM nicotine, 3.75 μM CycN showed an increase in absorbance typical for reduced cytochrome c at 410 and 550 nm (solid line), indicating that CycN had become reduced. Arrows indicate the directionality of change. Both NicA2 and nicotine are required to produce this change, as adding either one individually failed to reduce CycN. This experiment was independently repeated twice with similar results.

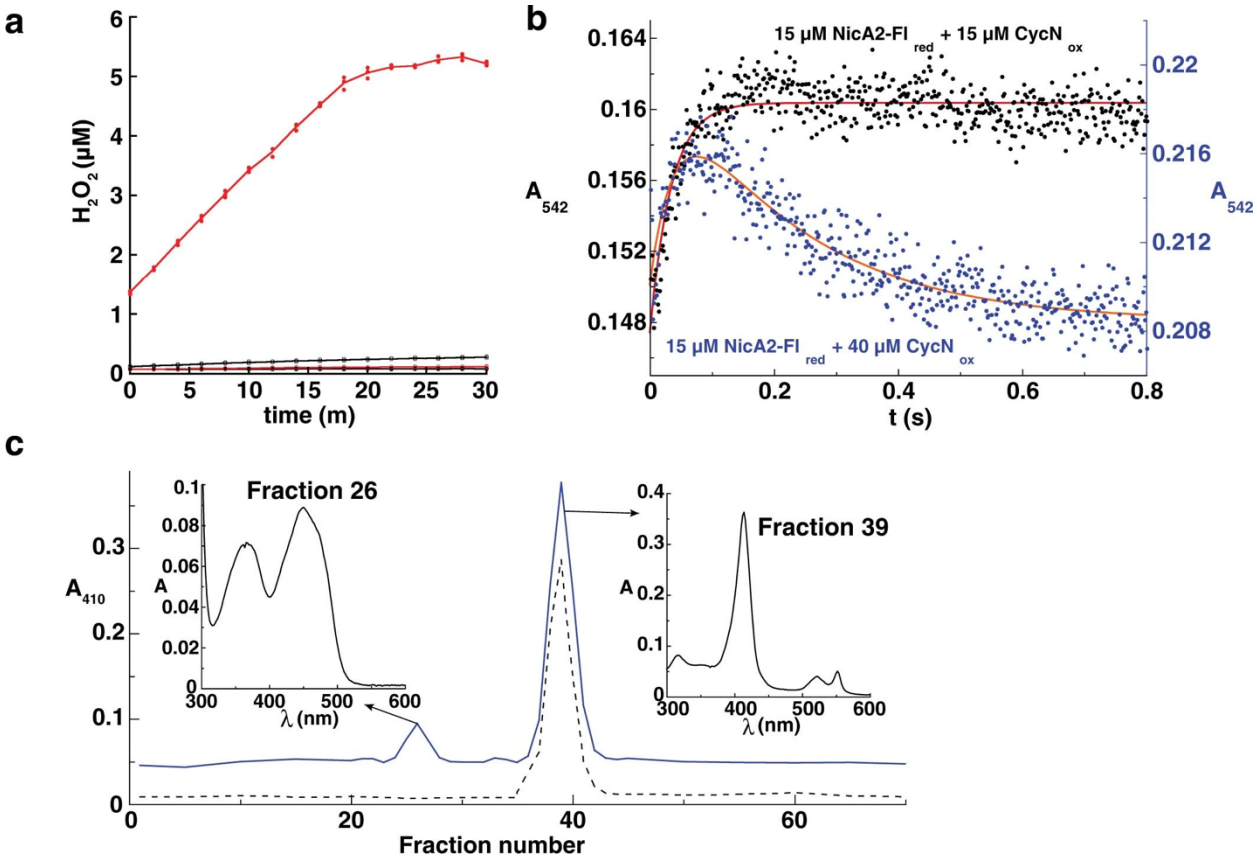

Figure 17. NicA2 and CycN's interaction.
a, Oxidized NicA2 was incubated with nicotine under aerobic conditions in the presence (black filled circles) and absence (red filled circles) of oxidized CycN, and the amount of H_2O_2 produced by the reaction was monitored using the Amplex Red assay. Also included were conditions of NicA2 without nicotine (black empty circles) and with CycN but without nicotine (red empty circles). Only in the condition where NicA2 was incubated with nicotine in the absence of CycN was a significant amount of H_2O_2 produced. Three independent replicates were obtained and plotted. **b**, Oxidized CycN and reduced NicA2 were combined in an anaerobic stopped-flow spectrophotometer and observed for change in absorbance at 542 nm. When mixed in equimolar amounts (black points), absorbance rose and was maintained at an increased value indicating transition to the flavin semiquinone state. When mixed with excess CycN (blue points), NicA2 first reaches the semiquinone state (observable as an increase in absorbance) before becoming fully oxidized (observable as a subsequent decrease in absorbance. **c,** 40 μM CycN alone (black dashed line) or 40 μM CycN with 200 μM NicA2 (blue line) were run over a HiLoad Superdex 75 pg size exclusion column. CycN in the presence of excess NicA2 eluted with the same retention time as CycN alone and was well-resolved from the NicA2 peak. The insets show the absorbance spectrum of the two peaks in the chromatogram. Fractions 26 and 39 have spectra consistent with clean NicA2 and CycN, respectively, indicating that the two proteins do not bind with high affinity.

2.2.5 NicA2-Fl$_{red}$ is rapidly re-oxidized by CycN

To measure the rate at which electrons are transferred from NicA2-Fl$_{red}$ to oxidized CycN (CycN$_{ox}$) *in vitro*, we performed stopped-flow absorbance experiments by anaerobically

mixing 15 μM NicA2-Fl_{red} with an excess of $CycN_{ox}$. Electron transfer between NicA2-Fl_{red} and $CycN_{ox}$ was complete in less than 1 second. The absorbance changes were dominated by signals associated with reduction of $CycN_{ox}$'s heme from the Fe^{3+} to the Fe^{2+} state ($CycN_{red}$) (**Figure 18a**).

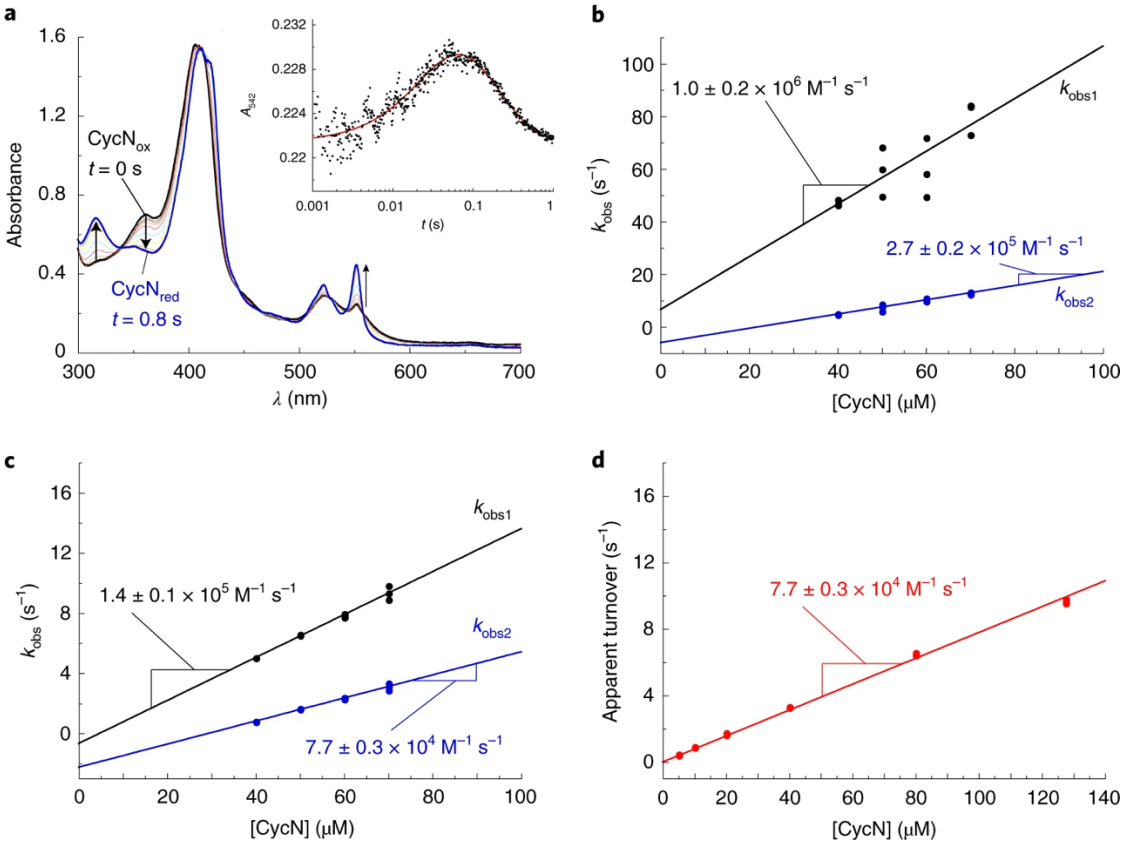

Figure 18. NicA2 is rapidly oxidized by CycN.

a, Oxidized CycN and reduced NicA2 were mixed in a series of anaerobic stopped-flow spectrophotometer experiments. Upon mixing, the absorbance changes were dominated by CycN reduction. Inset: The signal was monitored at 542 nm (an isosbestic point for CycN reduction/oxidation) in order to observe spectral changes only associated with NicA2 FAD absorbance. Note the logarithmic timescale. Traces at this wavelength fit well to two exponentials. See **Figure 21a** for kinetic traces at all CycN concentrations. **b**, k_{obs} values determined for the first phase were plotted against the concentration of CycN in each experiment, demonstrating linear dependence. The y-intercept was 6 ± 12 s^{-1}. The k_{obs} values for the second phase were also linearly dependent with CycN concentration. The negative y-intercept for k_{obs2} (–5.9±1.0 s^{-1}) is likely a result of the CycN concentration for the second phase being lower than the initial CycN concentration since roughly one NicA2 equivalent worth of CycN is consumed in the first phase. **c,** the k_{obs} values obtained for the reaction of oxidized CycN with N-methylmyosmine-bound NicA2 containing reduced FAD. The k_{obs} values for both phases increased linearly with CycN concentration. The y-intercept for k_{obs1} and k_{obs2} was –0.6 ± 0.3 s^{-1} and –2.2 ± 0.2 s^{-1}, respectively. The large negative y-intercept for k_{obs2} was again likely due to the consumption of some CycN in the first phase. **d,** The apparent steady state turnover number for NicA2 using saturating nicotine (1 mM) and varying amounts of CycN. When fit by a line, the slope of the steady state data matched that of the second NicA2-CycN oxidation event for N-methylmyosmine-bound NicA2. Values reported are the mean ± s.e.m. of the fit for all panels. These experiments were independently repeated twice with similar results.

We analyzed the kinetics of the reaction at 542 nm because: (1) the absorbance of $CycN_{ox}$ and $CycN_{red}$ is identical at 542 nm so this readout is unaffected by changes in CycN's oxidation state (**Figure 19**), and (2) NicA2's flavin semiquinone (NicA2-Fl_{SQ}) absorbs at this wavelength, unlike NicA2-Fl_{ox} and NicA2-Fl_{red} (**Figure 11c**). This wavelength therefore allowed us to monitor the expected transient formation of NicA2-Fl_{SQ}, since $CycN_{ox}$ is an obligate one-electron acceptor and two $CycN_{ox}$ molecules must react sequentially with NicA2-Fl_{red} in order to fully oxidize it back into NicA2-Fl_{ox}. Kinetic traces of the reaction with more than a two-fold molar excess of $CycN_{ox}$ indeed showed an increase, followed by a decrease in absorbance at 542 nm (**Figure 18a inset**), in agreement with the formation of NicA2-Fl_{SQ} followed by its conversion to NicA2-Fl_{ox}.

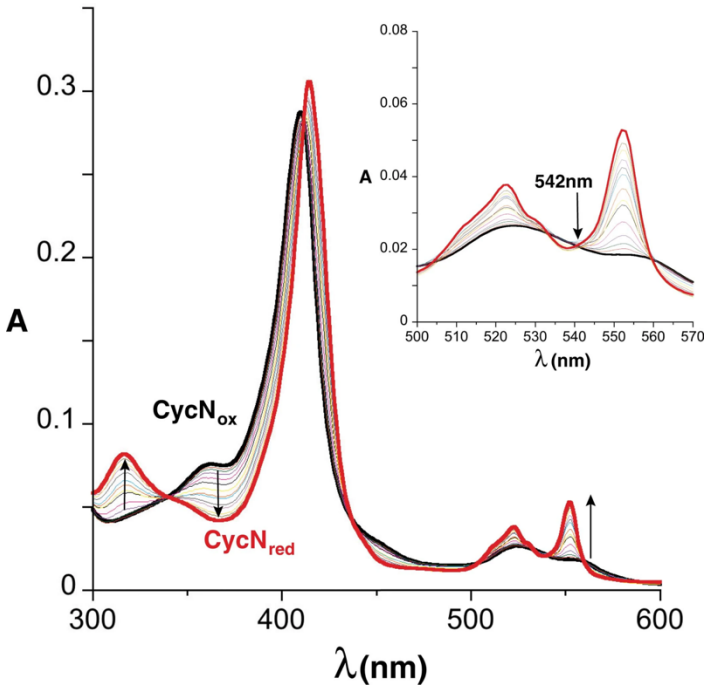

Figure 19. Reduction of CycN by dithionite.
UV-VIS spectra were recorded as sodium dithionite was serially titrated into a solution of oxidized CycN until it became fully reduced. Arrows represent the directionality of change during the titration. Inset: zooming in on just a small section of this titration, an isosbestic point is visible at 542 nm marked with an arrow. This wavelength was used to monitor the changes in absorbance for NicA2's FAD in the experiments in **Figure 18**.

We further tested that the signal changes at 542 nm report on NicA2-Fl_{SQ} by mixing NicA2-Fl_{red} with an equimolar amount of $CycN_{ox}$. Here we should only observe the increase at 542 nm, as there only enough $CycN_{ox}$ to react once on average with NicA2-Fl_{red} given that the first phase is faster than the second. Reaction of 15 μM NicA2-Fl_{red} with 15 μM $CycN_{ox}$ showed only an increase in absorbance at 542 nm without any subsequent decrease, confirming we are observing formation of the NicA2-Fl_{SQ} at this wavelength (**Figure 17b**).

Stopped-flow traces at 542nm using an excess of $CycN_{ox}$ could be fit using a double exponential function. k_{obs} for both phases increased linearly with the $CycN_{ox}$ concentration, indicating that they both report on the bimolecular association of NicA2 with $CycN_{ox}$ (NicA2-Fl_{red} and NicA2-Fl_{SQ} in the first and second phase, respectively). Linear fitting of the k_{obs} plots yielded bimolecular rate constants (k_{on}) of $1.0 \pm 0.2 \times 10^6$ $M^{-1}s^{-1}$ and $2.7 \pm 0.2 \times 10^5$ $M^{-1}s^{-1}$ for the first and second phase, respectively (**Figure 18b**). Strikingly, these values are ~4-5 orders of magnitude greater than that for the oxidation of NicA2-Fl_{red} by O_2 (which is 27 $M^{-1}s^{-1}$). The fact that both phases are bimolecular indicates that electron transfer between $CycN_{ox}$ and NicA2-$Fl_{red/SQ}$ is rate-limited by association between the two proteins; electron transfer between the two redox centers must therefore be extremely rapid after the complex has formed, and $CycN_{red}$ produced by the first electron transfer must dissociate from NicA2-Fl_{SQ} faster than the second $CycN_{ox}$ binds (**Figure 20**).

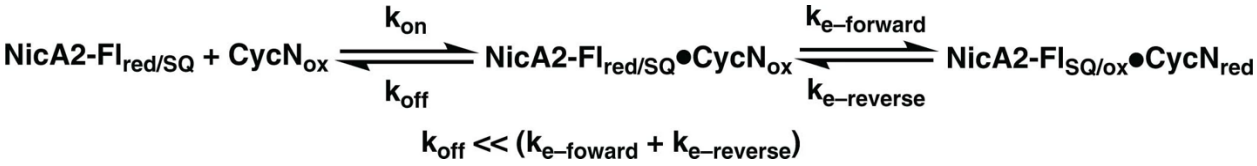

Figure 20. Kinetic model for NicA2 oxidation by CycN.
In a two-step mechanism where rate-limiting $CycN_{ox}$ binding to NicA2-Fl_{red} is followed by rapid electron transfer between the two redox centers, k_{obs} should be linearly dependent on [$CycN_{ox}$] at low $CycN_{ox}$ concentrations and should saturate at the sum of the rate constants for electron transfer ($k_{e-forward}$ + $k_{e-reverse}$) at high $CycN_{ox}$ concentrations[77]. Our data indicate that we have used $CycN_{ox}$ concentrations at the low end of this concentration regime, where k_{obs} increases linearly with $CycN_{ox}$ concentration with a slope equal to k_{on} for $CycN_{ox}$ binding to NicA2-Fl_{red}. We presume that k_{obs} would eventually reach a saturating value at high $CycN_{ox}$ concentrations; however, we are not able to produce enough $CycN_{ox}$ to explore the mM concentrations of $CycN_{ox}$ that would be needed to achieve saturation. Notably, the rate constant for $CycN_{ox}$ dissociation from NicA2-Fl_{red} (k_{off}) should not contribute to the y-intercept of the k_{obs} plot for the mechanism shown in this figure[53]. The k_{obs} for the second phase also increased linearly with $CycN_{ox}$ concentration, indicating that the above logic also applies for the reaction of the second $CycN_{ox}$ with NicA2-Fl_{SQ}. This finding also indicates that $CycN_{red}$ resulting from the first one-electron transfer must dissociate from NicA2-Fl_{SQ} fast enough such that the second one-electron transfer event is also rate-limited by $CycN_{ox}$ binding. In the kinetic scheme, the labels NicA2-$Fl_{red/SQ}$ and NicA2-$Fl_{SQ/ox}$ indicate that NicA2-Flred conversion to NicA2-Fl_{SQ} and NicA2-Fl_{SQ} conversion to NicA2-Fl_{ox} are observed in the first and second phases, respectively.

CycN does not form a stable complex with NicA2, in agreement with a large dissociation rate constant for the interaction (**Figure 17c**). Reaction traces at 552nm, where the signal for $CycN_{red}$ formation dominates, also fit to two phases with k_{obs} values similar to those obtained using the 542nm data (**Figure 21b**), confirming that reduction of two $CycN_{ox}$ molecules accompanies the two one-electron oxidations of NicA2's flavin in the reaction.

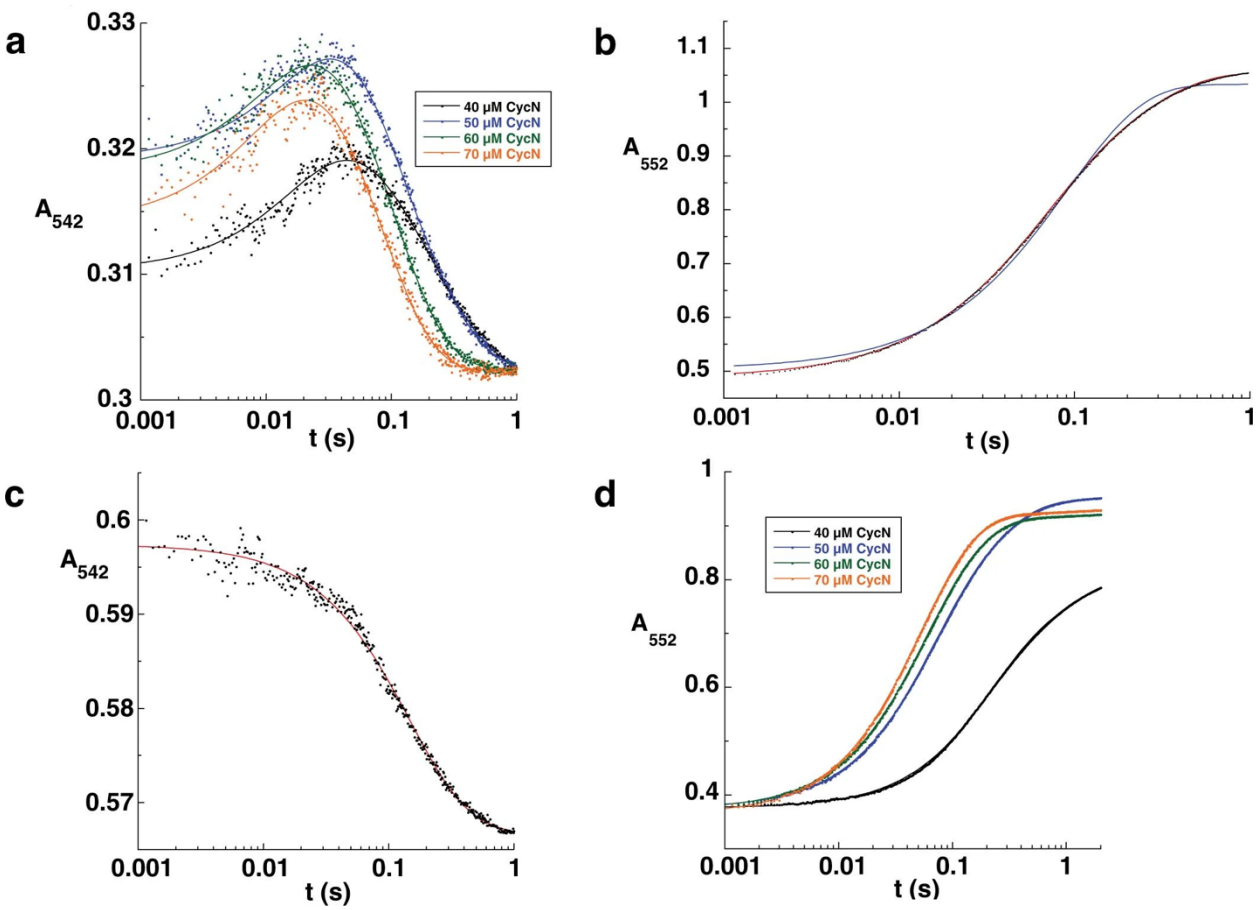

Figure 21. CycN stopped-flow data.
a, Absorbance traces for the stopped flow reaction between ligand-free NicA2-Fl_{red} with variable concentrations of $CycN_{ox}$. In this case, the traces were able to capture formation and depletion of NicA2-Fl_{SQ} that occurred as the reaction proceeded. CycN contributes a substantial amount of absorbance at 542 nm. Accordingly, the traces were adjusted so that they all end at the same absorbance value to facilitate comparison. Note the logarithmic timescale. **b**, Signal change for the stopped-flow reaction was also monitored at 552 nm, a wavelength suitable for observing reduction of CycN. The trace required two exponentials (red curve) with similar amplitudes to fit properly, as one exponential (blue curve) was insufficient. Signal change occurred at the same time as NicA2 oxidation monitored at 542 nm, indicating that the processes occurred simultaneously. Note the logarithmic timescale. **c,** Signal change at 542 nm for the reaction of NMM-NicA2-Fl_{red} with $CycN_{ox}$. Curiously, traces at 542 nm, where NicA2-Fl_{SQ} is detectable, did not show the increase in absorbance that we observed with ligand-free NicA2-Fl_{red}; traces at this wavelength showed a decrease in absorbance that occurred in two phases, with the first phase contributing 80-90% of the total absorbance. This observation suggests that N-methylmyosmine in the active site inhibits NicA2's FAD from populating a semiquinone state during the reaction with CycN. The decrease in absorbance at 542 nm may simply be due the small decrease in charge-transfer absorbance of N-methylmyosmine bound NicA2 that occurs when the flavin gets oxidized (**Figure 14b**). Reaction traces at 552 nm still showed the two kinetic phases with increasing absorbance (**Figure 21b**). Note the logarithmic timescale. **d,** Absorbance traces at 552 nm for the stopped flow reaction between NMM-NicA2-Fl_{red} and variable concentrations of $CycN_{ox}$. Traces fit best to two exponentials and the k_{obs} values are reported in **Figure 18c** of the main text. The traces were adjusted so that they all begin at the same absorbance value for comparison. Note the logarithmic timescale.

We also monitored the kinetics of electron transfer between nicotine-reduced NicA2 and $CycN_{ox}$ to see if the presence of N-methylmyosmine impacts electron transfer between the two proteins. Reaction traces again showed two kinetic phases, consistent with two stepwise one-electron transfers to two $CycN_{ox}$ molecules required to fully oxidize N-methylmyosmine bound NicA2-Fl_{red} (**Figure 21c,d**). The k_{obs} for both phases increased linearly with $CycN_{ox}$ concentration, indicating that each phase still reports on the two different bimolecular association steps. Linear fitting of the two data sets yielded bimolecular rate constants of $1.4 \pm 0.1 \times 10^5$ $M^{-1}s^{-1}$ and $7.7 \pm 0.3 \times 10^4$ $M^{-1}s^{-1}$ for the first and second phase, respectively (**Figure 18c**). Importantly, both of these values are more than 10,000-fold larger than the k_{ox}^{O2} of 5 $M^{-1}s^{-1}$ for oxidation of N-methylmyosmine-bound NicA2-Fl_{red} by O_2, indicating that CycN is a much more effective oxidant for NicA2-Fl_{red} than O_2 when N-methylmyosmine is bound.

2.2.6 Electron transfer to CycN limits turnover by NicA2

We next used steady state kinetic experiments of the NicA2-catalyzed electron transfer from nicotine to CycN to identify the rate-determining kinetic event. The reaction rate using saturating concentrations of nicotine increased linearly with CycN concentration over the accessible range of CycN concentrations (5 – 128 μM CycN). Presumably the reaction rate would saturate at higher [CycN]. Converting the rate data to apparent turnover numbers revealed that the apparent turnover number data was nearly identical to that of the second $CycN_{ox}$ binding event for N-methylmyosmine-bound NicA2-Fl_{red} (**Figure 18d**). This observation suggests that N-methylmyosmine remains bound to NicA2-Fl_{red} during electron transfer to $CycN_{ox}$ and that binding of $CycN_{ox}$ to NicA2-Fl_{SQ} is rate-determining at CycN concentrations ≤128 μM. This also suggests that the third phase

in the reductive half-reaction with nicotine is not catalytically relevant since our measured apparent turnover numbers are larger than the k_{obs} of ~6.6 s^{-1} for that step.

2.2.7 NicA2-Fl$_{red}$ reacts poorly with bovine cytochrome c

Is reactivity with NicA2 specific to CycN or will any cytochrome c work? Bovine cytochrome c (43% sequence identity to CycN), which is commonly used in the study of the electron transport chain, was tested as an electron acceptor for NicA2. It was not efficiently reduced, suggesting that NicA2 is specific for CycN (**Figure 22a**). Structural models of CycN reveal that the surface of bovine cytochrome c is enriched in positive charge relative to CycN, especially in the region near exposed heme **(Figure 22b**). Positively charged lysines are important for bovine cytochrome c binding to cytochrome oxidase[78], so this difference in charge distribution between CycN and bovine cytochrome c may be partially responsible for their specificities.

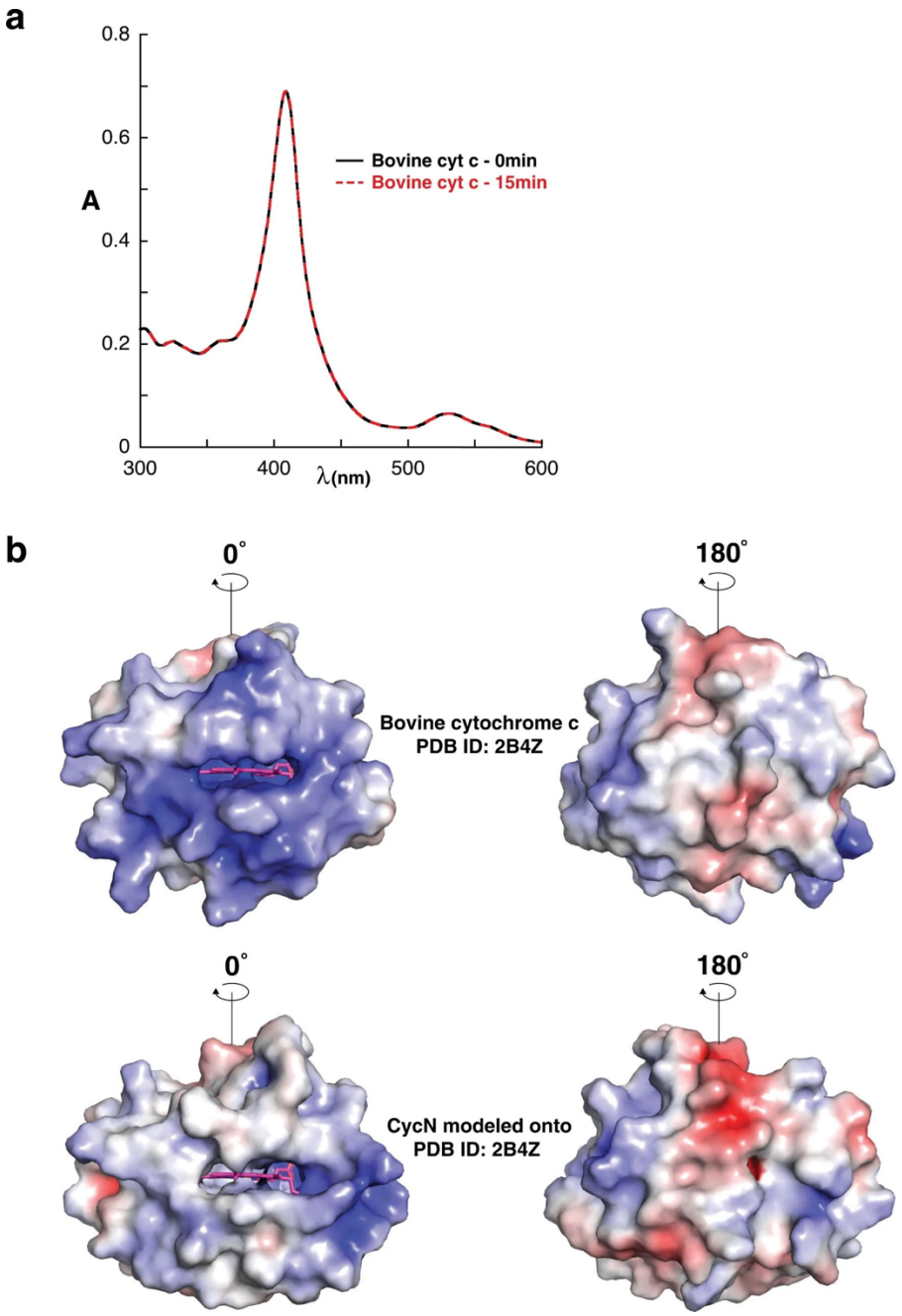

Figure 22. Bovine cytochrome c is not reduced by NicA2 and has different surface charge distribution than CycN.

a, Bovine cytochrome c combined with nicotine and NicA2 did not result in any reduction of the cytochrome c over 15 min of incubation, unlike the assay performed with CycN (**Figure 16**). **b,** CycN was modeled onto the structure of bovine cytochrome c (PDB ID: 2B4Z) using the SWISS-MODEL online server[79]. Surface charge distribution of CycN and bovine cytochrome c was calculated using the APBS electrostatics plugin for PyMOL[80]. Bovine cytochrome c (top) is enriched for positive charge in the region where the heme is surface-exposed, whereas CycN (bottom) is closer to neutral/hydrophobic. Red color indicates negative charge density; blue color indicates positive charge density; heme cofactor is colored in magenta for both structures.

2.3 Discussion

We have demonstrated that a novel cytochrome c, CycN, is the physiological oxidant for NicA2, not O_2. NicA2 is therefore a dehydrogenase, making it a notable outlier within the flavin-containing amine oxidase superfamily. We found that biphasic hydride transfer between nicotine and NicA2-Fl_{ox} in the reductive half-reaction occurs rapidly. This is followed by a slower kinetic event that may correspond to dissociation of N-methylmyosmine. However, this slow step is unlikely to be relevant during turnover since our data suggest that N-methylmyosmine remains bound when NicA2 reacts with CycN. Re-oxidation of NicA2-Fl_{red} by CycN must occur in a sequence of two one-electron transfer reactions since each molecule of CycN can only receive one electron. Based on our data, both of these one-electron transfers appear to be rate-limited by the interaction between NicA2 and CycN; the subsequent electron transfer must be significantly faster than binding. These points are summarized in **Figure 23**. Oxidation of NicA2-Fl_{red} by O_2 is unlikely to contribute significantly to nicotine turnover *in vivo* since O_2 oxidizes NicA2-Fl_{red} with a rate constant ~10,000–15,000 times lower than its oxidation by CycN.

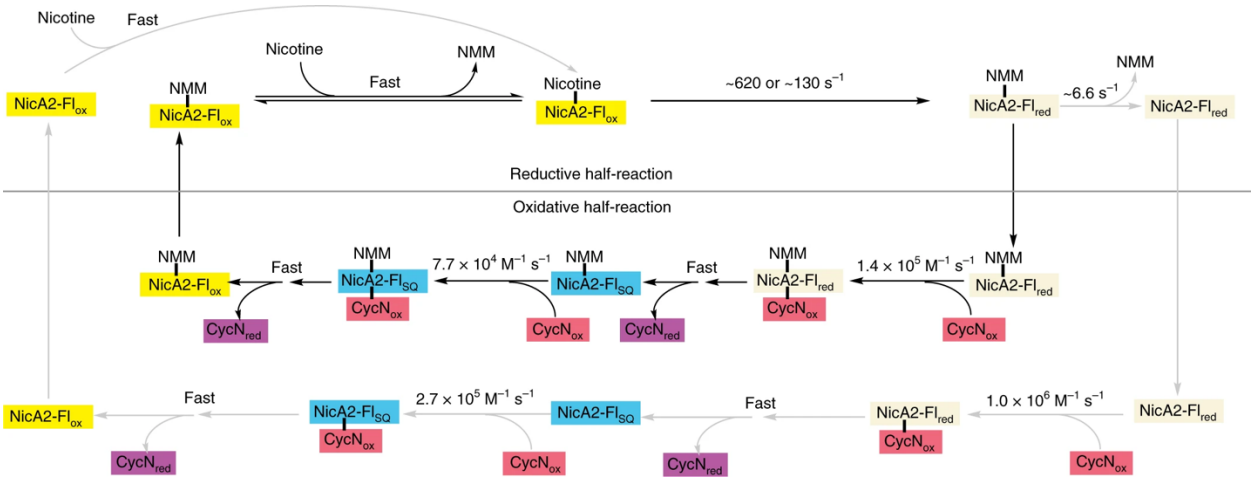

Figure 23. Proposed kinetic mechanism for the catalytic cycle of NicA2.

NMM, N-methylmyosmine, the product resulting from the NicA2-catalyzed oxidation of nicotine; NicA2-Fl$_{ox}$, NicA2 containing oxidized FAD; NicA2-Fl$_{red}$, NicA2 containing $FADH_2$; NicA2-Fl$_{SQ}$, NicA2 containing a flavin semiquinone. Only the black path is relevant during catalytic turnover by the enzyme.

Our discovery that NicA2 is a dehydrogenase that uses CycN as an electron acceptor raises many interesting questions about how NicA2 discriminates between CycN and O_2. NicA2 appears to be specific for CycN since bovine cytochrome c is a poor recipient of electrons from NicA2, suggesting that CycN contains structural features that optimize its reactivity or are important for NicA2 binding. Structures show that the isoalloxazine of NicA2's FAD is buried within the protein core, >10 Å away from the surface. Can one-electron transfers between NicA2's isoalloxazine and CycN's heme span this distance, or are major conformational changes or protein-derived wires required for electron transfer between these redox centers? NicA2's poor reactivity with O_2 is difficult to rationalize based on structures, as NicA2's FAD binding site is very similar to that in a homologous protein that reacts rapidly with O_2, namely 6-hydroxy-L-nicotine oxidase[37,81,82]. Two recent studies attempted to screen NicA2 variants with residue mutations near the isoalloxazine or the presumed product exit site for improved O_2-dependent nicotine-degrading activity[6,83]. However, NicA2 variants with only modest improvements were identified,

suggesting that O_2 reactivity in NicA2 is not controlled by structural features near the isoalloxazine. How reactivity with O_2 is suppressed in NicA2 is thus currently unclear.

Microorganisms sometimes find ways to obtain energy and nutrients from surprising sources. For *P. putida* S16, CycN provides an illustration of one such adaptation. Rather than transferring electrons from nicotine directly to O_2, which would waste valuable reducing equivalents and create H_2O_2, electrons are shuttled from NicA2 to CycN. Cytochrome c proteins are not known to be terminal electron acceptors. Thus, the electrons obtained by CycN from nicotine oxidation must be passed to another electron acceptor to enable continued turnover by NicA2. Where these electrons are transferred, and their eventual fate, is unknown. Other *Pseudomonas* subspecies conduct aerobic respiration using cytochrome c oxidases such as the cbb3 cytochrome oxidase of *Pseudomonas aeruginosa*[84,85]. Since *P. putida* S16 seems to contain similar machinery (**Figure 24**), this may provide an avenue for CycN re-oxidation. Regardless of the pathway electrons take from CycN, clearly CycN is required for robust growth of the organism on nicotine.

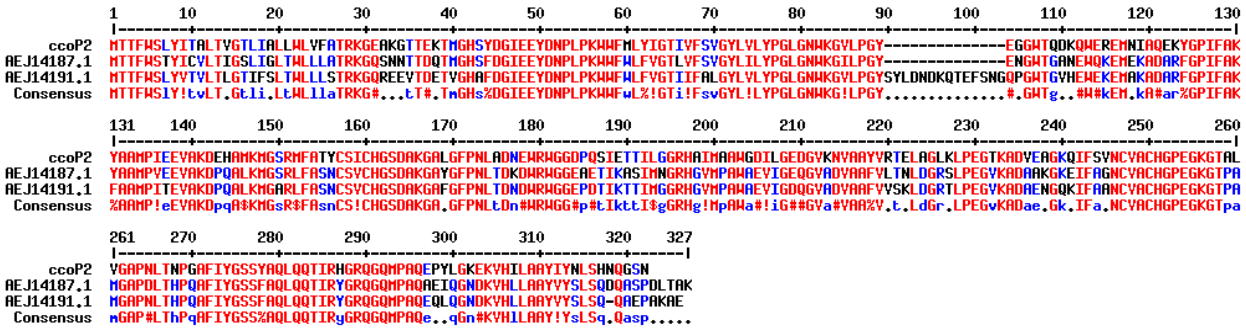

Figure 24. *P. putida* S16 contains terminal oxidases similar to those in other *Pseudomonas* subspecies.

The protein sequence for ccoP2, a cbb3 cytochrome c oxidase subunit from *P. aeruginosa* PAO1, was used for a NCBI BLAST homology search against the genome of *P. putida* S16, resulting in two highly significant hits (e values of 7e-168, 4e-163) also annotated as cytochrome c oxidase subunits. These proteins had 67% and 64% sequence identity, respectively. The sequence alignment image was generated using MultAlin software version 5.4.1[86].

Several recent studies have demonstrated NicA2's potential utility as treatment for nicotine dependence[5,7]. One significant caveat to these studies is the prohibitively large protein amounts required to achieve effective treatment—at least 10 and up to 70 mg kg^{-1} daily[5], considerably more than is feasible for humans. Accordingly, there is interest in generating NicA2 variants with increased nicotine turnover rates. One avenue for enhancing therapeutic nicotine turnover suggested by our work is to co-administer CycN alongside NicA2. Another option would be to engineer NicA2 to enhance its oxidase activity. This may be possible given that NicA2 belongs to a family where most members react rapidly with O_2. Using site-saturation mutagenesis of NicA2's active site, Thisted et al[6] identified several mutations that allowed for an up to 19-fold increased turnover rate of nicotine with O_2. These are relatively modest increases given that NicA2 can re-oxidize at >10,000 times the rate of re-oxidation with O_2 when provided its physiologic electron acceptor, implying that activity with O_2 could perhaps be further improved.

Applying the lessons learned from NicA2 more generally, members of the flavin-dependent amine oxidase family are assumed to undergo oxidation by O_2 *in vivo* and typically readily re-oxidize with O_2 *in vitro*[11]. That NicA2 transfers electrons to a c-type cytochrome prompts reconsideration of this generalization and raises the possibility that other members of this family use alternative physiologic oxidants. When amine oxidases use O_2 as an oxidant, reactive oxygen species such as H_2O_2 are released as a byproduct[16]. It may therefore be more desirable to shunt electrons elsewhere *in vivo*, as we have shown occurs with NicA2 in *P. putida* S16. Furthermore, just because an amine oxidase *can* rapidly be oxidized by O_2 *in vitro* does not necessarily mean that it uses O_2 as its electron acceptor *in vivo*. There is circumstantial evidence for the existence of one such example in human monoamine oxidases (MAOs) A and B[87]. These enzymes are bound to the outer mitochondrial membrane by a transmembrane tail anchor[88–90]. In their presumed catalytic cycle, MAOs are thought to be re-oxidized by O_2, producing potentially damaging H_2O_2[91]. Recent work, however, has demonstrated that human MAOs are not creating H_2O_2 as previously thought, and instead seem to transfer electrons from amine oxidation to complex IV of the electron transport chain[87]. Given that cytochrome c exists in the mitochondrial intermembrane space, we propose that cytochrome c may be the link facilitating electron transfer to the electron transport chain from MAOs. A re-evaluation of the mechanistic paradigm of these enzymes is indicated. MAOs are frequent targets for *in vitro* drug studies, and it may be that they are deprived of vital redox cofactors in these studies. Given the role of MAOs in neuropsychiatric disease, this topic warrants further consideration.

In summary, we have demonstrated that NicA2 is a flavin-dependent dehydrogenase that uses CycN as its redox partner. In the continued study of flavoenzymes, the “oxidase” paradigm for flavin-dependent amine oxidases should be reconsidered, as structural similarity alone clearly cannot determine oxygen reactivity.

2.4 Methods

Strains and culture conditions

P. putida S16 was obtained from American Type Culture Collection (ATCC® BAA-2546™). Culture was performed in lysogeny broth (LB) media unless otherwise specified. M9 salts with nicotine media was made with the following: 6 g L^{-1} Na_2HPO_4, 3 g L^{-1} KH_2PO_4, 1 mM $MgSO_4$, 0.1 mM $CaCl_2$, 1 μg mL^{-1}; thiamine, 1 g L^{-1} nicotine. M9 salts with nicotine agar was made with the same recipe, with an additional 15 g L^{-1} bacto agar (Thermo Fisher Scientific). All liquid cultures were inoculated from single colonies streaked out onto selective media. *E. coli* BL21 (DE3) cells were used for protein expression. Protein expression media (PEM) contains 12 g L^{-1} tryptone, 24 g L^{-1} yeast extract, 50.4 g L^{-1} glycerol, 2.13 g L^{-1} K_2HPO_4, and 12.54 g L^{-1} KH_2PO_4.

Construction of vectors

Standard cloning techniques were used. pEC86 helper vector was obtained from the Culture Collection of Switzerland. pJN105 vector was obtained as a gift from Ute Römling (Karolinska Institute). Genes codon optimized for expression in *E. coli* were purchased from Genscript for *cycN* and *nicA2* and cloned via restriction digest into pET28a, pJN105, or pET22b vectors. The *nicA2* gene, including its N-terminal signal sequence, was cloned into pET28a containing an N-terminal His-SUMO tag. For the complementation

experiments, full-length *cycN*, including its native signal sequence, was cloned into pJN105. For protein expression and purification, the sequence for mature *cycN* lacking its signal sequence was cloned downstream of the *pelB* leader sequence in pET22b.

Estimating NicA2 turnover rate *in vivo*

When grown on nicotine as its sole carbon and nitrogen source, *P. putida* S16 obtains nearly all of its biomass from this metabolite. Using the known values for doubling time, bacterial mass, and the amount of nicotine that must be turned over to sustain growth, we can estimate the minimal nicotine turnover rate for NicA2. A single bacterium's carbon and nitrogen content has a mass of ~0.3 pg, *P. putida* S16 doubles in roughly 90 min when grown on nicotine[23], and nicotine has a molecular weight of 162 g mol^{-1}. Therefore, each bacterium must turn over 2 x 10^{-15} mol of nicotine to double its mass. Assuming that NicA2 accounts for no more than 5% of total cell mass, there can be no more than 2.8 x 10^{-19} mol of NicA2 expressed for a single cell. We thus estimate the NicA2 *in vivo* turnover rate as 2 x 10^{-15} mol nicotine degraded by 2.8 x 10^{-19} mol NicA2 in 90 min, resulting in a turnover rate of ~1.3 s^{-1}.

NicA2 expression and purification

The pET28a-based expression vector for NicA2 was transformed into *E. coli* BL21 (DE3) cells and grown in 4 L PEM at 37 °C with shaking to an OD600 of 1.0. The temperature was then lowered to 20 °C and expression induced with 100 μM IPTG. The culture was grown overnight at 20 °C. After harvesting, the cells were lysed at 4 °C by sonication in 50 mM Tris HCl, 400 mM NaCl, 15 mM imidazole, 10% glycerol, pH 8.0 (lysis buffer) with DNase I and cOmplete™ protease inhibitor cocktail. The lysate was cleared by centrifugation and the supernatant was loaded on three 5 mL HisTrap columns pre-

equilibrated in lysis buffer. The columns were washed with 20 mL lysis buffer, then 20 mL lysis buffer + 20 mM imidazole, and NicA2 was then eluted in lysis buffer + 0.5 M imidazole. NicA2 was then exchanged into 40 mM Tris-HCl, pH 8 + 0.2 M NaCl in the presence of protease ULP1 to cleave off the His-SUMO tag and subsequently passed over the HisTrap column again in 25 mM Tris HCl, pH 8 + 0.2 M NaCl to remove the His-SUMO tag. Protein was then exchanged into 25 mM Tris pH 8.5 and loaded onto three 5 mL HiTrap Q columns equilibrated into the same buffer. NicA2 was eluted by linear salt gradient using 25 mM Tris pH 8.5 + 1 M NaCl. Fractions containing NicA2 were concentrated, then run over a HiLoad Superdex 200 column in 40 mM HEPES 100 mM NaCl pH 7.4. Purified protein was concentrated and flash frozen, then stored at -80 ºC until use (**Figure 25**).

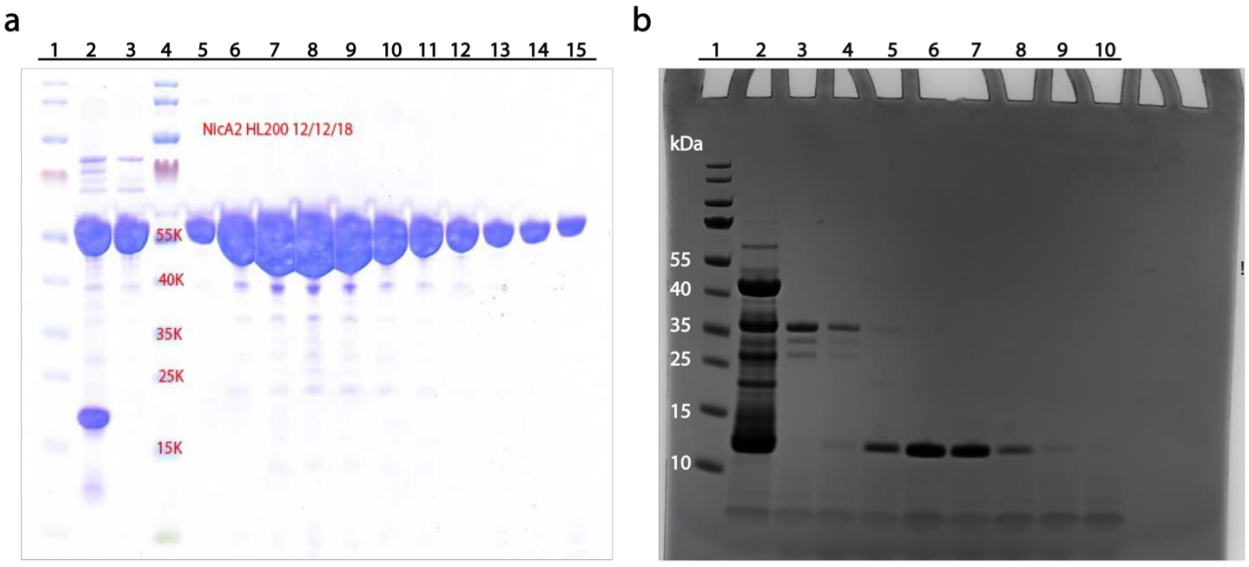

Figure 25. Purity of NicA2 and CycN.

a, NicA2 as collected from size exclusion, fractions corresponding to lanes 5-15 were collected for in vitro experiments. **b,** CycN as collected from size exclusion, fractions corresponding to lanes 6-8 were collected for in vitro experiments. Both gels are representative for all NicA2 and CycN purified for use in this study.

CycN expression and purification

The methods in enzymology subsection describing expression and purification of cytochrome c protiens was followed[92]. Antibiotic selection was maintained with chloramphenicol 17 μg mL^{-1} and ampicillin 100 μg mL^{-1} throughout. All incubations were performed at 30 °C. *E. coli* BL21 (DE3) cells were transformed with both pEC86 helper vector and pET22b-*cycN* for periplasmic expression. A single colony of the resulting transformation was inoculated into overnight culture, then subcultured into 3L PEM and incubated at 200 rpm. Cultures were grown to a density of OD 0.6–0.8, then induced with 10 μM IPTG. Cells were left to express overnight for 18–22 h. Red pellets were visible after spinning down at 4,000*g* for 20 min.

Pellets were immediately resuspended for periplasmic extraction by osmotic shock in ice-cold osmotic shock buffer (0.5 M sucrose, 0.2 M Tris HCl, pH 8.0, and 0.5 mM EDTA), 50 mL buffer per L of culture. 33 mL ice-cold water was added after resuspension, and the resulting mixture was incubated on ice with gentle shaking for 2 h. Suspensions were spun down at 12,000*g* for 20 min, and the red supernatant saved. These supernatants were dialyzed against 4 L of pH 4.0 30 mM sodium citrate + 38 mM Na_2HPO_4 overnight, then dialyzed into an additional 4 L of 25 mM NaH_2PO_4 at pH 4.0. The next day, samples were loaded onto a HiTrap SP HP cation exchange column (GE Life Sciences) equilibrated in the same buffer, and eluted against 25 mM NaH_2PO_4, pH 4.0 + 1 M NaCl in a salt gradient. Final cleanup was performed by running over a HiLoad Superdex 75 size exclusion column equilibrated in 40 mM HEPES 100 mM NaCl pH 7.4. Purified protein was flash frozen and stored at -80 ºC until use.

Generation of *cycN* knockout

A *cycN* knockout was generated by two-step allelic exchange according to the protocol established by Hmelo et al.[73]. Briefly, PCR of *P. putida* S16 genomic DNA was used to amplify regions upstream and downstream of *cycN* using the listed primers (**Table 2**). CycN_del_down primers created a DNA fragment containing the stop codon, the last few amino acids for CycN, and ~500 bp of downstream sequence. CycN_del_up primers created a fragment with ~500 bp of upstream sequence, including the start codon and first few amino acids for CycN. An additional PCR reaction using the set of both products and the primers CycN_del_up_Fwd and CycN_del_down_Rev was used to assemble the fragments together, creating a substrate for homologous recombination against the *P. putida* S16 genome. This was cloned into pEX18-Gm vector by restriction digest. Upon recombining, the *P. putida* S16 homologous fragment will insert next to the *cycN* gene along with the pEX18-Gm sequence containing a gentamycin marker and *sacB* marker for sucrose counterselection. pEX18-Gm cannot replicate in *P. putida* S16, and gentamycin resistance can only be passed on in this strain by genomic integration. Therefore, by first selecting for gentamycin resistance, we generate clones with the integrated genomic marker. Then, counterselecting by plating onto sucrose afterward, we select for clones that undergo a secondary recombination event, removing remaining pEX18-Gm sequence with *sacB* and the majority of *cycN* coding sequence, resulting in a scarless knockout.

pEX18-Gm was electroporated into the mating strain *E. coli* S17. Both *E. coli* S17 and *P. putida* S16 strains were grown at 30 °C until an OD of 1.0 was reached, at which point 5 mL of culture was spun down and resuspended in 1 mL LB. An equal mixture of each

strain, 200 μL each, was then spotted onto an LB agar plate for mating overnight at 30 °C. The next day, the spot was scraped and washed three times with 1 mL 150 mM NaCl. The resulting washed cells were resuspended in 500 μL 150 mM NaCl, and serial dilutions were plated on M9 salts + 0.4% glucose + 25 μg mL^{-1} gentamycin plates for selection of *Pseudomonas* with genomic integration of antibiotic marker. This resulted in >100 colonies, 8 of which were re-streaked onto 20% sucrose no-salt LB agar for secondary selection. This resulted in many single colonies, 16 of which were chosen for colony PCR screening using the listed CycN_verify primers, identifying which colonies successfully recombined *cycN* out. Three colonies appeared positive by size of PCR band; these were then gel extracted and submitted for Sanger sequencing, confirming the location and fidelity of knockouts.

Table 2: Primers used in Chapter 2.

Primer name	Sequence (5' to 3')
CycN_del_down_Fwd	TCCTCTAACTGAAACTTTTGAAAG
CycN_del_down_Rev	ATCCGGGGATCCGCTCTTTTGACATTATCCTCTG
CycN_del_up_Fwd	ATCCGGGAATTCGTTCATGTTAAGCAGAATCTCG
CycN_del_up_Rev	CTTTCAAAAGTTTCAGTTAGAGGACGCTTGTTTCATTTTTTATCCTC
CycN_verify_Fwd	GATTCATCAAAGAGGGGCAG
CycN_verify_Rev	GTATTCGTTACAGGCAGAGC

Phenotyping wild-type, knockout, and complemented *P. putida* S16

Single colonies of each strain grown from LB agar plates were streaked onto M9 salts + 1 mg mL^{-1} nicotine plates to examine for growth. Only the WT grew well on these plates. WT and Δ*cycN* strains were grown overnight in LB media and electroporated with pJN105 empty vector and pJN105-*cycN* for the complementation assay. These were plated onto LB + 25 μg mL^{-1} gentamycin selection plates. Single colonies from these plates were then

streaked onto fresh plates containing M9 salts + 1 mg mL^{-1} nicotine additionally supplemented with 25 μg mL^{-1} gentamycin and 0.01% arabinose to observe for growth at 30 °C for 2–5 days.

***In vitro* assays**

The buffer used in all *in vitro* experiments was 40 mM HEPES-KOH, pH 7.5, 100 mM NaCl, 10% glycerol. NicA2 is in its fully oxidized form under ambient conditions in the absence of nicotine. The absorbance spectrum of oxidized FAD was used to determine the concentration of NicA2, using an extinction coefficient of 11,300 M^{-1} cm^{-1} at 450 nm. 20 μM NicA2 was combined with 40 μM nicotine and rapidly transferred to an absorbance cuvette to measure reduction of NicA2 under ambient conditions.

CycN was fully oxidized by addition of 5 mM ferricyanide. Excess ferricyanide was then exchanged out of the sample by running over a PD-10 desalting column before use. Concentrations of CycN were determined using the extinction coefficient of oxidized cytochrome c at 410 nm (101,600 M^{-1} cm^{-1}). NicA2 and CycN were observed for characteristic spectrophotometric changes in a Shimadzu UV-1900 UV-VIS spectrophotometer. 3.75 μM CycN was combined with either 100 μM nicotine alone, 30 nM NicA2 alone, or both together and monitored for change between 250–600 nm. The same assay was performed with bovine cytochrome c (Sigma-Aldrich), except that the concentration of bovine cytochrome c was 6.84 μM. It was monitored for change in absorbance in the same region (250–600 nm) for 15 min. Oxidized CycN was additionally titrated with increasing amounts of sodium dithionite to achieve a fully reduced state, with absorbance scans taken at each titration step.

Nicotine degradation assay

This assay was performed to determine both the amount of nicotine degraded and the concentration of NicA2 enzyme in cultures of *P. putida* S16 grown in the presence of nicotine. Both wild-type and Δ*cycN* strains were grown overnight in LB. The next day, these cultures were diluted to OD 0.1 in 5 mL M9 salts + 0.4% glycerol and allowed to grow for 2 h. At this time point, nicotine was added to a final concentration of 1 mg mL^{-1} in each sample. The point of nicotine addition was considered time = 0. From then on, the cultures were sampled at 2, 4, 8,16, 24, and 48 h. 200 μL of culture extracted at each time point was spun down at 16,000*g* for 10 min. The supernatant was isolated, and 100 μL supernatant was mixed with 300 μL methanol to prepare HPLC samples. The cell pellet was resuspended in 100 μL Bacterial Protein Extraction Reagent (B-PER; Thermo Fisher) and allowed to incubate at room temperature for 15 min to complete lysis. After this time had elapsed, 25 μL of 5x reducing gel loading buffer was added to each sample.

Samples for HPLC were further clarified by spinning at 16,000*g* for 30 min. 100 μL of each clarified sample was placed into autosampler vials. These were injected then separated for analysis using a Vydac C18 4.6x250 mm column (Catalog: 218TP54) and an isocratic water + 0.1% TFA mobile phase. A nicotine standard concentration gradient from 10 mM down to 1 μM was run. 10 μL of standards and experimental samples were injected for analysis. Samples and standards were within the linear range of detection, and the absorbance peaks were integrated for quantification.

Samples for western blot analysis were boiled for 5 min. Protein standards of purified NicA2 were prepared at known concentrations from 1 μM to 1 nM. 10 μL of each sample and standard were loaded onto a Bio-Rad 12% SDS-reducing gel and run at 150 V until

completion. The gel was transferred to nitrocellulose blot via the Trans-Blot Turbo system (Bio-Rad). Blots were blocked in 5% milk TBST and stained with 1:10,000 rabbit-derived NicA2 antisera (Pacific Immunology) overnight at 4 °C. Blots were washed with 5% milk TBST three times, and then incubated with 1:20,000 goat anti-rabbit IR800 dye (LI-COR Biosciences) for 2 h at room temperature. Membranes were washed with TBST and then imaged using a LI-COR Odyssey Clx. Protein bands were quantified using LI-COR Odyssey software, and the NicA2 standard curve was used to determine the linear range of detection and concentration of NicA2 at each time point from the experiment.

Sedimentation velocity analytical ultracentrifugation (SV-AUC)

SV-AUC was carried out using 400 µl sample loaded into two-sector titanium centerpieces with 1.2 cm path-length in an An60Ti rotor in a Beckman Optima Xl-I analytical ultracentrifuge. Measurement was completed in intensity mode. All SV-AUC data were analyzed using UltraScan 4 software, version 4.0 and fitting procedures were completed on XSEDE clusters at the Texas Advanced Computing Center (Lonestar, Stampede) through the UltraScan Science Gateway (https://www.xsede.org/web/guest/gateways-listing)[93]. The partial specific volume (vbar) of NicA2 was estimated within UltraScan III based on the protein sequence[94]. Raw intensity data were converted to pseudo-absorbance by using the intensity of the air above the meniscus as a reference and edited. 2-dimensional sedimentation spectrum analysis (2DSA) was performed to subtract time-invariant noise and the meniscus was fit using ten points in a 0.05-cm range[95]. First arrays with a broad S range were fitted to account for possible large oligomeric states. Final arrays were fit using an S range 1-10, an f/f0 range of 1–4 with

64 grid points for each, 10 uniform grid repetitions and 400 simulation points. 2DSA was then repeated at the determined meniscus to fit radially invariant and time-invariant noise together using ten iterations. The 2DSA solution was refined by a genetic algorithm (GA), which uses an evolutionary based approach using random cross-over, mutations and deletion operations to alter the solute characteristics of the 2DSA solutes to eliminate false positive solutions[96]. The results from the genetic algorithm were evaluated using a Monte Carlo algorithm.

Transient kinetics

All stopped-flow experiments were performed in 40 mM HEPES-KOH, pH 7.5, 100 mM NaCl, 10% glycerol at 4 ºC. NicA2 and CycN solutions were made anaerobic in glass tonometers by repeated cycles with vacuum and anaerobic argon[97]. When needed, NicA2's FAD was reduced in the anaerobic tonometer by titrating with a dithionite solution or anaerobic nicotine solution housed in a gas-tight Hamilton syringe. The dithionite or nicotine solutions were slowly added up to the point where NicA2's flavin reached the fully-reduced hydroquinone state, and the redox status of the flavin was spectrophotometrically monitored during the titration using a Shimadzu UV-1900 UV-VIS spectrophotometer (UV Probe software). Nicotine-containing buffer solutions were made anaerobic by sparging for at least 10 min with anaerobic argon. Buffer containing O_2 at specific concentrations was prepared by sparging different O_2/N_2 gas ratios through buffer in a gas-tight syringe for at least 15 min at room temperature. The various O_2/N_2 gas ratios were prepared from O_2 and N_2 gas cylinders using a Maxtec MaxBlend 2 gas mixer, and the dissolved O_2 concentration in the buffer solution was calculated using a Henry's law constant for O_2 of 770 atm M^{-1}.

Stopped-flow experiments were conducted using a TgK Scientific SF-61DX2 KinetAsyst stopped-flow instrument (with Kinetic Studio software) that had been previously equilibrated with a glucose/glucose oxidase solution to make the internal components of the system anaerobic. ~30 μM NicA2 (flavin concentration before mixing) was loaded onto the instrument and mixed with substrate (nicotine, O_2, or CycN) at a range of concentrations. The reactions were monitored either using the instrument's multi-wavelength CCD detector (1.6 ms data interval time) or a single wavelength detector with photomultiplier tube. Kinetic traces were fit to sums of exponentials using KaleidaGraph (Synergy Software) to determine observed rate constants.

Steady state assays

Anaerobic steady state assays were performed in a stopped-flow spectrophotometer in 40 mM HEPES-KOH, pH 7.5, 100 mM NaCl, 10% glycerol at 4 ºC. NicA2 and nicotine were made anaerobic in a glass tonometer with the nicotine in a side arm separated from the NicA2 solution. After achieving anaerobiosis, the nicotine was added to the NicA2 solution, resulting in a solution containing 200 nM NicA2 (flavin concentration) and 2 mM nicotine. The NicA2/nicotine solution was then mixed with various concentrations (10-255 μM before mixing) of anaerobic, oxidized CycN and the reduction of CycN was observed at 550 nm over 80 s. The linear rate was obtained over the first 5 s of the reaction and 21,000 $M^{-1}cm^{-1}$ was used as the difference in extinction coefficient at 550 nm between reduced and oxidized CycN[98].The rate data were divided by two since two CycN molecules are used in a single turnover by NicA2 and then divided by the NicA2

concentration (100 nM after mixing in the experiment) to obtain the apparent turnover number for each CycN concentration.

Amplex Red Assay

For H_2O_2 detection, these assays were performed similarly to what has been previously reported for NicA2[8,68] following the recommendations provided in the Amplex Red Assay Kit (Thermo Fisher Scientific). Assays were performed in 40 mM HEPES-KOH, pH 7.5, 100 mM NaCl. Reactions were measured in a platereader with excitation wavelength of 530 nm and emission wavelength of 590 nm. Samples were combined to have end concentrations of the following constituents in a 100 μL reaction: 1 μM NicA2 (flavin concentration), 20 μM oxidized CycN, 10 μM nicotine, 0.1 units mL^{-1} horseradish peroxidase, 50 μM Amplex Red. These were mixed and immediately observed at room temperature in the plate reader for 30 min. A standard curve of H_2O_2 stock concentrations was used to determine the linear range of the assay and assign the concentration of H_2O_2 produced in each case.

Chapter 3

Directed Evolution Unlocks Oxygen Reactivity for a Nicotine Degrading Flavoenzyme‡

‡The contents of this chapter reflect a manuscript in preparation. I performed the aerobic in vitro and in vivo experiments, including the mutant library preparation and running of the selection, assisted by Joshua Li and Xiaomeng Liu. Rishav Mitra and I designed and performed the ^{19}F NMR experiments. Kevin Wu solved the crystal structures of NicA2 enzymes. Karli Boer, Zhiyao Zhang, Chris Clark, Kaitrin Funckes, and Cristian Vasquez performed the stopped-flow and anaerobic experiments in the lab of Frederick Stull.

3.1 Background

Nicotine oxidoreductase (NicA2) is a flavin-dependent enzyme with the ability to catalyze degradation of nicotine into a non-psychoactive metabolite, N-methylmyosmine (NMM)[7]. For this reason, it has garnered interest as an injectable therapeutic to aid in the cessation of smoking, and several preclinical studies in rats have demonstrated promising impact[5,6,67,68]. One major caveat of this approach, however, is the very large dose of NicA2 necessary to achieve benefit in these studies: 10 – 70 mg kg^{-1} [5,67]. The reason such sizeable amounts of NicA2 are required is likely due to the poor oxygen reactivity of the enzyme[18,19].

As a member of the flavin amine oxidase family, NicA2 catalyzes reduction and oxidation reactions by first accepting electrons from an amine-containing substrate, resulting in its bound flavin adenine dinucleotide (FAD) becoming a reduced

hydroquinone ($FADH_2$). After this reductive step, $FADH_2$ must oxidize before NicA2 can facilitate another round of catalysis. There are a wide variety of oxidative substrates available in nature, but molecular oxygen (O_2) is the canonical electron acceptor for flavin amine oxidases. When O_2 is the only substrate available to oxidize flavin, which is presumably the case in the bloodstream when this enzyme is used as a treatment, NicA2 turns over extremely slowly with a k_{cat} of 0.007 s^{-1} [7,8]. In its native organism *Pseudomonas putida* S16 it can achieve a rate of catalysis that is much faster due to the presence of an alternative electron acceptor to O_2: a cytochrome c we previously characterized called CycN[19]. We found CycN oxidizes NicA2's bound flavin at a rate that is 4 orders of magnitude greater than that achieved using O_2. The presence of CycN is critical for the ability of *P. putida* S16 to grow using nicotine as carbon source, but supplementation of CycN is unlikely to be useful therapeutically. This is in part due to the observation that cytochrome c proteins are not terminal electron acceptors, and so any electrons transferred from NicA2 will sequester CycN in a reduced state, rendering it unable to further assist in the oxidation of NicA2. Thus, without reconstitution of an entire electron transport chain to re-oxidize CycN, including the membrane-bound cytochrome oxidase, addition of catalytic quantities of CycN alone will not aid NicA2 in the process of nicotine degradation. To develop NicA2 as a treatment-suitable enzyme, a direct solution would be to increase its rate of reaction with O_2, which is readily available in the bloodstream. However, this is a challenging task, since the molecular features that govern the specificity for O_2 as an oxidative substrate of flavoenzymes remain obscure[16].

Due to the high redox potential of the O_2/H_2O_2 couple versus that of flavins, all reduced flavins are thermodynamically poised to be oxidized by O_2 in an essentially

irreversible reaction[13]. In the case of flavin-containing oxidases, O_2 is a ready reactant, with rate constants for oxidation typically falling between 10^3-10^6 $M^{-1}s^{-1}$ [14]. Conversely, flavin-containing dehydrogenases do not efficiently facilitate a reaction between their bound flavins and O_2, irrespective of the thermodynamic driving force, having rate constants for oxidation that can approach zero. This implies there are mechanisms in place that act to slow the reaction with O_2[12]. Despite roughly one hundred years of study[15], the molecular rules that govern oxidase activity for a given flavoenzyme have remained obscure[14,16,17]. The behavior of NicA2 is particularly perplexing because, defying the trend within its enzyme family, it reacts poorly with O_2 as an oxidant and it is thus better classified as a dehydrogenase[18,19]. NicA2 therefore provides an appealing opportunity to address how flavoenzymes can control their reactivity with O_2, since NicA2 can be compared to a large group of structurally similar enzymes that unlike NicA2 are reactive with molecular oxygen.

Previously characterized flavin amine oxidases facilitate rapid oxidation of $FADH_2$ using O_2 as a terminal electron acceptor[14,99]. NicA2 apparently stifles the ability of its bound $FADH_2$ prosthetic group to react with dioxygen, resulting in an oxidation rate well below that of even free $FADH_2$. Since other flavin amine oxidases readily use O_2, we hypothesized that it should be possible to adapt NicA2 to favor O_2 as a substrate. It is inherently difficult to do this with rational substitutions because of the obscurity of the structural features that control O_2 reactivity of this class of enzymes, and likely as a result, previous studies have achieved only modest increases in the catalytic rate constant for nicotine degradation in NicA2[6,18,45]. To gain more insight into the structural features that govern oxygen accessibility and reactivity for this class of enzymes we decided to exploit

the severe growth defect exhibited by null mutants of NicA2's in vivo electron acceptor, CycN, to develop a selection to isolate NicA2 variants that can effectively use oxygen as an electron acceptor. *cycN* deletions in *P. putida* S16 grow poorly using nicotine as a sole carbon source, presumably because in the absence of CycN, NicA2 is forced to use alternative electron acceptors such as O_2. We reasoned that expressing variants of NicA2 that can more effectively use oxygen as an electron acceptor should allow *cycN* deletion strains of *P. putida* S16 to grow more rapidly on nicotine, thereby allowing the isolation of increased activity variants. This approach does not require detailed mechanistic knowledge and proved to be very efficient, allowing us to rapidly select for more rapidly growing NicA2 variants. Our selection also proved to be very specific, essentially all variants isolated from the selection proved to show improved catalytic rates in their reaction directly with oxygen, rates that improved up to 200-fold. It appears that the mechanism by which this acceleration occurs is via control of an oxygen accessible tunnel in the variant NicA2s. These NicA2 variants may be more useful for treatment as an aid to smoking cessation, as they would require a much lower dose of enzyme to achieve clearance of nicotine from the blood.

3.2 Results

3.2.1 Pseudomonas putida S16 ΔcycN mutation provides a powerful selection for more O_2-reactive NicA2 variants

Rapid degradation of nicotine is required for the growth of *P. putida* S16 on nicotine[19]. The first step in this catabolic pathway is oxidation of nicotine by NicA2. The electrons

liberated by nicotine breakdown are donated from NicA2 to a cytochrome c we call CycN. Deletions of the gene for *cycN* arrest the natural pathway for nicotine degradation, and result in a severely impaired ability to grow on nicotine as a sole carbon source (**Figure 26a**). This is very likely a consequence of the inability of NicA2 to be efficiently oxidized directly by molecular oxygen[18,19]. *P. putida* S16 containing a *ΔcycN* mutation thus provides a genetic background that links bacterial growth to the ability of NicA2 to be oxidized by O_2. Demanding that *P. putida* S16 *ΔcycN* strains grow on nicotine in the presence of air then provides a convenient and powerful selection for O_2-reactive NicA2 enzyme variants. We transformed this *ΔcycN* knockout strain with mutant libraries of NicA2 and isolated variants that grow on media containing nicotine as a sole carbon source better than the abysmally poor growth shown by the *ΔcycN* knockout strain containing wild type NicA2. NicA2 variant proteins identified in the selection were then purified from *E. coli* and their activity with nicotine characterized using a spectrophotometric assay. This selection worked extremely well, essentially all of the variants of NicA2 that exhibited faster growth, as measured by colony size or in liquid culture, contained missense mutations in NicA2 that improved its ability to function using oxygen as an electron acceptor (**Figure 26b,c; Table 3**). Multiple rounds of enrichment, random mutagenesis, and reselection (see materials and methods for a detailed procedure), yielded variants with successive, increasingly rapid k_{cat} values. (**Figure 26d**). The k_{cat} values of the encoded variants are proportional to their growth rates in liquid culture, supporting our hypothesis that growth of the deletion strain is directly limited by the oxygen-dependent activity of NicA2. We were able to obtain variants with k_{cat} values up to 1.3 s^{-1}, an approximately 200-fold improvement over the 0.006 s^{-1} value of wild-type

NicA2. After iterative random mutagenesis and re-selection for 4 generations, the k_{cat} values roughly plateaued suggesting that we may be approaching saturation of the variants easily accessible using our approach.

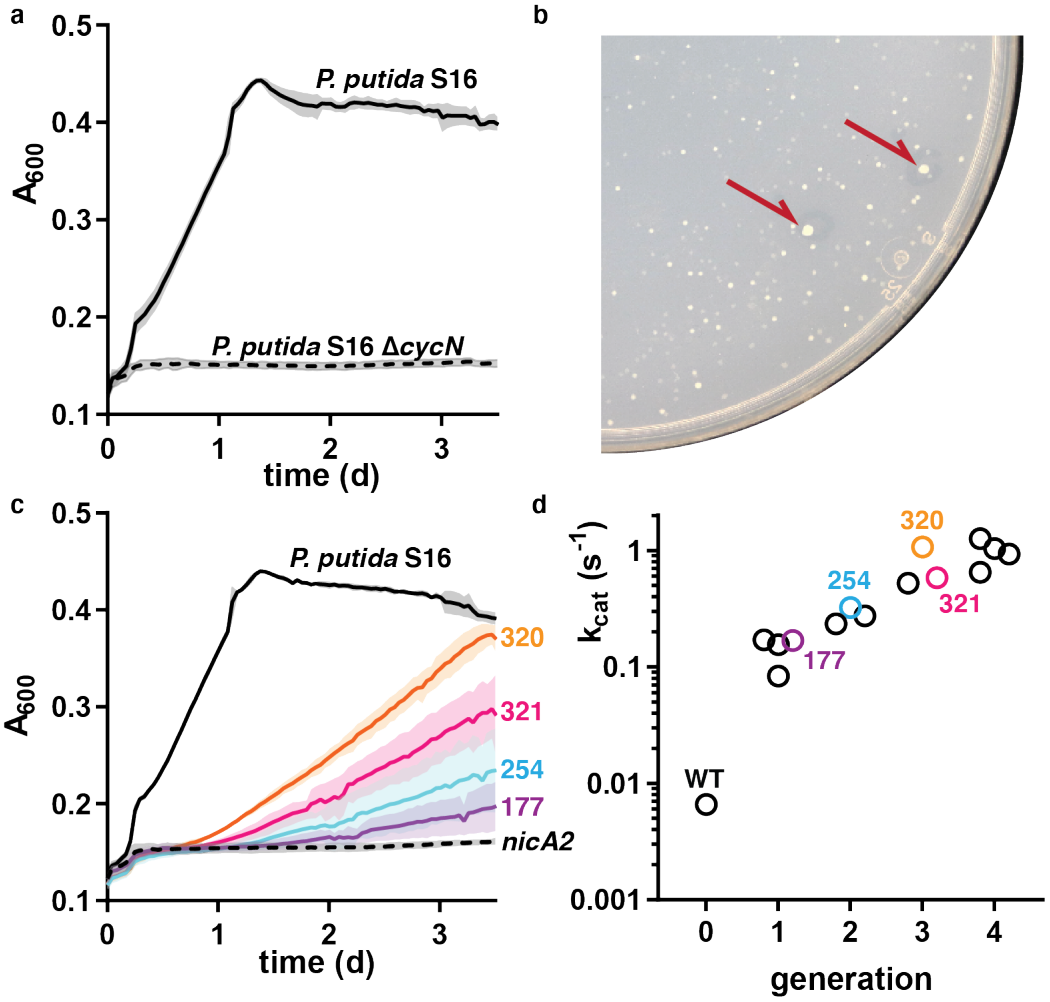

Figure 26. *Pseudomonas putida* S16 *ΔcycN* provides a platform for genetic selection.

a, Growth of *P. putida* S16 wild-type and *ΔcycN* in liquid culture with nicotine as sole carbon source. The grey error bands represent the standard deviation of three biological replicates. **b,** Image of a nicotine agar plate spread with a NicA2 mutant library transformed into *P. putida* S16 *ΔcycN*. Red arrows point to the substantially larger, and thus faster growing, colonies that were typically selected for further analysis. **c,** Growth of *P. putida* S16 wild-type in liquid culture with nicotine as sole carbon source is shown in solid black. Growth of *P. putida* S16 *ΔcycN* strains transformed with the wild-type sequence of *nicA2*, shown in dashed black, and the *nicA2* variants from the selection are shown in the colored curves with their allele numbers indicated. Note that the color scheme of the variants carries over between the growth curves and part d of this figure. Error bands represent the standard deviation of three biological replicates. **d,** NicA2 variants isolated from different generations of the selection were purified and characterized for their steady-state kinetic parameters (**Table 3**). Note that the y axis has a logarithmic scale.

The apparent K_M of NicA2 variants was prone to increase in the high activity variants (**Table 3**). **Figure 27** shows that the k_{cat}/K_M was not reliably selected for in our conditions. This is not surprising, given that the selection was carried out using a concentration of nicotine in the agar plates of ~3 mM. This is the concentration is required for robust growth of the organism (data not shown) but is well above the apparent K_M of the wild-type enzyme for nicotine (114 nM)[8]. As has previously been noted, NicA2's reaction with nicotine and oxygen most likely follows a ping-pong mechanism[18]. In this case, the apparent K_M for nicotine turnover under ambient conditions is directly linked to the rate of oxidation by O_2, and so would be expected to rise when that oxidation rate is increased, as we observe[100]. Despite this, the comparatively larger increases in k_{cat} resulting from the selection led to variants with up to a 10-fold increase in specificity constant.

Table 3. Steady-state kinetic data of NicA2 wild-type and variants.

NicA2 variant	Encoded mutations	k_{cat} (s^{-1})	K_M (μM)	k_{cat}/K_M (s^{-1} M^{-1})
WT		$0.0066 \pm 2 \times 10^{-4}$	0.114[a]	5.4×10^{4} [a]
6	H368R	0.0837 ± 0.008	ND	ND
15	A107T, D130N, S192N, M265I, T397A	0.155 ± 0.004	1.8 ± 0.2	8.6×10^{4}
16	E249G, H368R	0.171 ± 0.004	1.9 ± 0.2	9.0×10^{4}
177	G145A, S192I, Q359L, Q366R, S379N	0.17 ± 0.01	60 ± 10	2.7×10^{3}
235	K49N, F93L, F104L, V127M, D130S, L132R, F174C, T319I, E454D	0.274 ± 0.004	23 ± 2	1.2×10^{4}
254	A107T, D130G, T267I, N462S	0.32 ± 0.01	15 ± 2	2.2×10^{4}
255	F104L, G317D, H368R, L449V, N462S	0.235 ± 0.006	0.8 ± 0.2	3.1×10^{5}
305	F93L, F104L, V127M, D130S, L132R, S213T, T222S, A281T, L374M, M403I	0.52 ± 0.01	140 ± 10	3.9×10^{3}
320	F104L, A107T, D130S, T319I, L449V, N462S	1.07 ± 0.02	7 ± 0.6	1.5×10^{5}
321	F104L, A107T, S146I, G317D, H368R, L449V, N462S	0.58 ± 0.01	1.3 ± 0.2	4.5×10^{5}
416	T67A, F104L, A107T, D130S, K165R, N462S	0.93 ± 0.04	8 ± 1	1.2×10^{5}
417	G50D, F104L, A107T, D130S, F422L, N462H	1.26 ± 0.04	8 ± 1	1.6×10^{5}
426	G50D, F104L, A107T, D130S, T319I, L410M, L449V, N462S	1.04 ± 0.02	7.8 ± 0.8	1.3×10^{5}
427	F104L, T280A, D294Y, T307S, G317D, N363S, H368R, S379N, N462S	0.65 ± 0.01	4.1 ± 0.4	1.6×10^{5}

Values reported with 95% confidence intervals from 3 replicates.
[a] denotes values reported in Tararina et al.[8]

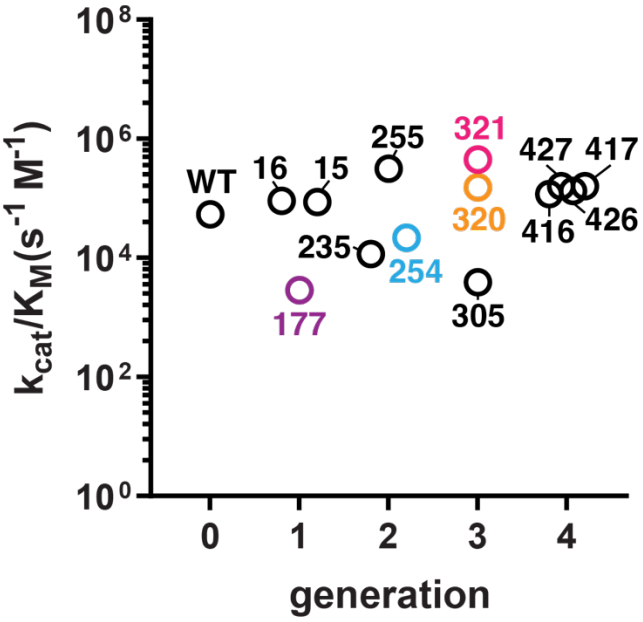

Figure 27. k_{cat}/K_M is not reliably selected for under plate selection conditions.

k_{cat}/K_M values for variants listed in **Table 3** are plotted based on the generation of the selection they were isolated from. The color scheme holds between this figure and **Figure 26**.

Over the course of isolation and DNA sequencing of positive clones from the selection, some amino acid locations were found to be mutated more frequently than others. F104, A107, D130, H368, and N462 are each found to be mutated in greater than 15% of sequenced variants (**Figure 28a**). Additionally, 96 out of 132 total individual variants sequenced contained a mutation at one or more of these resides. When visualized in the context of the protein structure, these frequently mutated residues clustered near the active site, specifically in the *Si*-flavin region (**Figure 28b**). We introduced the consensus substitution from each position into the background of wild-type NicA2 (**Figure 29**). This allows us to determine if, and how much, each of these mutations singly increase the catalytic activity of NicA2 when present alone. We find that F104L, A107T, and N462S mutations had minimal effect on activity, which is evidence for an epistatic or additive effect upon combining multiple mutations (**Figure 28c**). Notably, the

two single substitutions of greatest benefit to the activity of the enzyme, D130S and H368R, are distant from FAD making them less likely to directly impact the chemical environment for activation of O_2, and thus more likely to impact oxygen access to FAD.

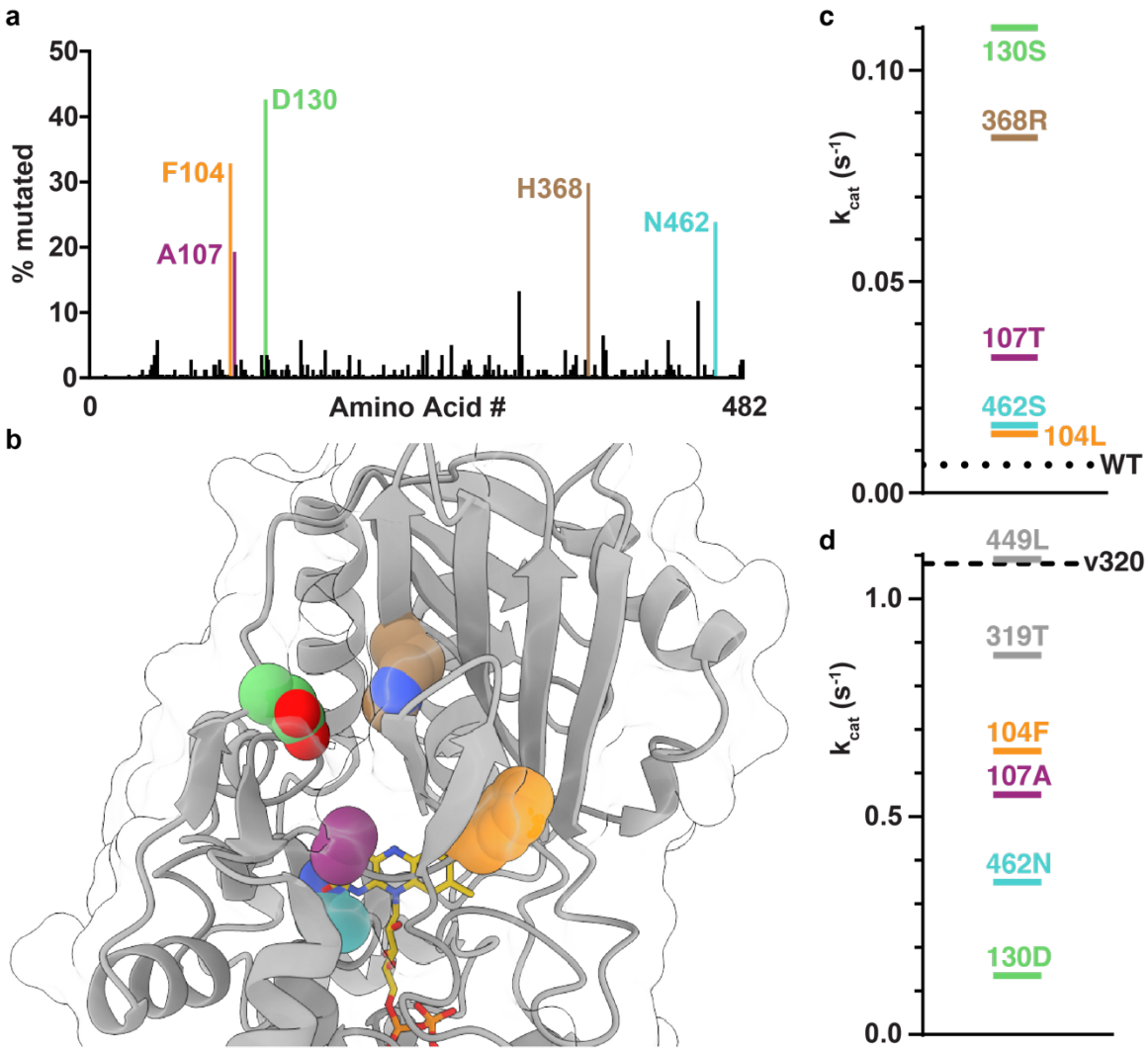

Figure 28. Mutations near FAD are critical for a gain in oxygen reactivity.

a, 133 variant sequences have been isolated from the selection. The likelihood of a variant containing a missense mutation occurring at each amino acid location along the protein is plotted above. Note that these variant sequences are not independent, since the iterative mutagenesis used to create new mutant libraries was based only using higher activity variants as template and is therefore subject to a founder effect between different generations of the selection. The color scheme in 2a carries over throughout the rest of the figure. **b,** The crystal structure of wild-type NicA2 (PDB: 5TTJ) with the 5 amino acids most often found to be mutated highlighted in color with spheres. Heteroatom oxygen is in red, and nitrogen is in blue. **c,** k_{cat} values determined for single mutations in the background of wild-type NicA2. The dotted line indicates the k_{cat} of value of wild-type NicA2. **d,** k_{cat} values determined for variants where mutations were removed from the background of variant 320; each line corresponds to the k_{cat} value corresponding to single mutations back toward the wild type. Note the 10-fold difference in scale from the plot of 2c. The dashed line indicates the k_{cat} value of NicA2 v320. The location of the amino acid positions L449 and T319 in the crystal structure can be seen in **Figure 30**.

Figure 29. Alignment of NicA2 variants tested for steady-state kinetic activity.

Red asterisks denote amino acid locations found to be mutated in greater than 15% of all sequences isolated from the selection. Sequences are colored for their degree of conservation using the BLOSUM62 score. Figure was prepared using Jalview[101].

The most active variants isolated from the selection contain several of these frequent mutations, implying that multiple mutations are required for robust activity. For example, NicA2 v320 contains four: F104L, A107T, D130S, and N462S; as well as two, less common, FAD distant mutations 319S and 449V. To establish which of these were most critical for the observed total increase in turnover rate from the wild-type k_{cat} of 0.006 s^{-1} to 1.1 s^{-1}, we serially removed mutations from NicA2 v320 (**Figure 28d**). Out of six total mutations in this variant, we find that the four highly enriched mutations proximal to the flavin or *Si*-flavin side (F104L, A107T, D130S, and N462S) are most important for activity, and that the two more distant mutations (319S and 449V) have little or no effect on the activity of the enzyme. Having multiple mutations in a single variant does not seem to put undue burden on protein thermostability, at least in the 4 variants we screened, as measured in a fluorescence based ThermoFAD melting assay (**Figure 31**)[102]. Since mutations are often destabilizing[103], this result may initially seem surprising, but since our selection demanded increased activity strongly destabilizing mutations were likely selected against.

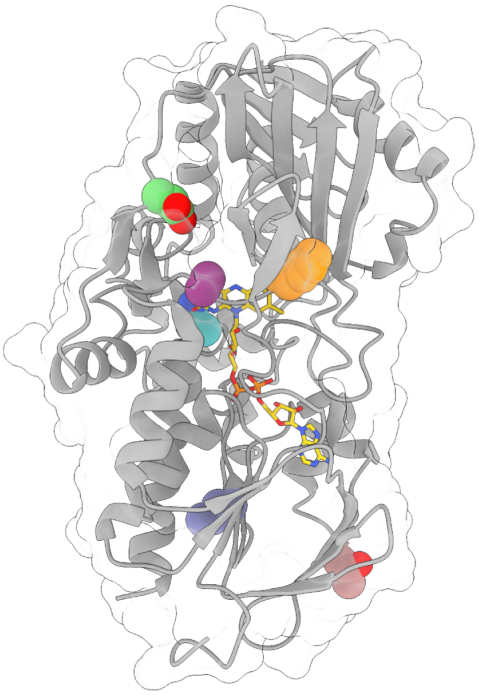

Figure 30. Mutation in NicA2 v320.

The crystal structure of wild-type NicA2 is displayed with residues highlighted that are mutated in NicA2 v320. Note F104 in orange, A107 in purple, D130 in green, T319 in salmon, L449 in cornflower blue, and N462 in turquoise. Heteroatom oxygen is in red and nitrogen in blue.

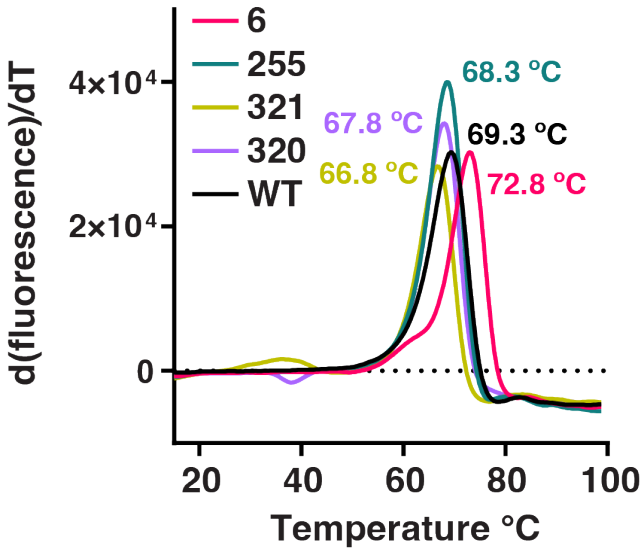

Figure 31. NicA2 wild-type and variants maintain a similar melting temperature.

NicA2 protiens as listed in the figure were subject to the ThermoFAD melting assay to determine the temperature at which they unfolded, releasing their bound FAD. The melting temperature of each variant is displayed in its corresponding color.

3.2.2 NicA2 variants have markedly higher oxidase activity than wild-type

NicA2 v320 had one of the highest k_{cat} values for O_2-dependent nicotine degradation of any of our variants, so we selected it for detailed analysis using stopped-flow spectroscopy to elucidate its mechanism of action. NicA2 v320 contains a spectrum of activating mutations consistent with the other highest k_{cat} variants (**Figure 29**), and so we expect the result to be representative of our improved activity variants on whole. Stopped-flow experiments that monitored the reaction of reduced NicA2 v320 with O_2 revealed that $FADH_2$ oxidation is indeed accelerated roughly 200-fold in this variant relative to wild-type NicA2. We found this enhanced reaction rate with O_2 is only observed when the reaction product, NMM, is bound to NicA2 v320. The bimolecular rate constant for flavin oxidation by O_2 ($k_{ox}^{O_2}$) is 4400 $M^{-1}s^{-1}$ for NicA2 v320 in the *presence* of NMM, however, $k_{ox}^{O_2}$ is only 230 $M^{-1}s^{-1}$ in the *absence* of NMM (**Figure 32a,c**). This indicates that NMM binding to NicA2 v320 substantially accelerates the rate at which its flavin can be oxidized by O_2. Notably, the opposite behavior occurs in wild-type NicA2. Here the addition of NMM decreases $k_{ox}^{O_2}$ to 31 $M^{-1}s^{-1}$ relative to the already low value of 120 $M^{-1}s^{-1}$ that is observed in the absence of NMM for wild-type NicA2 (**Figure 32b,c**). Spectrophotometric titrations indicate that, like with wild-type, reduced NicA2 v320 binds NMM tightly with a K_D in the nM range or lower (**Figure 33a**) We previously determined that the NMM product resulting from nicotine oxidation remains bound to wild-type NicA2 during catalysis when NicA2 is oxidized by its natural electron acceptor, CycN[19]. That appears to be the case for NicA2 v320 oxidation by O_2 as well since the apparent rate constant for oxidation of NMM-bound NicA2 v320 at 250 μM O_2 (ambient concentration) is 1.1 s^{-1}, which matches the measured

k_{cat} for this variant. This indicates that the NMM-bound $k_{ox}^{O_2}$ value is rate-limiting during turnover, at least for this variant, and that the mechanism by which our mutations improve the catalytic rate of the enzyme is by directly increasing the oxidation rate by O_2.

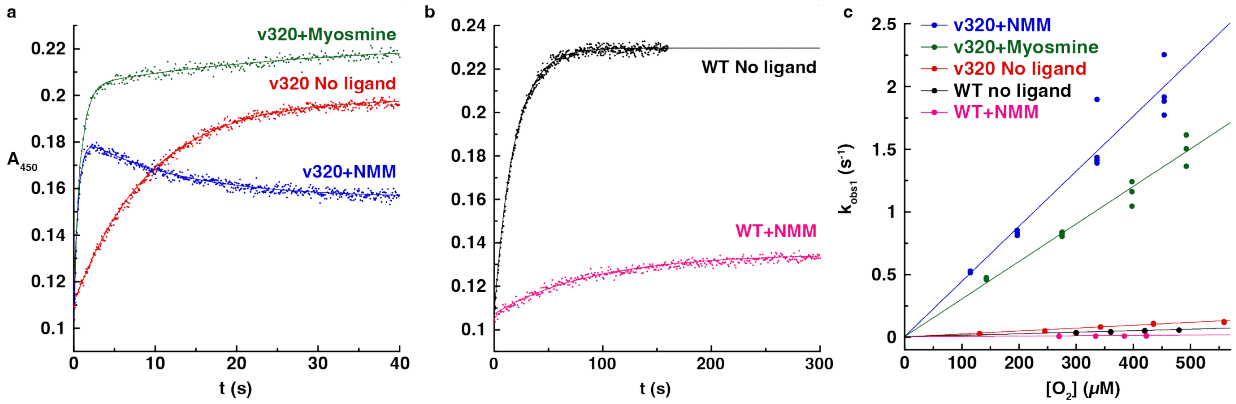

Figure 32. NicA2 variants are rapidly oxidized by O_2.

a, Example traces for the stopped-flow reaction of reduced NicA2 v320 with O_2 under the described conditions. The decrease in absorbance that occurs after flavin oxidation for the NMM-bound trace is caused by an interaction between NMM and NicA2 containing oxidized FAD[19]. This decrease in absorbance is not observed in the equivalent experiment with wild-type NicA2 because flavin oxidation by O_2 is very slow and therefore rate limiting. **b,** Example traces for the reaction of reduced NicA2 wild-type with O_2. **c,** k_{obs} values for the first phase of oxidation are plotted against the concentration of O_2 and fit to a line. The slope of these lines define the bimolecular rate constant for oxidation by O_2, and are listed in the text.

Substrate/product binding has also been shown to accelerate flavin oxidation for other amine oxidases like monoamine oxidases A and B. In these cases, it is thought to be because the product supplies a positive charge that stabilizes the transient superoxide intermediate that occurs during flavin oxidation by O_2[14,104]. NMM is also a positively charged product, in this case at the pyrrolidine nitrogen, so we wondered if this positive charge may be responsible for accelerating the reaction of NicA2 v320 with O_2 when NMM is bound. To test this possibility, we measured $k_{ox}^{O_2}$ for reduced NicA2 v320 in the presence of myosmine, which is structurally similar to NMM but lacks the positive charge

on the pyrrolidine nitrogen. The $k_{ox}^{O_2}$ value for myosmine-bound NicA2 v320 was 2900 $M^{-1}s^{-1}$, which is comparable to that of NMM-bound NicA2 v320, suggesting that the positive charge of NMM is not important to the enhanced reactivity of NicA2 v320 with O_2 when bound to NMM (**Figure 32a,c**).

To investigate the reductive half-reaction we then measured kinetics for the reaction of oxidized NicA2 v320 with nicotine by stopped-flow under anaerobic conditions, which allows us to determine if the mutations present in this variant impact its reaction with nicotine. The reaction, as monitored by following absorbance changes that accompany flavin reduction, occurred in two kinetically observable events, both of which appeared to correspond to flavin reduction based on the observed changes in absorbance (**Figure 33b**). We previously saw similar behavior with wild-type NicA2, which can be attributed to the two different subunits of the NicA2 homodimer reacting with different rate constants[19]. The observed rate constants for both kinetic events were invariant with nicotine concentration, suggesting that the binding affinity of NicA2 v320 for nicotine is substantially lower than the lowest nicotine concentration we could use (50 μM) and still maintain pseudo first order conditions. Somewhat surprisingly, the two rate constants for this reaction with NicA2 v320 were 19 s^{-1} and 4.1 s^{-1}; these values are 42- and 29-fold lower for the first and second phase, respectively, than the corresponding values with wild-type NicA2 (800 s^{-1} and 120 s^{-1}), indicating that the mutations in NicA2 v320 *negatively* impacted the enzyme's ability to react rapidly with nicotine (**Figure 33c,d**). Notably, the rate constant for the second phase of flavin reduction (4.1 s^{-1}) of NicA2 v320 is only 4-fold greater than the apparent rate constant for the reaction with O_2 at ambient O_2 concentrations. This result may explain why variants selected for in our growth

selection plateaued at a k_{cat} of ~1.3 s^{-1}, as the compromised reaction with nicotine in these variants would become rate limiting with significant further improvement in the oxidase activity of the enzyme. While the mutations in NicA2 v320 negatively affect the enzyme's reaction with nicotine, they do not have a major impact on its ability to transfer electrons to CycN, as reduced NicA2 v320 reacts rapidly with CycN, having k_{obs} values similar to wild-type NicA2 (**Figure 33e**).

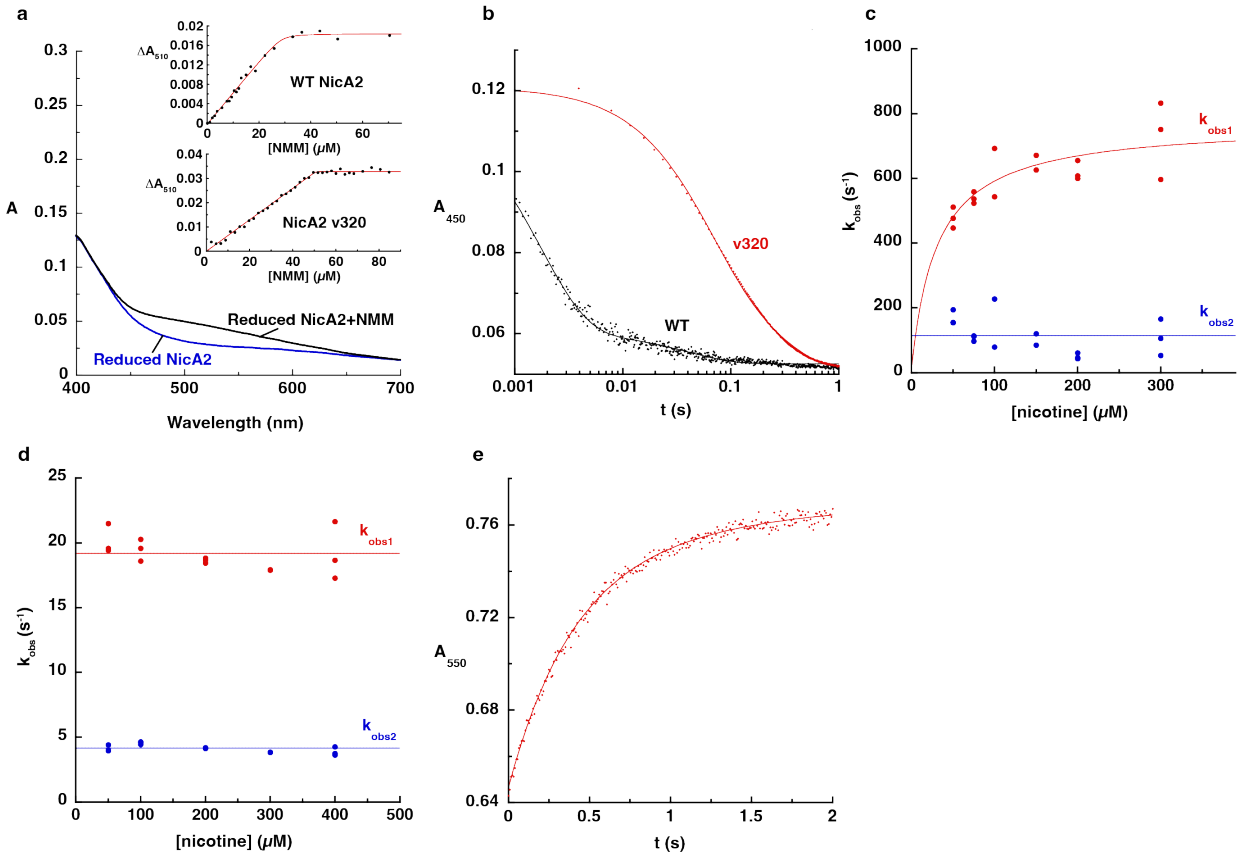

Figure 33. Binding and stopped flow reactions of wild-type and v320 NicA2.

a, Reduced NicA2 wild-type and v320 were titrated with NMM, monitoring change in absorbance at 510 nm to determine the binding coefficient. The inset shows the data points from the titration fit the the tight binding equation. **b,** Raw traces for the reactions of NicA2 wild-type and v320 with nicotine, both demonstrating biphasic traces. **c,** k_{obs} values for the reaction of wild-type NicA2 are plotted against the concentration of nicotine. k_{obs} values from first phase was fit to a hyperbola, k_{obs} from the second phase was invariant to nicotine concentration. **d,** k_{obs} values for the reaction of NicA2 v320 are plotted against the concentration of nicotine, both invariant to the nicotine concentration. **e,** The reaction of reduced NicA2 v320 with oxidized CycN was rapid, finishing in under 2 seconds similar to the reaction of wild-type NicA2[19].

3.2.3 A change in tunnel accessibility enhances catalysis in a NicA2 variant

Although these stopped flow experiments have allowed us to gain some insights into the similarities and differences between the enzymatic mechanism used by this variant and wild type NicA2, they do not give us a clear understanding of the molecular basis of our increased oxidation rate. To explain its better reactivity toward oxygen, we decided to closely examine the structural properties of our enzymes. Flavoenzyme oxidases often contain tunnels for the guided diffusion of dioxygen into the protein core that houses the flavin cofactor. These tunnels can be a permanent feature that is evident from crystal structures, such as that of cholesterol oxidase[105], or they can form transiently in the catalytic cycle as is apparently the case for alditol oxidase[50], in which case they are considerably more difficult to characterize experimentally. Inspection of the solvent-accessible surface area in the crystal structure of wild type NicA2 revealed several interconnected cavities that can potentially form tunnels that extend from the *Si*-side of the FAD moiety to the surface (**Figure 34**). One such tunnel is located in a region that is rich with the mutations we discovered that improve the oxidase activity of NicA2 (**Figure 35**). This led us to wonder if the observed gain in activity is at least partially due to structural perturbations that might make this tunnel more accessible to dioxygen.

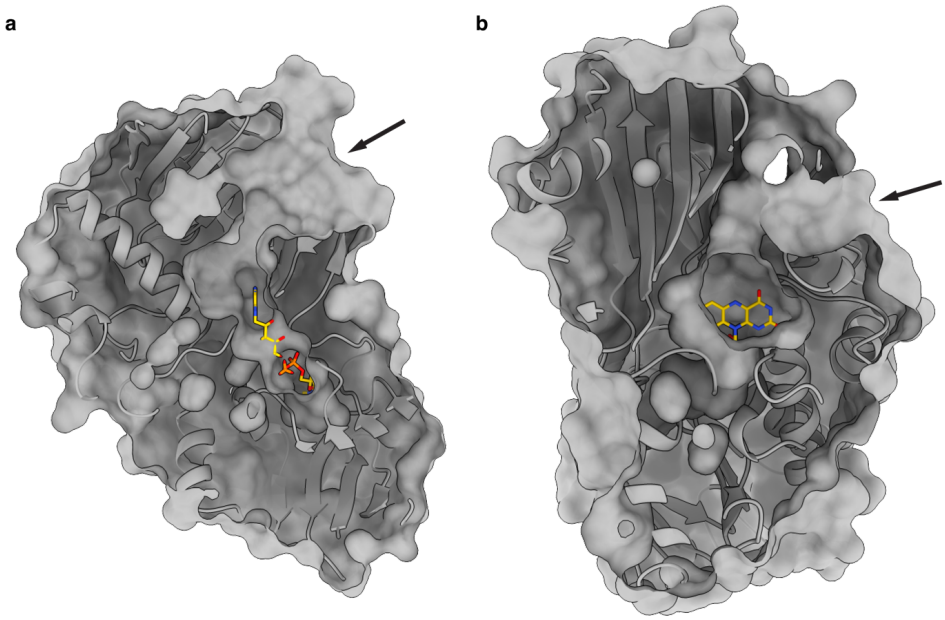

Figure 34. NicA2 wild-type has solvent exposed cavities.

a, The crystal structure of wild-type NicA2 is rendered with the solven accessible surface area. The arrow marks a solvent exposed channel into the active site of NicA2. **b,** A different view of wild-type NicA2. The arrow marks a cavity on the surface of the protein that approaches the active site.

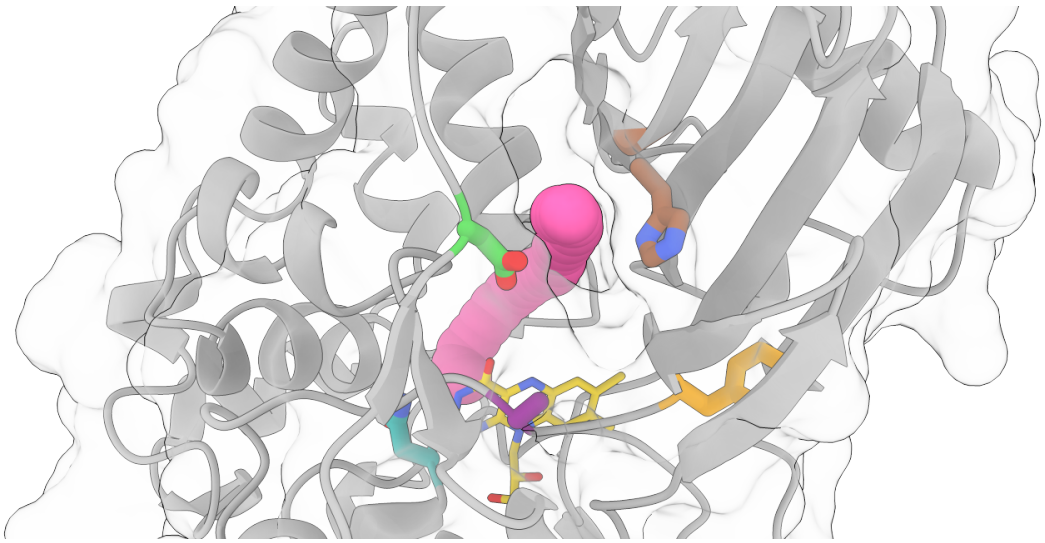

Figure 35. Mutations in variant NicA2 enzymes cluster around a putative tunnel.

The crystal structure of NicA2 wild-type (PDB ID: 5TTJ) is displayed with an ~1.4 Å diameter tunnel identified by CAVER simulation rendered in pink. FAD is rendered in yellow. Frequently mutated residues (as defined earlier) are rendered F104 in orange, A107 in purple, D130 in green, H368 in brown, N462 in turquoise.

We first attempted to crystallize NicA2 v320, but none of our crystals diffracted to adequate resolution for structure determination. In screening through our various high activity mutants, we were fortunate to obtain well diffracting crystals of NicA2 v321 in both the apo and NMM-bound forms. The constellation of mutations that comprise this variant (F104L, A107T, S146I, G317D, H368R, L449V, N462S) well represent most of those found in other high activity variants (**Table 3**). Additionally, NicA2 v321 demonstrates similar kinetic qualities as v320. The most obvious difference between the apo-structures of wild-type and v321 enzymes is that the active site of v321 appears *less* accessible to solvent (**Figure 36a**). The NMM-bound structures of v321 and wild type NicA2 are very similar with an overall RMSD of < 0.5 Å (**Figure 36c**). Enzymes that have a buried active site need to facilitate substrate migration for catalysis to occur. The observed increase in the oxidation rate of NMM-bound NicA2 in the variant then raises an intriguing possibility, that the collection of mutations in this variant alter the transport pathway of O_2 through tunnels like the one we observed in the static structure of wild-type NicA2. To further investigate the dynamics of the mutationally dense region of NicA2 in both our wild-type and mutant proteins, we decided to use nuclear magnetic resonance (NMR) spectroscopy.

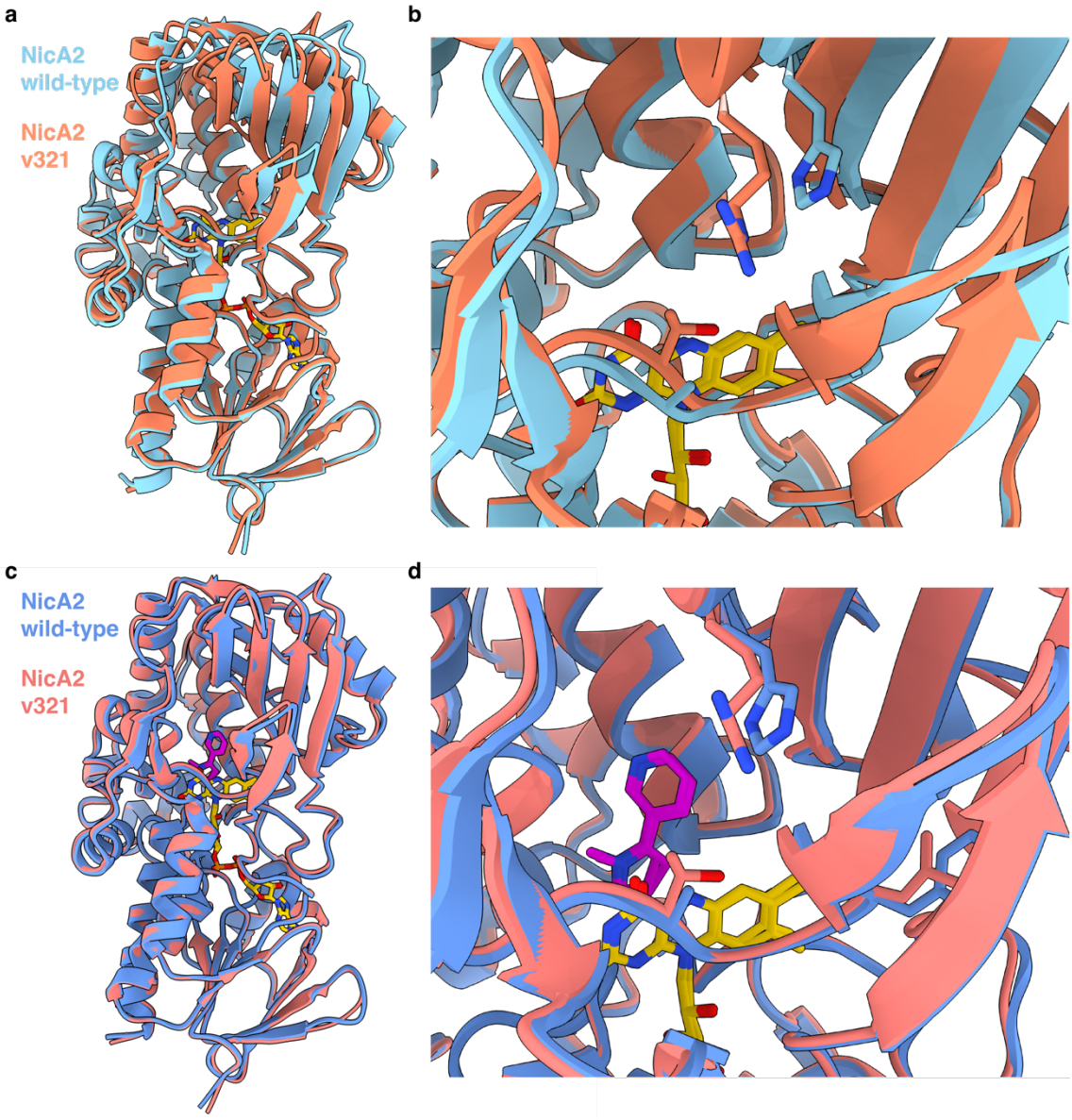

Figure 36. NicA2 wild-type and v321 have similar structures when bound by N-methylmyosmine.

a, Ligand-free NicA2 wild-type (PDB: 5TTJ) and v321 enzyme structures were overlaid, aligned at their flavin binding domains. **b,** overlay of the active sites of the enzymes with A107T and H368R mutations highlighted. **c,** NicA2 wild-type and v321 enzyme structures bound to N-methylmyosmine were overlaid, aligned at their flavin binding domains. **d,** overlay of the active sites with A107T and H368R mutations highlighted. Wild-type enzyme is rendered in cyan/blue, v321 in orange/salmon, Flavin adenine dinucleotide in yellow, and N-methylmyosmine in magenta.

Although hitherto under-utilized for the study of flavoenzymes, NMR spectroscopy can provide both structural and kinetic information on transient events in enzyme dynamics[106]. Given the large size of the NicA2 homodimer (110 kD) and the subtle conformational changes we wish to probe, we chose one-dimensional ^{19}F NMR over ^{1}H, ^{15}N based two-dimensional NMR. We used an amber codon suppression strategy to site-specifically incorporate an unnatural amino acid, p-trifluoromethylphenylalanine (tfmPhe) in the tunnel interior[107]. We chose Y342 located in the tunnel interior as the site of fluorine incorporation as it is unlikely to affect enzyme function or block the opening of the tunnel. (**Figure 37a**). Indeed, mutating Y342 into tfmPhe leads to only minor changes in the secondary structure, and stability, catalytic rate of wildtype and mutant NicA2 (**Figure 38**). The fluorine in tfmPhe are an exquisitely sensitive structural probe for side-chain dynamics in the tunnel since anything other than a single peak in the ^{19}F NMR spectrum indicates conformational heterogeneity in the local environment of the fluorine nucleus.

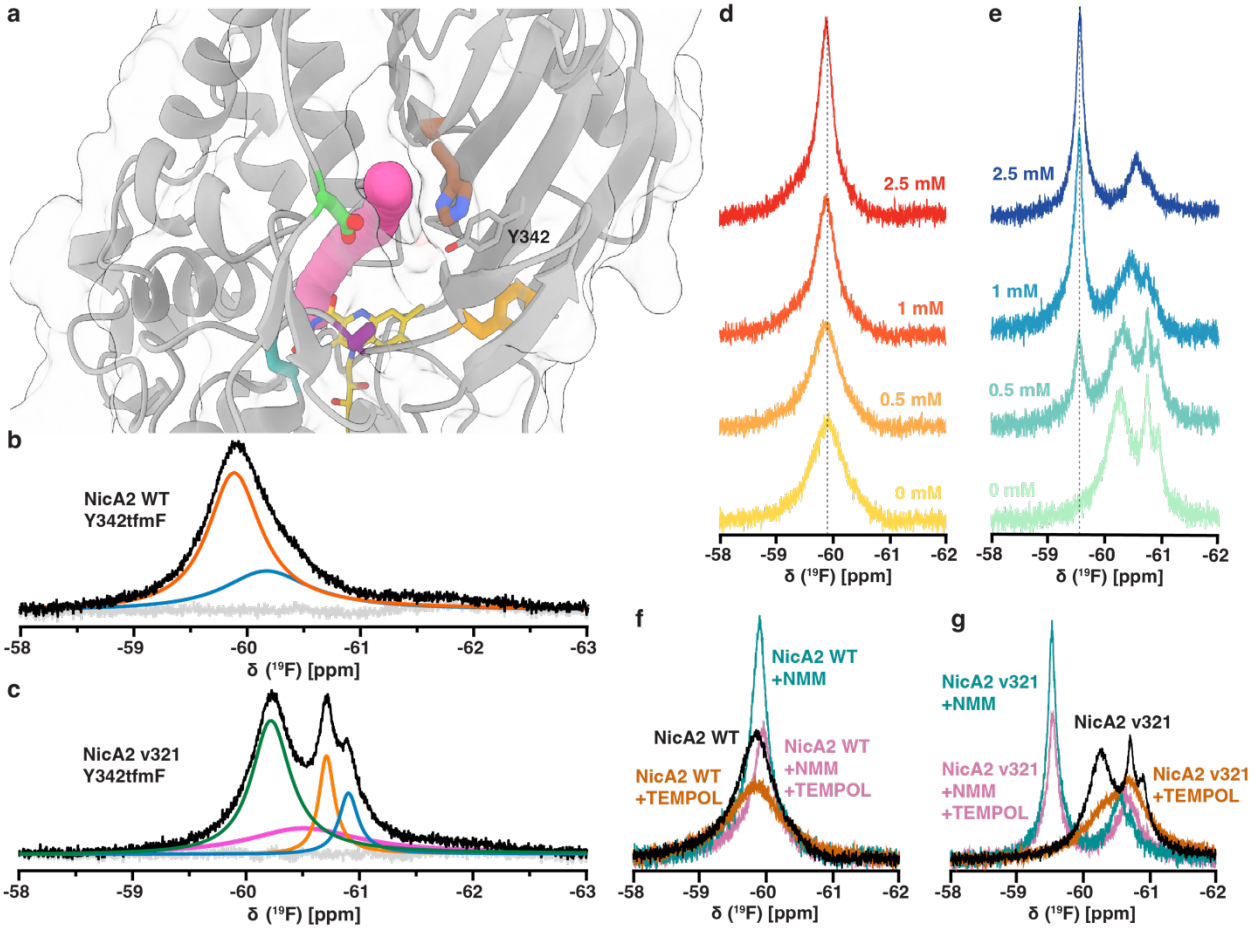

Figure 37. NicA2 wild-type and v321 populate distinct conformational landscapes.

a, NicA2 wild-type's crystal structure (PDB ID: 5TTJ) is displayed with an ~1.4 Å diameter tunnel identified by CAVER simulation rendered in pink. FAD is rendered in yellow, Y342 is rendered in grey and labeled, frequently mutated residues are rendered F104 in orange, A107 in purple, D130 in green, H368 in brown, N462 in turquoise. **b,** ^{19}F NMR spectrum of wild-type NicA2 with the Y342tmfF substitution. The black trace represents the raw data, the colored curves represent fits deconvoluted using *decon1d*[108], and the grey trace represents residuals from the fit. **c,** ^{19}F NMR spectrum of NicA2 v321 with the Y342tmfF substitution. **d,** Wild-type NicA2 Y342tmfF titrated with 0, 0.1, 0.5, and 2.5 mM NMM which narrows with increasing NMM, indicating a more restricted sampling of local conformations. **e,** NicA2 v321 Y342tmfF titrated with NMM of the same concentrations as labeled, showing collapse into a single population. **f,** Scans were taken before and after TEMPOL was added to samples of wild-type NicA2 Y342tmfF with and without 5 mM NMM included. In the samples with TEMPOL added, the peaks are observed to broaden in accordance with their exposure to solvent. **g,** NicA2 v321 Y342tmfF samples prepared in the same manner.

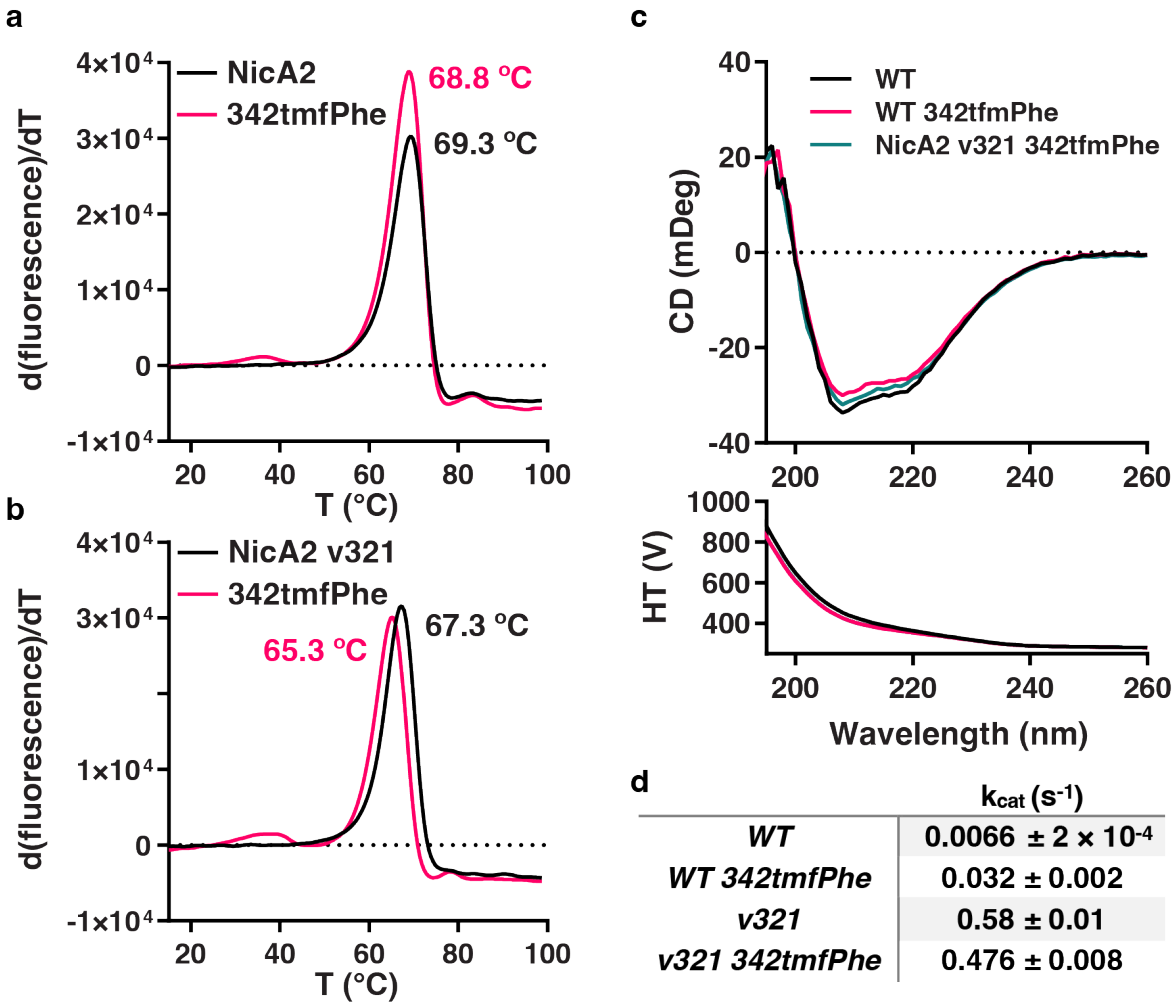

Figure 38. Qualities of NicA2 ^{19}F-containing variants.

a, NicA2 wild-type and NicA2 wild-type with tfmPhe substituted at position 342 have a similar melting temperature. Traces represent an average of 3 replicates. **b,** NicA2 v321 and NicA2 v321 with tfmPhe substituted at position 342 have a slightly different, but still similar melting temperature. Traces represent an average of 3 replicates. **c,** Circular dichroism spectra of wild-type and the two ^{19}F containing constructs maintain secondary structure. **d,** Steady-state kinetic data for the reaction of NMR variants with nicotine. Values are reported with 95% confidence intervals from 3 replicates.

There is a single, broad signal in the ^{19}F spectrum of wild type NicA2 that can be deconvoluted into two highly overlapping peaks, indicating that there is conformational motion in intermediate-to-slow exchange in the interior of the tunnel (**Figure 37b**). The ^{19}F spectrum of NicA2 v321 is strikingly different. The spectrum of the variant is composed of distinct, well-populated peaks: a broad up-field shifted major peak at -60.2 ppm and

three highly overlapping down-field minor peaks (**Figure 37c**). The broadness of the resonance at the major -60.2 ppm peak indicates that the most abundant sub-ensemble of v321, like that of the wild type enzyme, contains multiple conformations with μs–ms lifetimes. In contrast to the ^{19}F NMR spectrum for the fluorine incorporated at the Y342 site, we observed narrow peaks in wildtype NicA2 and v321 at a control substitution position Y313 that lies far from the tunnel region (**Figure 39a**). This suggests that the multiple peaks we detect with a single tfmF incorporated at Y342 cannot be explained solely by global structural perturbation. The greater conformational heterogeneity in v321 cannot be explained by a lower stability of the mutant variant either, since the wildtype and mutant enzymes exhibit nearly identical thermal denaturation curves (**Figure 38**). We excluded the possibility that the chemical shift differences between the wildtype and v321 enzymes arise from higher molecular weight species in v321 by dynamic light scattering (DLS) measurements that did not detect any aggregates in solution (**Table 4**). There was a noticeable difference in the measured hydrodynamic radius between ligand-free v321 and the wild-type or NMM-bound proteins, which could indicate that ligand-free v321 exists as a monomer in solution. It is difficult to say whether this is relevant to catalysis without further investigation, but it is unlikely to explain the increased oxidation rate observed in our variant proteins. This is because NMM-bound v321, the species that has an increased rate of oxidation by O_2, has the same hydrodynamic radius as the wild-type, which is known to exist as a homodimer under these conditions. Additionally, the DLS experiments that I have performed so far have only used proteins with the 342tmfF substitution. An important follow-up to is to use DLS and other techniques such as analytical ultracentrifugation to characterize v321 and other NicA2 variants, with and

without the 342tmfF substitution. In summary, the ^{19}F NMR spectra of the two apo NicA2s clearly demonstrate the existence of a dynamic access tunnel whose motional properties have been altered by the mutations in v321.

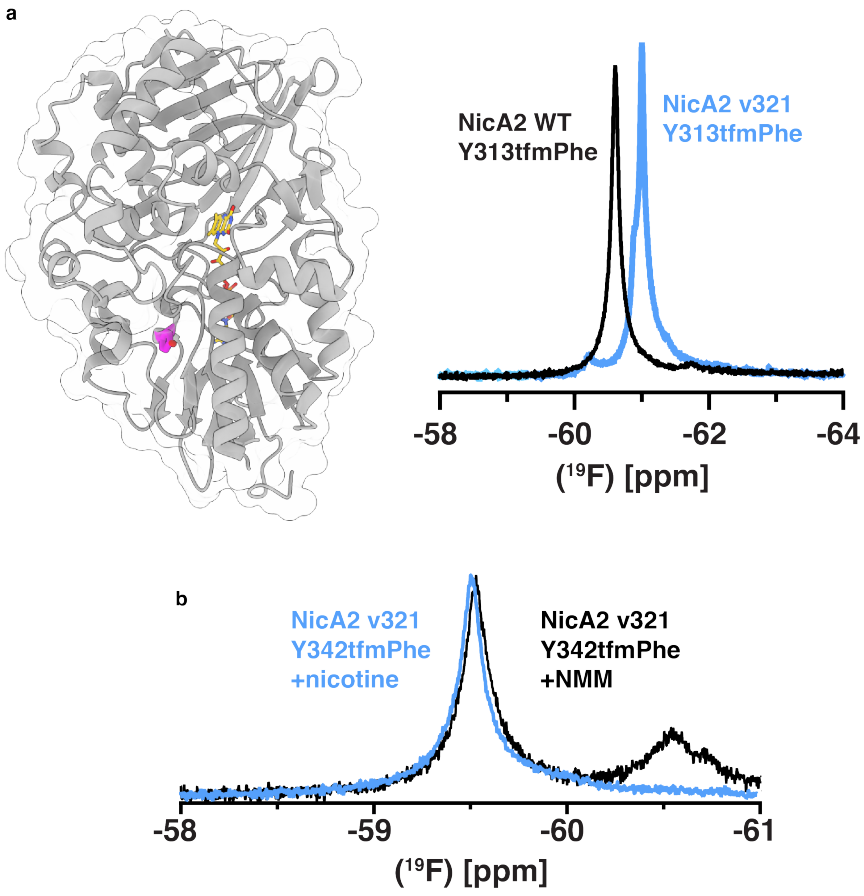

Figure 39. NicA2 NMR control substitutions, and addition of nicotine.

a, Y313 (magenta) was mutated to the amber stop codon, and tfmPhe incorporated into this position to serve as a prove for ^{19}F NMR. This position was chosen because it is conservative substitution distant from the tunnel region and buried in the core of the flavin-binding domain. It should therefore be an independent readout about global protein dynamics that is not influenced by local tunnel dynamics. Also displayed are the ^{19}F NMR spectra of the Y313tfmPhe for wild-type and variant NicA2s, which are similar. **b,** Nicotine was titrated into NicA2 v321 Y342tmfPhe to achieve the reduced, NMM-bound state. NMM was also titrated into the oxidized enzyme. These spectra overlay closely, indicating that they sample a very similar conformational landscape around this probe.

Table 4. Dynamic light scattering of NicA2 enzymes.

NicA2 enzyme was prepared at NMR concentrations (100 μM) with and without 5 mM NMM in solution. Data were collected on a Dynapro Nanostar DLS with 30 scans per sample. No significant aggregates were observable upon the addition of NMM.

	Radius (nm)	*% Mass*
WT -Apo	5.3	99.8
WT -NMM	5.5	99.8
v321 -Apo	3.1	93.0
v321 -NMM	5.4	95.8

Our stopped-flow experiments only demonstrate an increased rate of oxidation when NicA2 is bound by the reaction product NMM. If we want to explore the structural basis of this effect, we must therefore observe the NMM bound state. We titrated the oxidized enzyme with NMM and observed a large chemical shift in the major peak of NicA2 v321, possibly due to extensive conformational rearrangement in the tunnel as a result of product binding (**Figure 37e**). At increasing molar ratios, NMM yields a narrow major peak whose intensity increases with a concomitant decrease in the intensity of the apo-state peaks. Thus, NMM binding “pulls” the four distinct apo-state sub-ensembles that are in slow exchange to a single major conformation that presumably resembles the crystalized conformation of the NMM-bound NicA2 v321 complex. In contrast, NMM addition does not cause any significant chemical shift perturbation in the wildtype NicA2, although the peak does narrow (**Figure 37d**), which suggests that ligand binding restricts conformational fluctuations in the interior of the tunnel. We confirmed that these conformational changes are relevant to catalysis by adding excess nicotine to the enzymes to achieve the NMM-bound, reduced enzyme state observed to have rapid

oxidation by O_2 in our kinetic experiments. The resulting spectra after addition of nicotine closely overlay with those that represent NMM-bound oxidized enzyme from the titration, indicating that NMM-bound oxidized and reduced states are conformationally indistinguishable (**Figure 39b**). Therefore, observations made using the NMM-bound oxidized enzyme report on the conformation of the enzyme relevant for the oxidation step observed in our stopped-flow experiments.

Paramagnetic relaxation enhancement (PRE) is widely used to obtain long-range distance restraints in NMR spectroscopy[109]. When a soluble paramagnetic reagent like 4-hydroxy-2,2,6,6-tetramethyl-piperidine-1-oxyl (TEMPOL) is added to the solvent, the extent of paramagnetic broadening depends on solvent accessibility of fluorine, which we use as a substitute to measure the ease of access of O_2 to the tunnel interior. In the presence of TEMPOL, we observed line broadening in the major peaks of both the unbound wild type and mutant NicA2 (**Figure 37f,g**). In contrast, the down-field peak at -60.7 ppm in NicA2 v321 showed little line broadening, consistent with the idea that this peak represents a more closed conformation of the enzyme tunnel. PREs in the free and NMM-bound states of wildtype NicA2 were similar, both losing about 50% of their peak height. The similar PRE values establishes that Y342 is as solvent-accessible in the free state as the NMM-bound state, which suggests that the tunnel in wildtype NicA2 is relatively open throughout its catalytic cycle. Although the major conformation of v321 is more-accessible in ligand-free oxidized form, as evidenced by losing 70% of its peak height, the same representative peak reproducibly loses only ~40% of its height in the NMM-bound state when TEMPOL is added to the buffer. NicA2 v321 thus appears to explore two distinct populations. In the unbound state, v321 samples a more open

conformation that allows unhindered entry and exit of O_2 through the tunnel. In the NMM-bound state however, the tunnel is occluded, being less exposed to solvent as evidenced by a mere 40% reduction in peak intensity due to PRE.

3.3 Discussion

Nicotine oxidoreductase (NicA2) is curiously discerning as to its preference for electron acceptors. Unlike the vast majority of flavin amine oxidase family members, the only other known exception being the recently documented pseudooxynicotine amine oxidase[110], NicA2 exhibits a limited capacity to react with O_2 as an oxidative substrate. Both enzymes are instead dehydrogenases, which appears to be an evolutionary adaptation by which *P. putida* S16 saves valuable reducing equivalents freed during the catabolism of nicotine, shuttling them to productive use via a cytochrome c. It is not entirely clear how widespread this adaptation is. Other organisms, such as *Arthrobacter nicotinovorans*, use the alternative pyridine pathway for the catabolism of nicotine and contain homologous flavoenzymes which react readily with O_2 [32]. The structural similarity between NicA2 and these O_2 utilizing flavin amine oxidases is undeniable[37], which makes NicA2 an attractive model protein with which to explore the control of oxygen reactivity in flavoenzymes.

We developed a genetic selection that links growth of *P. putida* S16 to the activity of NicA2 in the absence of its physiologic electron acceptor CycN, and isolated variants of NicA2 with up to a 200-fold increase in both NicA2's k_{cat} and $k_{ox}^{O_2}$. Discovering that NicA2 variants only display increased oxidation rates when bound by the reaction product NMM was a surprise, and it is additionally perplexing that this rate enhancement is independent of the positive charge of NMM, which was thought to be a common paradigm

among this enzyme class. That the product analogue myosmine provides a comparable rate enhancement seems to imply that it is either a shift in the product-bound conformation of the protein, or the displacement of solvent in the active site upon the binding of NMM, that is actually important for increasing the rate constant for oxidation by O_2. Since NMM is already known to remain bound during CycN dependent catalysis[19], and CycN appears to inhabit a binding site that is distinct from the location of most of our mutations[110], it is not surprising that the oxidation rate with CycN is not impaired.

A unifying framework that describes how flavoproteins suppress or enable their reactivity with O_2 is intensely sought after, but the title of a review on this subject, "The enigmatic reaction of flavins with oxygen," well summarizes how much there is yet to learn on this topic[16]. $FADH_2$ free in solution can be oxidized by O_2 with a bimolecular rate constant of 250 $M^{-1}s^{-1}$ [13]. When $FADH_2$ is bound to an enzyme, the oxidation rate may be enormously depressed or accelerated to between 2 and 10^6 M^{-1} s^{-1} [12]. There are two primary features that have been carefully investigated and are known to contribute to this variability. One way by which flavoenzymes may modulate oxidation of $FADH_2$ is by changing the accessibility of the protein interior to O_2. This makes intuitive sense, given that O_2 must be in the proximity of N5 or C4a of flavin for oxidation to occur. Dissolved oxygen is thought to penetrate enzymes through either "breathing" motions intrinsic to the dynamics of the protein, or by predefined oxygen channels which have been uncovered in some flavoenzyme oxidases[48–53]. It has been shown that obstruction or modification of these channels can lead to a decrease of oxidase activity, which supports a direct role of channels in bringing O_2 to the active site[48,49,53].

The rate limiting step for oxidation of flavoenzymes by O_2 is formation of an energetically unfavorable superoxide-flavin semiquinone intermediate[12,55]. This is thought to occur via two consecutive one electron transfers from $FADH_2$ to O_2, ending with the production of H_2O_2 for flavin oxidases[13]. For this reaction to occur rapidly, it is therefore critical to maintain a suitable environment near $FADH_2$ that can stabilize the superoxide-semiquinone intermediate. It is generally accepted that a positively charged residue is required for the activation of O_2, and flavin amine oxidases usually accomplish this using a lysine residue poised on the *Si*-face of FAD.

Wild-type NicA2 appears to meet both of these functional requirements for activity, and yet is not an oxidase. This demonstrates that our understanding of the evolution of oxidase activity is limited. The location of the mutations in our NicA2 variants led us to suspect that it is the migration of O_2 to the active site FAD through a putative tunnel that is altered by the mutations in our variants. Examination of crystal structures revealed no obvious difference between the product (NMM)-bound forms of the WT and the 321 variant proteins. In the NicA2 variant 321 there is no steric relief around the N5 or C4a of FAD facilitated by our mutations, as was seen in previous dehydrogenase-oxidase switch mutations[57,58]. In fact, the N5 region is somewhat more crowded in most of our increased activity variants due to the presence of the A107T mutation (**Figure 36b,d**). Additionally, crystal structures did not reveal any static tunnel for guided diffusion of O_2 that was absent in the WT protein but present in the variants. This does not, however, exclude the possibility of a tunnel that can form transiently. We placed an NMR-sensitive, ^{19}F containing non-canonical amino acid in the interior of the putative tunnel most affected by the dehydrogenase-oxidase switch mutations to probe the local chemical environment

and also to look for differences between our wild-type and v321 NicA2. In their apo- state, both enzymes product populate distinct conformational substates that differ in conformational exchange rates. However, the major population of both these enzymes is accessible to solvent. NicA2 v321 appears to have greater exposure to solvent relative to wildtype, while also being more conformationally heterogenous and populating substates that exchange slowly, implying that the lifetime of the open state is longer in the variant as compared to the intermediate exchange regime of the wild-type. In the catalytically relevant NMM-bound state, the peak for wild-type NicA2 becomes is narrower, indicating less flexibility in this tunnel region, while remaining accessible to solvent. We suspect that this restricted conformation is representative of the crystallized compact structure of NMM-complexed NicA2. NicA2 v321 similarly demonstrates peak narrowing, and a large chemical shift that is indicative of major rearrangements in the tunnel region that results in the formation of a new conformational state that appears to have an interior that is less polar and less solvent-accessible than the apo-state tunnel.

With the limited window into the conformational landscape of this tunnel granted by a single probe, we are unable to thoroughly characterize the distinct substates of NicA2 in various catalytically-relevant states seen in our experiments. It is interesting to note that a difference in accessibility or flexibility of the tunnel region does not fully explain why our variants have enhanced reoxidation by oxygen, however, it is impossible to rule out effects that our mutations have on NicA2 v321 that are outside of the measurement capabilities of our Y342tfmF site. The effect that our mutations have on steering and orienting O_2 to a catalytically productive location near flavin remain unknown. Regardless of the mechanism by which our introduced mutations increase the catalytic rate, we have

created variants of NicA2 that may be more practical as a therapeutic to aid in the cessation of smoking.

Nicotine dependence is a notoriously difficult habit to kick, with < 5% of quit attempts in the absence of medical management ending in success[1,2]. Medical management most commonly consists of nicotine replacement therapy, nicotine receptor partial agonists, or a norepinephrine-dopamine reuptake inhibitor; but these therapeutic options are estimated to increase the chance of a successful quit attempt less than 4 fold, to < 20%[3]. Given that nicotine dependence is expected to be responsible for at least 1 in 10 deaths worldwide for the foreseeable future, this is clearly lower than is desired[4]. Treatment with NicA2 provides an exciting new direction to neutralize the pharmaceutical effect of nicotine, though previous studies suggest a dose that is unfeasibly high for administration to humans. Ideally NicA2 would degrade most of the nicotine absorbed when smoking before it is able to reach the tissues upon which it acts. There is only about 7 seconds of "dead time" after inhaling nicotine before it reaches the brain[9]. Given the slow catalytic rate of wild-type NicA2, an extremely large dose is necessary to enact degradation of this much nicotine in this short time frame. Using directed evolution, we now have succeeded in isolating variants of NicA2 that are much more capable of reacting with O_2 than the wild-type enzymes's k_{cat} of 0.006 s^{-1}, our variants having a k_{cat} of up to 1.3 s^{-1}, much closer to the catalytic rates exhibited by other flavin oxidases. We have thus come a considerable distance in restoring the oxidase activity of this enzyme implied by its enzyme family. We have succeeded in doing this without disrupting the enyzme's dehydrogenase activity or overall thermodynamic stability. Our increased activity variants react much more rapidly than the wild type NicA2, which should translate to a lower

effective dose necessary to achieve the beneficial effects observed in rats. Hopefully, such a dose will be within a range suitable for administration to humans if indicated. Further investigation of these improved activity variants applied to addiction cessation models is indicated.

3.4 Methods

Strains and culture conditions

Pseudomonas putida S16 was obtained from American Type Culture Collection (ATCC BAA-2546). *P. putida* S16 *ΔcycN* was created as previously described[19]. Bacterial culture was performed in lysogeny broth (LB) medium for general maintenance and growth of strains. Antibiotic selection was maintained using 100 μg mL^{-1} kanamycin or 25 μg mL^{-1} gentamycin for pET28 and pJN105 plasmids, respectively. Nicotine liquid media was based on M9 minimal medium and included: 6 g L^{-1} Na_2HPO_4, 3 g L^{-1} KH_2PO_4, 1 g L^{-1} ammonium chloride, 1 mM $MgSO_4$, 0.1 mM $CaCl_2$, 1x trace metals (Teknova T1001), 1 μg mL^{-1} thiamine, and 0.5 g L^{-1} nicotine. Nicotine selection plates were made with the same recipe as the liquid media, but instead used 1 g L^{-1} nicotine and 15 g L^{-1} agarose was added (Thermo Fisher Scientific). Protein expression medium (PEM) was 12 g L^{-1} tryptone, 24 g L^{-1} yeast extract, 50.4 g L^{-1} glycerol, 2.13 g L^{-1} K_2HPO_4 and 12.54 g L^{-1} KH_2PO_4. *E. coli* BL21 (DE3) cells were used for protein expression.

NicA2 variant library production

A high diversity library of NicA2 variants containing ~10^8 independent clones with an average mutation density of 8.9 nucleotide mutations per gene was obtained from Genewiz (Chelmsford, MA) cloned into the arabinose inducible pJN105 vector[111]. This library was used for the first generation of the selection. Following generations were obtained using serial error-prone PCR of pooled higher activity variants from the previous rounds of selection as follows. Error-prone PCR was performed using the Mutazyme II kit (Agilent) according to the manufacturer guidelines with primers P01/P02. 100 ng of pooled variants was routinely used as the substrate for the reaction. PCR products were run out on an agarose gel and the *nicA2* band purified with a gel extraction kit (Macherey-Nagel). This mutagenized band was then used for a MEGAWHOP reaction onto pJN105-nicA2 template as follows[112]. 400 uL of Phusion PCR (Thermo Fisher) reaction was prepared with 400 ng pJN105-nicA2 wild-type as template and 1500 ng mutagenic PCR product as megaprimer. PCR products were DpnI digested for 3 hours before ethanol precipitation with Pellet Paint (Sigma) additive, resuspension in 5 uL ddH_2O and transformation into MegaX DH10b electrocompetent cells (Thermo Fisher). 100uL cell stocks were split into 25 uL volumes and each electroporated at 2000 V in a 0.1 mm cuvette. Each electroporation reaction was resuspended in 1 mL SOC media and recovered shaking at 37 °C for 1 hr. Serial dilutions were plated onto LB-gentamycin plates to determine the size of resulting libraries. Recovered media was subcultured into LB with gentamicin, grown overnight, and then miniprepped (QIAprep Spin Miniprep Kit, QIAGEN) to isolate the pJN105-*nicA2* libraries used in the selection. Homemade libraries ranged from 10^5-10^6 unique sequences in size.

Selection of NicA2 variants with enhanced activity

The selection of NicA2 variants was performed using nicotine agar plates. *Pseudomonas putida* S16 *ΔcycN* was grown overnight at 30 °C. The next day, 0.25 mL of overnight culture was subcultured into 5 mL fresh LB with 25 μg mL^{-1} gentamycin and grown for 3-4 hours before being spun down and washed 3 times with 4 mL ice cold 300 mM sucrose. After these washes, cells were resuspended in 80 μL 300 mM sucrose. Selection libraries in pJN105 were added to this concentrated cell stock, then electroporated at 2500 V (Electroporator 2510, Eppendorf). 1 mL SOC media was added and the cells allowed to recover shaking at 30 °C for one hour.

These library transformed strains were grown in LB and then washed with M9 salts to remove any residual nutrient sources before being plated onto nicotine agar plates in a 10x serial dilution using glass beads. Plates contained arabinose concentrations between 0.01 and 0.001% (w/v) as an inducer for NicA2 expression. Nicotine selection plates were incubated at 30 °C for 2 – 8 days until visible growth of colonies. The largest colonies were picked and streaked onto nicotine agar plates to purify fast growing strains from any contaminants on the original plate. Single colonies were picked from these streakouts and were then evaluated for activity in a platereader based secondary screen (See platereader growth assay, below) to determine which variants were most promising. The top performers from this secondary screen were sequenced and then subcloned via MEGAWHOP reaction into pET28a-His-SUMO for purification and analysis as detailed below.

Platereader growth assay

Strains of *Pseudomonas putida* S16 were streaked onto LB or nicotine-agar plates to obtain single colonies. Strains containing pJN105 plasmid were maintained under 25 μg mL^{-1} gentamicin selection throughout. 3 distinct colonies were picked as biological replicates and grown in LB-medium shaking at 30 °C overnight. The next day, 2 μL of stationary phase culture for each replicate was transferred to 200 μL nicotine media supplemented with 0.001% (w/v) arabinose in a 96-well plate. A breathe-easy plate cover (Sigma) was applied. The plate was set to shake at 30 °C and monitored at 600 nm in a Tecan M200 platereader for 4 days.

Purification of NicA2 variants for crystallography and stopped-flow assays

pET28a-His-SUMO-nicA2 vectors were transformed into *E. coli* BL21 (DE3) for expression. Overnight cultures were diluted into 2-3 L PEM and grown to an OD of ~0.8 before being transferred to a 20 °C shaker and induced with 100 uM IPTG overnight. The following day, cultures were spun down and cell pellets stored at -20 °C before use. Cells were lysed by sonication at 4 °C in 50 mM Tris HCl, 400 mM NaCl, 15 mM imidazole, 10% glycerol, pH 8.0 (lysis buffer) with DNase I and cOmplete™ protease inhibitor cocktail. The lysate was cleared by spinning twice at 30,000 g 4 °C for 30 min. The clarified supernatant was then loaded onto three 5 mL HisTrap columns pre-equilibrated in lysis buffer. Columns were washed with 20 mL lysis buffer, 20 mL lysis buffer supplemented with 20 mM imidazole, and then protein eluted in lysis buffer with added 0.5 M imidazole. NicA2 was dialyzed into 40 mM mM Tris-HCl pH 8.0, 0.2 M NaCl in the presence of protease ULP-1 to cleave the His-SUMO tag. Dialyzed, cleaved protein was subsequently passed back over the HisTrap columns to remove the tag. Protein was then

diluted into 25 mM Tris pH 8.5 and loaded onto three HiTrap Q columns equilibrated in the same buffer. NicA2 was eluted using a linear salt gradient to 1 M NaCl. Fractions containing NicA2 were then concentrated before a final gel filtration over a HiLoad Superdex 200 column equilibrated in 40 mM HEPES 100 mM NaCl pH 7.4. Purified protein was supplemented with glycerol to 10% before being flash frozen in liquid nitrogen and stored at -80 °C until use (**Figure 40**).

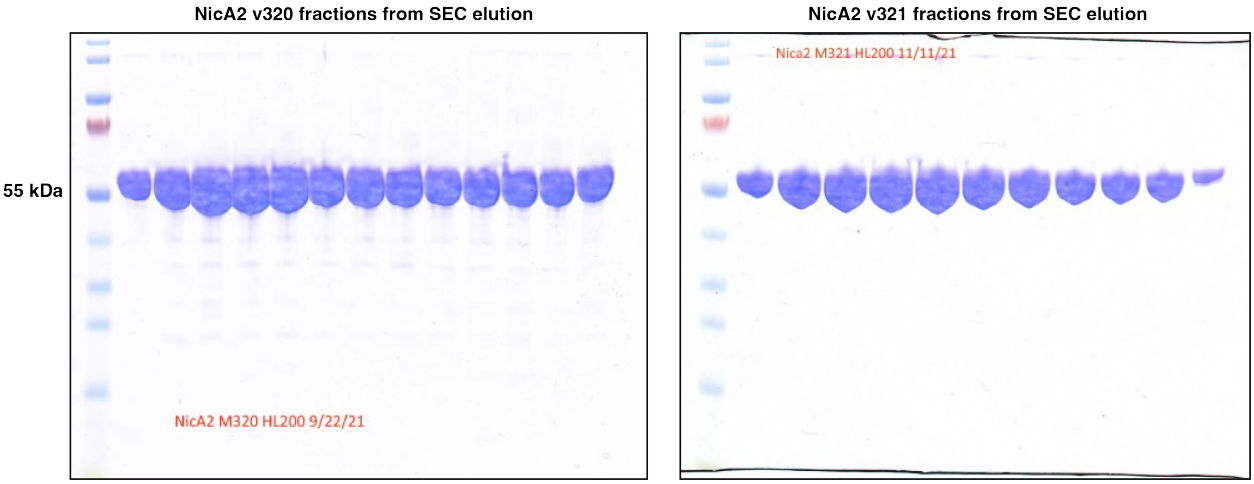

Figure 40. Purity of NicA2 used in this study.

Purification of NicA2 variants for steady-state reactions

NicA2 variants were PCR amplified from pJN105 vectors isolated from the selection using primers P01/P02. The PCR products were gel extracted then used as megaprimers in a MEGAWHOP reaction onto template pET28a-His-SUMO-nicA2 to create expression constructs. The MEGAWHOP reaction was DpnI digested for 2-4 hours before being transformed into *E. coli* 10b to isolate variants, which had their sequence confirmed by Sanger sequencing.

pET28a-His-SUMO-nicA2 variant plasmids were transformed into *E. coli* BL21 (DE3) for expression. Overnight cultures were diluted into 1 L PEM and grown until an OD of ~0.8

before being transferred to a 20 °C shaker and induced with 200 uM IPTG overnight. The next day, samples were spun down and cell pellet stored at -20 °C before purification. Cell pellets were resuspended in 50 mM sodium phosphate pH 8.0, 100 mM NaCl, 10% (w/v) glycerol lysis buffer supplemented with PMSF, lysozyme, and benzonase nuclease. These samples were sonicated on ice for 5 min, then spun at 25,000 g for 30 min. The supernatant was removed, and added to 5 mL Ni-NTA beads equilibrated in the lysis buffer. The supernatant and bead mixture was set to rotate at 4 °C for 2 hours before being washed with at least 3 column volumes of lysis buffer. Proteins were eluted with lysis buffer supplemented with imidazole to 500 mM. The eluate was set to dialyze overnight at 4 °C to dilute imidazole in the presence of ULP-1 protease. The next day, samples were re-loaded onto Ni-NTA beads and passed through. Cleaved His-SUMO tag and ULP-1 protease remained on the column, while NicA2 variants were eluted in dialysis buffer. Proteins were concentrated and flash-frozen before being stored at -80 °C.

Steady-state kinetic assays

All experiments were performed in 40 mM HEPES pH 7.4, 100 mM NaCl, 10% (w/v) glycerol at 22 °C. The concentration of NicA2 was determined using the absorbance of bound FAD cofactor with an extinction coefficient at 450 nm of ε = 11,300 M^{-1} cm^{-1}. Purified NicA2 of flavin concentration between 200 nM – 2 μM, depending on the variant, was mixed 1:1 with solutions of nicotine ranging from 4 - 1000 μM then transferred to a cuvette. Concentration of substrate was always at least 5 times greater than that of enzyme. Due to low signal change, it was not possible to determine activity with nicotine less than 2 μM end concentration. Change in absorbance at 280 nm was monitored over

time, and the linear portion of the resulting curves fit to determine the initial velocity of the reaction. This value was divided by the difference between extinction coefficients of nicotine and N-methylmyosmine at 280 nm (ε = 2914 M^{-1} cm^{-1}) and the enzyme concentration in the reaction in order to obtain V_0/E_0 values. Initial velocities were then fit to the Michaelis-Menten equation in order to determine the steady-state kinetic parameters for each enzyme variant. Point mutants were generated using the Quikchange method with primer pairs P03-P24.

Stopped-flow experiments

All stopped flow experiments were completed in 40 mM HEPES pH 7.4, 100 mM NaCl, 10% glycerol at 22 °C using a TgK Scientific SF-61DX2 KinetAsyst stopped-flow instrument. 35 μM NicA2 variant (flavin concentration) was placed in a glass tonometer and made anaerobic by cycling with vacuum and anaerobic argon[97]. For experiments monitoring the reaction with O_2 or CycN, NicA2 was stoichiometrically reduced by titration with dithionite in buffer in a gas tight syringe until the visible absorbance spectrum reached that of reduced flavin. After flavin reduction, NMM or myosmine (kept in a tonometer side arm during anaerobic flavin reduction) was mixed with the reduced enzyme to a concentration of 2 mM ligand. The tonometer was then loaded on the stopped-flow instrument and mixed with buffer containing various O_2 concentrations (prepared by sparging buffer with various N_2/O_2 ratios made using a gas blender) or anaerobic CycN (prepared in a tonometer), and the reaction monitored using the instrument's multi wavelength CCD detector. For experiments monitoring the reaction with nicotine, oxidized anaerobic NicA2 was mixed with various concentrations of nicotine

(made anaerobic by sparging with argon) and the reaction monitored using the instrument's single wavelength PMT detector at 450 nm.

Stopped-flow data were analyzed using KaleidaGraph. Kinetic traces at 450 nm for the reaction with O_2 in the absence of ligand and reaction of WT NicA2-NMM with O_2 were fit to a single exponential function (eq 1) to determine observed rate constant (k_{obs}) values for each O_2 concentration. Kinetic traces for all other experiments were fit to a sum of two exponentials (eq 2) to determine k_{obs} values for the first and second kinetic phase. In eq 1 and eq 2, ΔA is the kinetic amplitude for each phase, k_{obs} is the apparent first order rate constant and A_∞ is the absorbance at the end of the reaction.

$$Y = \Delta A e^{-k_{obs}t} + A_\infty \quad (1)$$

$$Y = \Delta A_1 e^{-k_{obs1}t} + \Delta A_2 e^{-k_{obs2}t} + A_\infty \quad (2)$$

Plots of k_{obs} against O_2 concentration for the flavin oxidation event were fit to a line, with the slope providing the second order rate constant for the reaction of reduced enzyme with O_2 ($k_{ox}^{O_2}$). Plots of k_{obs} against nicotine concentration were invariant for NicA2 v320. However, the plot of k_{obs1} vs [nicotine] for WT NicA2 showed a hyperbolic dependence and was therefore fit to eq 3 to determine the rate constant for flavin reduction (k_{red}) for this reaction phase.

$$k_{obs} = \frac{k_{red}[S]}{K_d + [S]} \quad (3)$$

Data collected for the titration of NMM into reduced NicA2 enzymes was fit to the quadratic equation for tight binding.

NicA2 crystallization and structure determination

Purified NicA2 variants and WT were prepared in phosphate buffered saline. Initial screening for crystallization conditions was performed using the National High-Throughput Crystallization Center at the Hauptman-Woodward Institute[113]. Crystals for NicA2 v321 were obtained using the hanging-drop vapor diffusion method. Protein solutions from 2.5 to 10 mg mL^{-1} were combined 1:1 with a reservoir solution. NicA2 v321 without added NMM was combined with 100 mM sodium citrate tribasic dihydrate pH 5.0, 18% PEG 6000 and set to incubate at 4 °C. For the NMM bound crystals, NicA2 v321 with NMM supplemented to 20 mM was combined with 80 mM sodium citrate tribasic dihydrate pH 5.0, 18% PEG 6000, then set to incubate at 4 °C. Crystals were harvested using the same buffer as the reservoir solution with ethylene glycol added to 25% (v/v) as a cryoprotectant before being flash frozen in liquid nitrogen. For the NMM-bound WT crystals, 15 mg/ml NicA2 WT was supplemented with 2.3mM NMM and combined 1:1 with 0.2M Ammonium citrate tribasic pH7.0, 20% PEG 3350, then set to incubate at 4 °C. Crystals were harvested using the same buffer with additional 15% PEG3350 as a cryoprotectant. Crystal diffraction data was collected at the Life Sciences Collaborative Access Team beamline 21-ID-G at the Advanced Photon Source (APS), Argonne National Laboratory. Data integration and scaling were performed with iMosflm[114] and AIMLESS respectively. The space group for NicA2 v321 apo crystal and NMM-bound crystal was determined to be $P4_3$; the space group for the NMM-bound NicA2 WT was determined to be $P2_12_12_1$. An asymmetric unit for all three crystals contains two molecules, forming a physiological dimer. All structures were solved by molecular

replacement using PHENIX Phaser-MR[115] with NicA2 WT apo structure (PDB: 7C4A) as an initial searching model. Multiple rounds of structural refinement and manual model building were performed in PHENIX Refine program[116] and Coot[117]. Crystallographic data and refinement statistics are given in **Table 5**.

Table 5. Refinement statistics for X-ray structures of NicA2.

	NicA2 v321-apo	NicA2 v321-NMM	WT-NMM
Data collection			
Space group	P43	P43	$P2_12_12_1$
Cell dimensions ***a*, *b*, *c* (Å)** **α, β, γ (°)**	 85.5, 85.5, 122.4 90.0, 90.0, 90.0	 86.3, 86.3, 122.5 90.0, 90.0, 90.0	 75.1, 86.7, 152.1 90.0, 90.0, 90.0
Resolution (Å)	42.76-2.10 (2.16-2.10)	32.64-1.90 (1.94-1.90)	57.18-2.50 (2.60-2.50)
R_{merge} (%)	7.6 (47.6)	8.0 (46.5)	10.3 (31.2)
R_{meas} (%)	8.2 (51.1)	8.6 (49.9)	11.1 (33.6)
***I*/σ(*I*)**	17.6 (4.3)	15.9 (4.2)	11.7 (5.2)
$CC_{1/2}$	0.907 (0.818)	0.823 (0.796)	0.894 (0.879)
Redundancy	7.6 (7.5)	7.6 (7.5)	7.0 (7.2)
Completeness (%)	100 (100)	100 (100)	97.2 (89.2)
Total/unique reflections	388225/51280 (31529/4187)	536368/70427 (34209/4531)	239376/34120 (24554/3430)
Refinement			
R_{work}, R_{free} (%)	15.1, 20.0	14.0, 17.7	16.4, 21.2
No. atoms	7279	7499	7149
Protein	6661	6704	6610
Ligand	172	192	275
Water	446	603	264
Rotamer outliers (%)	0.59	0.15	0.6
Clashscore	4.2	3.57	2.72
RMSD **Bond lengths (Å)** **Bond angles (°)**	 0.012 1.05	 0.016 1.19	 0.004 0.69
Average B factors (Å^2)	29.18	21.77	34.90
Wilson B-factor (Å^2)	26.80	20.07	31.88
Ramachandran statistics **Favored regions (%)** **Allowed regions (%)** **Outliers (%)**	 97.56 2.44 0.00	 98.49 1.51 0.00	 97.33 2.44 0.23

Statistics for the highest-resolution shell are shown in parentheses.

Circular dichroism of NicA2 variants

10 μM NicA2 proteins (flavin concentration) were prepared in 10 mM potassium phosphate pH 7.4, 2.5% (w/v) glycerol for circular dichroism experiments. Solutions were

added to 1 mm quartz cuvettes (Jasco 0556). 5 room temperature scans were averaged from 260-195 nm using a Jasco J-1500 circular dichroism spectrophotometer.

ThermoFAD melting assay

This assay was performed as previously described[102]. The intrinsic fluorescence of FAD is quenched upon being bound by protein. As the temperature of the protein is raised and it begins to unfold, the released FAD is once again fluorescent. This signal is monitored in a qPCR machine. 20 uL of 10 μM NicA2 enzymes were pipetted to the bottom of a qPCR tray. This was monitored for fluorescence as the temperature was ramped at 0.5 °C per second with a 30 second hold time per step in a QuantStudio 3 Real-Time PCR System.

Preparation of tmfPhe labeled NicA2 for NMR

^{19}F labeled proteins were prepared as described in previous methods[118,119]. Quikchange mutagenesis was used to place the amber stop codon (TAG) into desired locations within the NicA2 gene using primers P25-P28. These genes were then restriction cloned into pET21 at NdeI and XhoI sites with a C-terminal His-tag. This way, any unlabeled proteins prematurely truncated at the amber stop codon will pass in the flow-through of a His-tag purification step. Overnight culture of *E. coli* BL21 containing the plasmid pDULE2-tmfP and pET21-nicA2 was subcultured into 1L PEM supplemented with 1 mM 4-trifluoromethyl-L-phenylalanine (Thermo Fisher). Antibiotic selection was maintained using 100 μg/mL spectinomycin and 200 μg/mL ampicillin. Cultures were grown to an optical density of 0.8, then transferred to a 20 °C shaking incubator and induced overnight

with 0.1 mM IPTG. The next day, cells were spun down and pellets stored at -20 °C before use. Cell pellets were suspended in 50 mL lysis buffer supplemented with PMSF, lysozyme, and benzonase nuclease, then sonicated until cleared. Lysates were spun at 25,000 g for 30 minutes, then filtered before loading onto a 5 mL HisTrap column (Cytiva) pre-equilibrated in lysis buffer. The HisTrap column was washed with 5 column volumes of lysis buffer, then eluted in lysis buffer with 300 mM imidazole. This eluate was diluted into 25 mM Tris pH 8.0 before loading onto a Q-column pre-equilibrated in the same buffer. The column was then washed with 25 mL of the equilibration buffer before elution in a salt gradient. Purified proteins were dialyzed into 40 mM HEPES pH 7.4, 100 mM NaCl, 10% (w/v) glycerol then snap frozen and stored at -80 °C before use.

NMR sample preparation

Purified NicA2 at a concentration of 100-300 μM in 40 mM HEPES pH 7.4, 100 mM NaCl, 10% (w/v) glycerol buffer was used in all NMR reactions unless otherwise specified. A Wilmad internal reference tube containing the same buffer with an added 10% D_2O and 1 mM TFA was used to reference the apo- protein spectra. NMM and TEMPOL titration experiments included 10% D_2O with the sample and were instead referenced to free tri-fluoromethyl phenylalanine at 5 μM concentration. N-methylmyosmine titrations used 100 μM NicA2 proteins and were referenced to 5 μM TFA in the NMR tube containing an added 10% D_2O. For PRE experiments TEMPOL was added to the sample to an end concentration of 8 mM. Samples with nicotine added to obtain the reduced product bound form of the enzyme were prepared as follows: NicA2 proteins at 300 μM concentration were combined with nicotine to 1 mM in order to fully reduce FAD. The samples were

introduced into NMR tubes and capped with a rubber septum stopper (Chemglass). Reduction of the protein throughout all NMR experiments was confirmed by monitoring the color of the protein in the tube.

^{19}F NMR spectroscopy

All NMR spectra were acquired at 298 K on a Bruker 600 MHz instrument equipped with Prodigy (^{1}H/^{19}F)-X broadband cryoprobe and operating at a basic transmitter frequency of 563.6701729 MHz for the ^{19}F nucleus. One-dimensional undecoupled ^{19}F spectra were recorded with 16K data points, 30 kHz sweep width, an acquisition time of 0.288 s, relaxation delay of 2 s, and a total of 1000 - 5000 transients accumulated per experiment. The ^{19}F chemical shifts were referenced to either TFA (set at -75.39 ppm) or tfmPhe (set at -62.0832 ppm). The spectra were processed in TopSpin 4.1.4 and deconvoluted using the Python-based *decon1d* fitting program that assumes Lorentzian peak shapes[108].

Table 6. Primers used in Chapter 3.

PRIMER NAME	PRIMER SEQUENCE (5' TO 3')
P01	ACCCAGAAGACCAACCGTG
P02	TTAGCTCAGCAGTTGTTTCACTTCACG
P03	CGGGTCAAGAGATCGAGTTAGGCGGTGCGT
P04	ACGCACCGCCTAACTCGATCTCTTGACCCG
P05	GATCGAGTTCGGCGGTACGTGGGTTCATTGG
P06	CCAATGAACCCACGTACCGCCGAACTCGATC
P07	CGGCCTGGGTGTGGTTGAAAGTCCGCTGACCAA
P08	TTGGTCAGCGGACTTTCAACCACACCCAGGCCG
P09	CTCGTCGCTATAATCGCGGGTTTGCACCCAGTT
P10	AACTGGGTGCAAACCCGCGATTATAGCGACGAG
P11	GGCTGGCACGCGAGCATTGATGGTGCG
P12	CGCACCATCAATGCTCGCGTGCCAGCC
P13	GTCAAGAGATCGAGTTCGGCGGTACGTGG
P14	CCACGTACCGCCGAACTCGATCTCTTGAC
P15	ATCGAGCTCGGCGGTGCGTGGGTTCATTG
P16	CAATGAACCCACGCACCGCCGAGCTCGAT
P17	CGGCCTGGGTGTGGTTGAAGATCCGCTGACCAA
P18	TTGGTCAGCGGATCTTCAACCACACCCAGGCCG
P19	TACAAACACATCGGCTTCACCCCGGCGCTG
P20	CAGCGCCGGGGTGAAGCCGATGTGTTTGTA
P21	CGGAGGGTCGTATCTTGTTTGCTGGTGCG
P22	CGCACCAGCAAACAAGATACGACCCTCCG
P23	CGGCTGGCACGCGAATATTGATGGTGCTG
P24	CAGCACCATCAATATTCGCGTGCCAGCCG
P25	GTGCCGCTGAACACCTAGAAACACATCGGCT
P26	AGCCGATGTGTTTCTAGGTGTTCAGCGGCAC
P27	GCAAGGGTGCGAAACTGTAGGTTCACGTGAAACAG
P28	CTGTTTCACGTGAACCTACAGTTTCGCACCCTTGC

Chapter 4
Conclusions and Future Directions

The focus of this thesis has been to study the flavoenzyme nicotine oxidoreductase (NicA2) encoded by the microorganism *Pseudomonas putida* S16, the reactivity of NicA2 with CycN, an encoded cytochrome c, and how NicA2's poor oxygen reactivity can be enhanced through directed evolution. Here I summarize the major conclusions of this work and discuss future directions of study.

4.1 NicA2 and flavin amine oxidases

4.1.1 The interaction between NicA2 and CycN

My work presented in Chapter 2 provides a detailed characterization of the in vivo electron acceptor for NicA2. It is clearly not O_2, as NicA2 only achieves a meagre rate constant of 5 $M^{-1}s^{-1}$ for donation of electrons to dioxygen. This is a very low number, especially for flavin amine oxidases, which generally have rate constants for oxidation by O_2 of 10^3-10^6 $M^{-1}s^{-1}$ [16,54]. This led us to hypothesize that there might be an alternative electron acceptor for NicA2 in vivo. There is a previously overlooked cytochrome c gene, CycN, within the same predicted operon that induces expression of NicA2. This seemed a likely candidate to be NicA2's in vivo electron acceptor, as cytochrome c proteins have previously been characterized as electron acceptors for flavoenzymes[75]. Purification of CycN and stopped flow spectrophotometric assays allowed us to measure the rate

constant for oxidation of NicA2 by CycN which has a value of 1.4 x 10^5 $M^{-1}s^{-1}$, 10,000 times larger than that with oxygen. In addition, a CycN knockout strain of *Pseudomonas putida* S16 barely grows on agar plates containing nicotine as the sole carbon source. These data establish CycN as the in vivo electron acceptor for NicA2.

That NicA2 donates electrons to a cytochrome c opens several possible avenues for further studies. The interaction between NicA2 and CycN is transient and allows for rapid electron transfer, but the nature of this interaction outside of our kinetic experiments is not well characterized. One plausible explanation for the mechanism by which electron transfer occurs is a direct transfer from NicA2's $FADH_2$ to the heme of CycN. However, how this occurs is unclear since NicA2's bound FAD is buried deep within NicA2's structure >10 Å from any solvent exposed surface. It therefore seems unlikely that electron transfer would occur directly, but instead by a radical transfer pathway composed of Tyr or Trp residues that runs within the interior of the protein to the surface where electrons may then be picked up by CycN[110]. The existence and identity of such a path is currently uncharacterized. I observed binding specificity between NicA2 and CycN, as bovine cytochrome c is not able to oxidize NicA2 despite very close structural homology (**See Appendix I**). The structural features that enable this specificity are not clear; though the fact that CycN is also the in vivo electron acceptor for Pnao directs speculation regarding possible binding sites to a shared interface identified by ridged body docking[110].

CycN is not a terminal electron acceptor. Therefore, there must be an electron transport chain that is able to accept electrons from CycN. Though there are two cytochrome c oxidases which may serve this purpose so far known within *P. putida* S16, it is not yet clear which of these, if either, are able to oxidize CycN. One way to test if

these serve as electron acceptors is by growing cytochrome c oxidase deletion strains on nicotine as a sole carbon source, this should result in a slow growth phenotype for whichever oxidase accepts electrons for CycN. This could line of inquiry could be further pursued in the future.

4.1.2 Variants of NicA2 with greater oxidase activity

Data presented in Chapter 3 have demonstrated that NicA2 may be engineered to increase its oxidase activity. Using a genetic selection that allows for the isolation of variants of NicA2 with greater ability to use O_2 as an electron acceptor, I characterized mutations in NicA2 which increase its oxidation rate by ~200-fold. An initial surprise in our transient kinetic workup of variant NicA2s was that the bimolecular rate constant for oxidation in these enzymes is only greatly increased in the product-bound state; with the apo- enzyme demonstrating a rate constant similar to that of the wild-type. In light of our more recent data this seems less surprising, as we now know that N-methylmyosmine likely remains bound during the oxidation of wild-type NicA2, and thus I was likely selecting for oxidation activity of the NMM-bound enzyme from the start of the directed evolution experiments[19].

In the crystal structures for apo- and NMM-bound wild-type enzyme, there is an obvious conformational change associated with the product-bound state. For NicA2 v321, however, there was no clear difference between the apo- and NMM-bound crystal structures. The mutations in this variant that lead to higher activity localize to the region of a putative oxygen tunnel. This led us to hypothesize that NicA2 v321 has altered structural dynamics of this tunnel, not observable in a static crystal structure.

We incorporated an NMR sensitive probe into this O_2 tunnel and observe that the wild-type enzyme maintains roughly similar solvent accessibility of this tunnel in the apo- and NMM-bound states. The tunnel in the variant enzyme is considerably more accessible to solvent in the apo- state but occluded in the NMM-bound state. This may imply that when bound by product O_2 is better poised for catalysis in the desolvated NMM-bound enzyme, contributing to the observed increased oxidation rate. Alternatively, it may due to effects that are outside of the window of observation provided by our single ^{19}F NMR probe.

To further elucidate the mechanism by which NicA2 becomes oxygen reactive, it would be useful to directly probe access and reactivity of O_2. The use of oxygen pressure crystallography, a powerful technique for determining the localization of oxygen in the active sites of proteins which use O_2 as a substrate, is one possible approach[120]. The crystal structures solved for our NicA2 variant 321 are very similar to those of the nicotine- or NMM-bound wild-type enzyme. If the presence of O_2 can be detected, there may be a difference in orientation or localization adjacent to FAD that is relevant to oxidation. Oxygen pressure NMR could also be used. O_2 can serve as an intrinsic paramagnetic probe in protein NMR, in which the local concentration of O_2 within a protein's structure contributes to paramagnetic relaxation enhancement of nearby residues, and these measurements can then be used to map oxygen access routes and binding sites[121,122]. This could be particularly useful in the case of NicA2, where variable-pressure O_2 NMR could probe the access of O_2 itself to our putative tunnel, or any other labeled site. Comparing PRE effects between wild-type and variant NicA2 could reveal that the difference in O_2 accessibility or residence that allows greater reactivity of the enzyme.

4.1.3 Oxygen control in flavoenzymes

There is a keen interest in determining a general mechanism for oxygen control within flavin-dependent enzymes[13,16,70]. A major takeaway from this work, and from other interesting work published by the Stull lab[110], is that the flavin amine oxidase family does not consist solely of oxidases. The enigmatic nature of the features that allow oxidation by O_2 makes it challenging to predict which enzymes of this family will be oxidases simply through sequence or structure comparison. It would be interesting to characterize additional dehydrogenases from this enzyme family. By characterizing more members of this enzyme family and determining which of those members are oxidases or dehydrogenases, it may be possible to elucidate the structural features that enable (or disable) oxidase activity within this enzyme class.

The development of oxidase activity in NicA2 is just one example of flavoenzymes that have been transformed by mutagenesis from dehydrogenases to oxidases[57,74,123]. In these other cases, it appears that a positively charged region near N5 of FAD already existed in the dehydrogenases that was capable of stabilizing oxidation, but steric hinderance of a single residue prevented oxygen from reaching that spot. By relieving this steric hinderance, oxygen reactivity was imparted to the enzyme in a straightforward way. To my knowledge, there are no analogous residues in NicA2, and no other single mutation that acts as a simple switch. An informative direction to further investigate how oxidase activity can be developed would be to pursue directed evolution of other flavin dehydrogenases in the absence of their native electron acceptors. If a genetic selection specific for oxidase activity, analogous to our *cycN* knockout strain, can be established; I would expect that enhanced-activity variants can be isolated for other dehydrogenases.

Characterizing the mutations that enable oxidation activity in these other directed evolution studies may assist in obtaining a general understanding of O_2 control.

4.2 Applications of NicA2 as a treatment

NicA2 is an attractive target for directed evolution in part because of its possible application as an aid to cessation of smoking. The apparent next step is to test improved activity variants of NicA2 for their efficacy in a preclinical model, comparing them to the established properties of the wild-type enzyme. There are, however, many possible pitfalls in the road to developing a successful protein therapeutic. In anticipation of NicA2's preclinical and clinical application, some of these concerns have been addressed by other groups in their previous investigations. Discussion of this work and areas for further study are summarized below.

4.2.1 Pharmacokinetic properties of NicA2

In order to remove nicotine from the bloodstream, NicA2 must remain *in* the bloodstream. Unfortunately for the development of protein therapeutics, our vascular system is a challenging environment fraught with hazards. For one, the kidney is rapid and effective at removing proteins from circulation, processing the entire blood volume within 30 minutes. Renal clearance of proteins from circulation occurs at the glomerulus where podocytes form a molecular sieve with a size cutoff of ~50 kDa[124]. NicA2 is a functional homodimer of ~110 kDa of size, but monomers are possibly filterable through the kidney. Renal clearance is, therefore, a concern. Additional depletion of proteins from

the bloodstream occurs via intracellular degradation after nonspecific pinocytic uptake in many tissues, including the vascular endothelium[125].

Several strategies have been developed to circumvent filtration by the kidney. These rely on engineering the protein to increase its effective size so that it is unable to pass through the glomerulus. One approach that has previously been applied to NicA2 is fusion of the therapeutic protein to an albumin binding domain[5,68]. Albumin being 70 kDa in size, it is excluded from excretion through the kidney. It also has the favorable property of undergoing FcRn mediated recycling, preserving bloodstream levels by escaping degradation mediated by pinocytic uptake[125]. The combination of these effects results in a serum half-life of albumin of ~3 weeks. In order for NicA2 to harness the desirable pharmacokinetic properties of albumin, it is necessary to tightly associate the two proteins. This can be achieved by the creation of a fusion of NicA2 to a domain that is optimized to bind with high affinity to albumin, also known as an albumin binding domain fusion. Albumin binding domains with femtomolar affinity to albumin have been previously characterized[126]. Fusion of one of these (ABD035) to NicA2 wild-type was previously shown to considerably extend its circulating half-life and is also likely to be effective in our variant forms of NicA2[5].

An alternate strategy is encapsulation of the therapeutic protein within red blood cells. This is a particularly attractive strategy since encapsulation within RBCs should isolate NicA2 from renal clearance, pinocytosis, and recognition by the immune system, another potential pitfall of protein therapeutics[127,128]. Unfortunately, this technology is early in the developmental stage. Nevertheless, several drugs have entered human clinical trials in RBC encapsulated formulations[128,129]. Current encapsulation methods

involve isolating patient RBCs, permeabilizing the cells for the introduction of drug, then autologous transfusion of the drug loaded cells back into the patient— a rather costly and inefficient procedure[127]. However, as the technology matures, it could be a practical platform for the delivery of NicA2.

The thermodynamic stability of proteins also contributes to their longevity in storage and in serum. NicA2 appears to have favorable thermodynamic stability, with a melting temperature of ~70 ºC. Our increased activity variants maintain a similar melting profile, and the protein demonstrates long term stability in solution[7]. At the current stage, it does not seem that thermodynamic stability is a significant barrier for the use of NicA2 as a protein therapeutic.

4.2.2 Immune tolerance

Another avenue of protein clearance is the activity of the immune system. The adaptive immune system is exquisitely sensitive to the presence of bacterial antigens. Any bacterially derived protein is thus vulnerable to recognition and clearance. An active immune response against a protein-based treatment greatly limits the therapeutic efficacy of the treatment, by either inactivation or destruction of the protein[130]. Methods that can limit or postpone the development of an immune response against the protein of interest are the subject of intense investigation.

One of the oldest “tried and true” methods for immune evasion is that of PEGylation[131,132]. Poly-ethylene glycol (PEG) is a polymer that can be formulated to coat proteins. Once coated with PEG (hence, PEGylated), there is a physical barrier preventing immune recognition and proteolysis of protein epitopes[133]. NicA2 is amenable

to PEGylation, and formulations of NicA2 with PEG have a lower immune sensitivity while maintaining activity[6].

As previously mentioned, encapsulation in red blood cells is a possible alternative that has several advantages, including immune escape, though it has not yet been widely implemented.

4.2.3 The multifactorial nature of nicotine dependence

Smoking cessation is challenging to achieve due to the complex factors which feed into nicotine dependence. Though pharmacologic addiction to nicotine is a major factor, especially in the early stage of a developing smoker, genetics, lifestyle and reward response patterning also appear to play major roles[134–137]. For these reasons, it is insufficient to approach a smoking cessation strategy by solely addressing the pharmaceutical effects of nicotine. So, though NicA2 may become an effective therapy to remove nicotine from the bloodstream, finding a personalized combination with lifestyle intervention or a medication that influences the reward response pathway is likely to be critical for the real-world efficacy of this approach.

Appendix

Pseudooxynicotine oxidase is not an oxidase

The following materials are adapted from work published in the following study, for which I am a co-author: Choudhary V., Wu K., Zhang Z., Dulchavsky M., Barkman T., Bardwell J.C.A., Stull F. The enzyme pseudooxynicotine amine oxidase from *Pseudomonas putida* S16 is not an oxidase, but a dehydrogenase. *Journal of Biological Chemistry*. Published online July 2022. I performed the work described in this appendix, and Kevin Wu assisted by solving our obtained crystal diffraction data.

Pseudooxynicotine oxidase (Pnao) is a flavin-dependent enzyme from the organism *Pseudomonas putida* S16. Like NicA2, it is a member of the flavin amine oxidase family. *pnao* is just downstream of *cycN* and *nicA2* in the genome of *Pseudomonas putida* S16 (**Figure 15a**), and their regulation as a unit implied that Pnao may also use CycN as an electron acceptor. We find that Pnao reacts poorly using O_2 as a terminal electron acceptor and reacts rapidly using CycN as an electron acceptor[19].

Reduced NicA2 is oxidized by O_2 with a bimolecular rate constant of 5 $M^{-1}s^{-1}$ when bound by N-methylmyosmine[19]. Pnao reacts more rapidly with O_2, with a rate constant of 600 $M^{-1}s^{-1}$, but this is considerably slower than its reaction with CycN: 1.4 x 10^5 $M^{-1}s^{-1}$. This implies that CycN is likely Pnao's in vivo electron acceptor. In order to confirm this hypothesis, I endeavored to elicit a CycN dependent phenotype in *Pseudomonas putida* S16 for the function of Pnao. In the background of a CycN deletion, *P. putida* S16 grows

extremely poorly using nicotine as a carbon source; likely due to the very slow turnover rate of NicA2 without CycN to rapidly oxidize it. This strain can also be grown using pseudooxynicotine as a carbon source, in which case we may expect a similar slow growth phenotype if Pnao uses CycN as an oxidant. In this media, *P. putida* S16 wild-type grows well (**Figure 41**). *P. putida* S16 *ΔcycN* grows slowly, in accordance with the presence of CycN being necessary to facilitate rapid degradation of pseudooxynicotine by Pnao. Importantly, this phenotype may be complemented, and rapid growth restored by the plasmid-based expression of CycN. Thus, the slow turnover of Pnao without CycN limits the growth of the organism, providing strong evidence that CycN serves as the in vivo electron acceptor for the reaction.

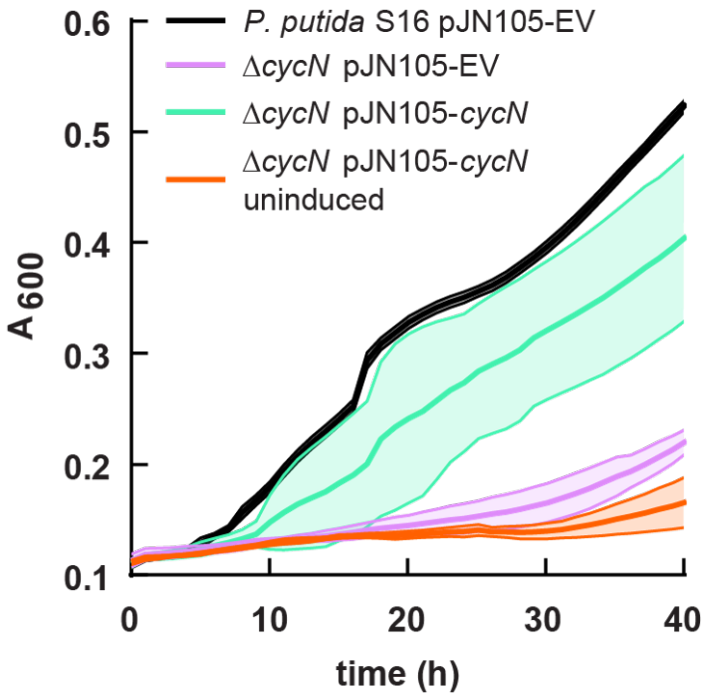

Figure 41. CycN is required by *P. putida* S16 for robust growth on pseudooxynicotine.

Growth of the *P. putida* S16 strains was monitored by absorbance at 600 nm in a plate reader growth assay with pseudooxynicotine as a carbon source. *ΔcycN* in the legend refers to *P. putida* S16 *ΔcycN*. EV denotes empty vector. Each curve is plotted as the mean of 5 biological replicates with error bands representing the standard deviation, note that the error bands for the wild-type strain are present but small.

One interesting aspect of the interaction between CycN and NicA2/Pnao is the specificity of their partnership. CycN is unable to react with other flavin amine oxidases, and NicA2/Pnao are unable to react with other cytochrome c proteins[19,110]. I crystallized CycN and determined its 3D structure. It has very high homology to other cytochrome c proteins (0.6 Å RMSD to bovine cytochrome c, **Figure 42**), and appears to differ only in its surface charge distribution. It seems likely, then, that it is this difference in surface charge that defines the specificity with which CycN interacts with NicA2/Pnao; though charge reversal mutations would be a more definitive method to test this hypothesis.

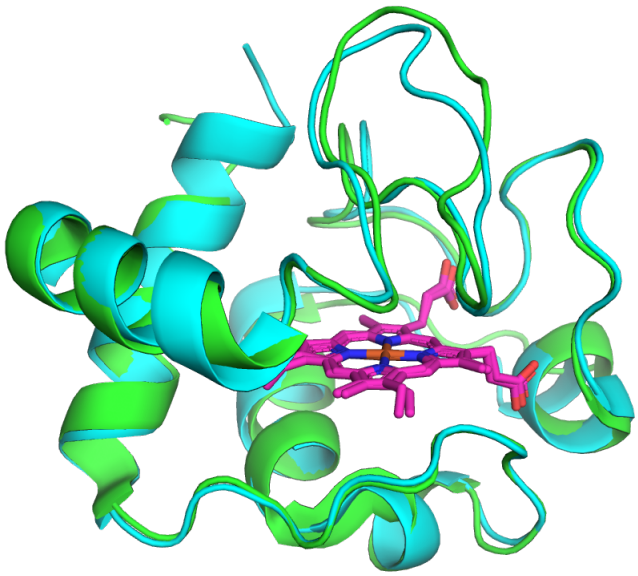

Figure 42. CycN and bovine cytochrome c are structurally similar.

A structural overlay of CycN (PDB 7TLX) rendered in green, and bovine cytochrome c rendered in cyan (PDB 2B4Z)[138]. Heme is rendered in magenta.

Methods

Pseudooxynicotine plate reader growth assay

Bacteria containing pJN105 plasmid were maintained under 25 μg mL^{-1} gentamicin selection when needed. *Pseudomonas putida* S16 was electroporated with either pJN105 empty vector or pJN105-*cycN* and plated onto LB-gentamicin and allowed to grow at 30 °C overnight. 5 distinct colonies were picked as biological replicates and grown in LB-medium supplemented with gentamicin shaking at 30 °C overnight. The next day, overnight cultures were subcultured into minimal media (6 g L^{-1} sodium phosphate dibasic, 3 g L^{-1} potassium phosphate monobasic, 0.5 g L^{-1} sodium chloride, 1 g L^{-1} ammonium chloride, 0.4% glycerol, 1 mg L^{-1} thiamine, 1 mM $MgSO_4$, 0.1 mM $CaCl_2$, 1x trace metals mixture (Teknova), 25 μg mL^{-1} gentamicin) and grown into log phase. The OD_{600} of cultures was determined, and all strains were adjusted to an OD_{600} of 1.0 in minimal media without a carbon source. 2 uL of OD_{600} 1.0 culture was added to 200 uL pseudooxynicotine media (Made with the same ingredients as minimal media, but with 0.5 g L^{-1} pseudooxynicotine as a carbon source instead of glycerol) supplemented with 0.2% arabinose, or without arabinose in the case of the uninduced control, in a 96-well plate covered with a Breathe-easy® sealing membrane (Sigma). The plate was set to shake at 30 °C and absorbance monitored at 600 nm in a Tecan M200 plate reader for 2 days.

CycN crystal studies

CycN was dialyzed into deionized H_2O and supplemented with potassium ferricyanide to ensure total oxidation of the protein. The end solution had 1.3 mM (15mg/mL) CycN and

5 mM potassium ferricyanide. This solution was mixed 1:1 with 0.1 M MES monohydrate pH 6.0, 20% polyethylene glycol monomethyl ether 2,000 and set to incubate at 20 °C using the hanging drop vapor diffusion method until crystal formation. Crystals were harvested and flash frozen in the same buffer with an added 20% glycerol as cryoprotectant. Crystal diffraction data was collected at the Life Sciences Collaborative Access Team beamline 21-ID-F at the Advanced Photon Source (APS), Argonne National Laboratory. Data integration and scaling were performed with iMosflm[114] and AIMLESS[139], respectively. The space group was determined to be C2 space group with unit cell parameters a=79.73 Å, b=30.17 Å, c=49.10 Å, which suggests an asymmetric unit containing a single molecule. The CycN structure was solved by molecular replacement using PHENIX Phaser-MR[115] with a horse cytochrome c structure (PDB 1CRC)[140] as a searching mode. Multiple rounds of structural refinements and manual model building were performed in PHENIX Refine program[116] and Coot[117]. Crystallographic data and refinement statistics are given in **Table 7**.

Table 7: Data collection and refinement statistics for CycN.

Protein	CycN (PDB ID: 7TLX)
Data Collection	
Wavelength (Å)	0.98
Resolution range	41.84-1.80
Space group	C2
Unit cell a, b, c (Å) a, b, g (°)	79.73, 30.17, 49.10 90.0, 121.6, 90.0
Total reflections	107297
Unique reflections	9383
Multiplicity	3.6
Completeness (%)	99.9 (99.7)
Mean I/sigma(I)	8.2
R_{merge} (%)	5.6 (17.2)
R_{meas} (%)	7.8 (23.8)
CC1/2	0.996 (0.963)
Refinement	
Reflections used in refinement	9379 (927)
R-work (%)	17.4 (19.0)
R-free (%)	19.1 (20.9)
Number of non-hydrogen atoms	856
macromolecules	740
Ligands	43
solvent	73
Protein residues	101
RMS(bonds)	0.013
RMS(angles)	1.09
Ramachandran favored (%)	97.98
Ramachandran allowed (%)	2.02
Ramachandran outliers (%)	0.00
Rotamer outliers (%)	0.00
Clashscore	4.00
Average B-factor	20.77
Wilson B-factor	15.12

Bibliography

1. Chaiton, M. *et al.* Estimating the number of quit attempts it takes to quit smoking successfully in a longitudinal cohort of smokers. *BMJ Open* **6**, e011045 (2016).
2. Stead, L. F. *et al.* Physician advice for smoking cessation. *Cochrane Database Syst. Rev.* (2013) doi:10.1002/14651858.CD000165.pub4.
3. Cahill, K., Stevens, S., Perera, R. & Lancaster, T. Pharmacological interventions for smoking cessation: an overview and network meta-analysis. *Cochrane Database Syst. Rev.* **2015**, (2013).
4. Mathers, C. D. & Loncar, D. Projections of Global Mortality and Burden of Disease from 2002 to 2030. *PLoS Med.* **3**, e442 (2006).
5. Pentel, P. R. *et al.* The nicotine-degrading enzyme NicA2 reduces nicotine levels in blood, nicotine distribution to brain, and nicotine discrimination and reinforcement in rats. *BMC Biotechnol.* **18**, 46 (2018).
6. Thisted, T. *et al.* Optimization of a nicotine degrading enzyme for potential use in treatment of nicotine addiction. *BMC Biotechnol.* **19**, 56 (2019).
7. Xue, S., Schlosburg, J. E. & Janda, K. D. A new strategy for smoking cessation: characterization of a bacterial enzyme for the degradation of nicotine. *J. Am. Chem. Soc.* **137**, 10136–10139 (2015).
8. Tararina, M. A. *et al.* Crystallography coupled with kinetic analysis provides mechanistic underpinnings of a nicotine-degrading enzyme. *Biochemistry* **57**,

3741–3751 (2018).

9. Rose, J. E. *et al.* Kinetics of brain nicotine accumulation in dependent and nondependent smokers assessed with PET and cigarettes containing11C-nicotine. *Proc. Natl. Acad. Sci. U. S. A.* **107**, 5190–5195 (2010).
10. Ouedraogo, D. & Gadda, G. Flavoprotein Oxidases. in *Flavin-Based Catalysis* 225–244 (Wiley, 2021). doi:10.1002/9783527830138.ch9.
11. Fitzpatrick, P. F. Oxidation of amines by flavoproteins. *Arch. Biochem. Biophys.* **493**, 13–25 (2010).
12. Massey, V. The reactivity of oxygen with flavoproteins. *Int. Congr. Ser.* **1233**, 3–11 (2002).
13. Massey, V. Activation of Molecular Oxygen by Flavins and Flavoprotein. *J. Chem. Inf. Model.* **53**, 1689–1699 (1994).
14. Mattevi, A. To be or not to be an oxidase: challenging the oxygen reactivity of flavoenzymes. *Trends Biochem. Sci.* **31**, 276–283 (2006).
15. Hare, M. L. C. Tyramine oxidase. *Biochem. J.* **22**, 968–979 (1928).
16. Chaiyen, P., Fraaije, M. W. & Mattevi, A. The enigmatic reaction of flavins with oxygen. *Trends Biochem. Sci.* **37**, 373–380 (2012).
17. Leff, J. A., Oppegard, M. A., Terada, L. S., McCarty, E. C. & Repine, J. E. Human serum catalase decreases endothelial cell injury from hydrogen peroxide. *J. Appl. Physiol.* **71**, 1903–1906 (1991).
18. Tararina, M. A. *et al.* Fast Kinetics Reveals Rate-Limiting Oxidation and the Role of the Aromatic Cage in the Mechanism of the Nicotine-Degrading Enzyme NicA2. *Biochemistry* **60**, 259–273 (2021).

19. Dulchavsky, M., Clark, C. T., Bardwell, J. C. A. & Stull, F. A cytochrome c is the natural electron acceptor for nicotine oxidoreductase. *Nat. Chem. Biol.* (2021) doi:10.1038/s41589-020-00712-3.

20. Tararina, M. A. & Allen, K. N. Bioinformatic Analysis of the Flavin-Dependent Amine Oxidase Superfamily: Adaptations for Substrate Specificity and Catalytic Diversity. *J. Mol. Biol.* **432**, 3269–3288 (2020).

21. Wang, S. N. *et al.* Biodegradation and detoxification of nicotine in tobacco solid waste by a Pseudomonas sp. *Biotechnol. Lett.* **26**, 1493–1496 (2004).

22. Tang, H. *et al.* Novel nicotine oxidoreductase-encoding gene involved in nicotine degradation by pseudomonas putida strain S16. *Appl. Environ. Microbiol.* **75**, 772–778 (2009).

23. Tang, H. *et al.* Systematic unraveling of the unsolved pathway of nicotine degradation in pseudomonas. *PLoS Genet.* **9**, e1003923 (2013).

24. Wang, S. N., Liu, Z. & Xu, P. Biodegradation of nicotine by a newly isolated Agrobacterium sp. strain S33. *J. Appl. Microbiol.* **107**, 838–847 (2009).

25. Li, J. *et al.* Comparative Genomics Reveals Specific Genetic Architectures in Nicotine Metabolism of Pseudomonas sp. JY-Q. *Front. Microbiol.* **8**, 1–11 (2017).

26. Wang, M. *et al.* Nicotine degradation by two novel bacterial isolates of Acinetobacter sp. TW and Sphingomonas sp. TY and their responses in the presence of neonicotinoid insecticides. *World J. Microbiol. Biotechnol.* **27**, 1633–1640 (2011).

27. Yu, H., Tang, H., Zhu, X., Li, Y. & Xu, P. Molecular Mechanism of Nicotine Degradation by a Newly Isolated Strain, Ochrobactrum sp. Strain SJY1. *Appl.*

Environ. Microbiol. **81**, 272–281 (2015).

28. Ma, Y. *et al.* Isolation, transposon mutagenesis, and characterization of the novel nicotine-degrading strain Shinella sp. HZN7. *Appl. Microbiol. Biotechnol.* **98**, 2625–2636 (2014).
29. Fitzpatrick, P. F. The enzymes of microbial nicotine metabolism. *Beilstein J. Org. Chem.* **14**, 2295–2307 (2018).
30. Brandsch, R. Microbiology and biochemistry of nicotine degradation. *Appl. Microbiol. Biotechnol.* **69**, 493–498 (2006).
31. Brandsch, R., Hinkkanen, A. E. & Decker, K. Plasmid-mediated nicotine degradation in Arthrobacter oxidans. *Arch. Microbiol.* **132**, 26–30 (1982).
32. Fitzpatrick, P. F., Chadegani, F., Zhang, S., Roberts, K. M. & Hinck, C. S. Mechanism of the Flavoprotein L-Hydroxynicotine Oxidase: Kinetic Mechanism, Substrate Specificity, Reaction Product, and Roles of Active-Site Residues. *Biochemistry* **55**, 697–703 (2016).
33. Yu, H. *et al.* Complete genome sequence of the nicotine-degrading pseudomonas putida strain S16. *J. Bacteriol.* **193**, 5541–5542 (2011).
34. Maeda, S., Matsushita, H., Mikami, Y. & Kisaki, T. Structural changes of N-methylmyosmine based on pH. *Agric. Biol. Chem.* **44**, 1643–1645 (1980).
35. Kopacz, M. M., Heuts, D. P. H. M. & Fraaije, M. W. Kinetic mechanism of putrescine oxidase from rhodococcus erythropolis. *FEBS J.* **281**, 4384–4393 (2014).
36. Vintém, A. P. B., Price, N. T., Silverman, R. B. & Ramsay, R. R. Mutation of surface cysteine 374 to alanine in monoamine oxidase A alters substrate turnover

and inactivation by cyclopropylamines. *Bioorganic Med. Chem.* **13**, 3487–3495 (2005).

37. Tararina, M. A., Janda, K. D. & Allen, K. N. Structural Analysis Provides Mechanistic Insight into Nicotine Oxidoreductase from Pseudomonas putida. *Biochemistry* **55**, 6595–6598 (2016).

38. Akyüz, M. A., Erdem, S. S. & Edmondson, D. E. The aromatic cage in the active site of monoamine oxidase B: effect on the structural and electronic properties of bound benzylamine and p-nitrobenzylamine. *J. Neural Transm.* **114**, 693–698 (2007).

39. Li, M., Binda, C., Mattevi, A. & Edmondson, D. E. Functional Role of the "Aromatic Cage" in Human Monoamine Oxidase B: Structures and Catalytic Properties of Tyr435 Mutant Proteins ,. *Biochemistry* **45**, 4775–4784 (2006).

40. Tan, T. C. *et al.* The 1.6 Å Crystal Structure of Pyranose Dehydrogenase from Agaricus meleagris Rationalizes Substrate Specificity and Reveals a Flavin Intermediate. *PLoS One* **8**, e53567 (2013).

41. Yildiz, I. Computational Analysis of the Nicotine Oxidoreductase Mechanism by the ONIOM Method. *ACS Omega* **6**, 22422–22428 (2021).

42. De Colibus, L. *et al.* Three-dimensional structure of human monoamine oxidase A (MAO A): Relation to the structures of rat MAO A and human MAO B. *Proc. Natl. Acad. Sci.* **102**, 12684–12689 (2005).

43. Binda, C. *et al.* Structural and Mechanistic Studies of Arylalkylhydrazine Inhibition of Human Monoamine Oxidases A and B. *Biochemistry* **47**, 5616–5625 (2008).

44. Kachalova, G., Decker, K., Holt, A. & Bartunik, H. D. Crystallographic snapshots

of the complete reaction cycle of nicotine degradation by an amine oxidase of the monoamine oxidase (MAO) family. *Proc. Natl. Acad. Sci.* **108**, 4800–4805 (2011).

45. Deay, D. O. *et al.* Improving the kinetic parameters of nicotine oxidizing enzymes by homologous structure comparison and rational design. *Arch. Biochem. Biophys.* **718**, 109122 (2022).

46. Deay, D. O. *et al.* An active site mutation in 6-hydroxy-L-Nicotine oxidase from Arthrobacter nicotinovorans changes the substrate specificity in favor of (S)-nicotine. *Arch. Biochem. Biophys.* **692**, 108520 (2020).

47. Russell, M. A., Jarvis, M., Iyer, R. & Feyerabend, C. Relation of nicotine yield of cigarettes to blood nicotine concentrations in smokers. *BMJ* **280**, 972–976 (1980).

48. Collazo, L. & Klinman, J. P. Control of the Position of Oxygen Delivery in Soybean Lipoxygenase-1 by Amino Acid Side Chains within a Gas Migration Channel. *J. Biol. Chem.* **291**, 9052–9059 (2016).

49. Coulombe, R., Yue, K. Q., Ghisla, S. & Vrielink, A. Oxygen Access to the Active Site of Cholesterol Oxidase through a Narrow Channel Is Gated by an Arg-Glu Pair. *J. Biol. Chem.* **276**, 30435–30441 (2001).

50. Baron, R. *et al.* Multiple pathways guide oxygen diffusion into flavoenzyme active sites. *Proc. Natl. Acad. Sci. U. S. A.* **106**, 10603–10608 (2009).

51. Brunori, M., Bourgeois, D. & Vallone, B. The structural dynamics of myoglobin. *J. Struct. Biol.* **147**, 223–234 (2004).

52. Saam, J., Ivanov, I., Walther, M., Holzhütter, H. G. & Kuhn, H. Molecular dioxygen enters the active site of 12/15-lipoxygenase via dynamic oxygen access channels. *Proc. Natl. Acad. Sci. U. S. A.* **104**, 13319–13324 (2007).

53. Saam, J. *et al.* O2 reactivity of flavoproteins: Dynamic access of dioxygen to the active site and role of a H+ relay system in D-amino acid oxidase. *J. Biol. Chem.* **285**, 24439–24446 (2010).

54. Gadda, G. Oxygen activation in flavoprotein oxidases: The importance of being positive. *Biochemistry* **51**, 2662–2669 (2012).

55. Bruice, T. C. Oxygen-Flavin Chemistry. *Isr. J. Chem.* **24**, 54–61 (1984).

56. Schreuder, H. A., Hol, W. G. & Drenth, J. Molecular modeling reveals the possible importance of a carbonyl oxygen binding pocket for the catalytic mechanism of p-hydroxybenzoate hydroxylase. *J. Biol. Chem.* **263**, 3131–3136 (1988).

57. Leferink, N. G. H. *et al.* Identification of a gatekeeper residue that prevents dehydrogenases from acting as oxidases. *J. Biol. Chem.* **284**, 4392–4397 (2009).

58. Zafred, D. *et al.* Rationally engineered flavin-dependent oxidase reveals steric control of dioxygen reduction. *FEBS J.* **282**, 3060–3074 (2015).

59. Zhao, G., Bruckner, R. C. & Jorns, M. S. Identification of the oxygen activation site in monomeric sarcosine oxidase: Role of Lys265 in catalysis. *Biochemistry* **47**, 9124–9135 (2008).

60. Bruckner, R. C., Winans, J. & Jorns, M. S. Pleiotropic Impact of a Single Lysine Mutation on Biosynthesis of and Catalysis by N -Methyltryptophan Oxidase. *Biochemistry* **50**, 4949–4962 (2011).

61. Iacovino, L. G. *et al.* Rational Redesign of Monoamine Oxidase A into a Dehydrogenase to Probe ROS in Cardiac Aging. *ACS Chem. Biol.* **15**, 1795–1800 (2020).

62. Horaguchi, Y. *et al.* Construction of mutant glucose oxidases with increased dye-

mediated dehydrogenase activity. *Int. J. Mol. Sci.* **13**, 14149–14157 (2012).

63. Massey, V. The chemical and biological versatility of riboflavin. *Biochem. Soc. Trans.* **28**, 283 (2000).

64. El-Gebali, S. *et al.* The Pfam protein families database in 2019. *Nucleic Acids Res.* **47**, D427–D432 (2019).

65. Van Erum, J., Van Dam, D. & De Deyn, P. P. Alzheimer's disease: Neurotransmitters of the sleep-wake cycle. *Neurosci. Biobehav. Rev.* **105**, 72–80 (2019).

66. Binda, C., Mattevi, A. & Edmondson, D. E. Structure-function relationships in flavoenzyme-dependent amine oxidations: a comparison of polyamine oxidase and monoamine oxidase. *J. Biol. Chem.* **277**, 23973–23976 (2002).

67. Kallupi, M., Xue, S., Zhou, B., Janda, K. D. & George, O. An enzymatic approach reverses nicotine dependence, decreases compulsive-like intake, and prevents relapse. *Sci. Adv.* **4**, eaat4751 (2018).

68. Xue, S. *et al.* An enzymatic advance in nicotine cessation therapy. *Chem. Commun.* **54**, 1686–1689 (2018).

69. Su, D., Kabir, M. P., Orozco-Gonzalez, Y., Gozem, S. & Gadda, G. Fluorescence properties of flavin semiquinone radicals in nitronate monooxygenase. *ChemBioChem* **20**, 1646–1652 (2019).

70. Mattevi, A. To be or not to be an oxidase: challenging the oxygen reactivity of flavoenzymes. *Trends Biochem. Sci.* **31**, 276–283 (2006).

71. Almagro Armenteros, J. J. *et al.* SignalP 5.0 improves signal peptide predictions using deep neural networks. *Nat. Biotechnol.* **37**, 420–423 (2019).

72. Lehninger, A. L., Nelson, D. L. & Cox, M. M. *Lehninger Principles of Biochemistry*. (W. H. Freeman, 2005).

73. Hmelo, L. R. *et al.* Precision-engineering the pseudomonas aeruginosa genome with two-step allelic exchange. *Nat. Protoc.* **10**, 1820–1841 (2015).

74. Leferink, N. G. H., Van Den Berg, W. A. M. & Van Berkel, W. J. H. L-Galactono-γ-lactone dehydrogenase from arabidopsis thaliana, a flavoprotein involved in vitamin C biosynthesis. *FEBS J.* **275**, 713–726 (2008).

75. Kuwahara, T., White, R. A. & Agosin, M. A cytosolic flavin-containing enzyme catalyzing reduction of cytochrome c in trypanosoma cruzi: kinetic studies with cytochrome c as substrate. *Arch. Biochem. Biophys.* **241**, 45–49 (1985).

76. Butt, W. D. & Keilen, D. Absorption spectra and some other properties of cytochrome c and of its compounds with ligands. *Proc. R. Soc. Lond. B. Biol. Sci.* **156**, 429–458 (1962).

77. Bagshaw, C. *Biomolecular Kinetics*. (CRC Press, 2017).

78. Döpner, S. *et al.* The structural and functional role of lysine residues in the binding domain of cytochrome c in the electron transfer to cytochrome c oxidase. *Eur. J. Biochem.* **261**, 379–391 (1999).

79. Waterhouse, A. *et al.* SWISS-MODEL: Homology modelling of protein structures and complexes. *Nucleic Acids Res.* **46**, W296–W303 (2018).

80. Jurrus, E. *et al.* Improvements to the APBS biomolecular solvation software suite. *Protein Sci.* **27**, 112–128 (2018).

81. Kachalova, G. S. *et al.* Crystal structure analysis of free and substrate-bound 6-hydroxy-l-nicotine oxidase from arthrobacter nicotinovorans. *J. Mol. Biol.* **396**,

785–799 (2010).

82. Fitzpatrick, P. F., Chadegani, F., Zhang, S. & Dougherty, V. Mechanism of flavoprotein l-6-hydroxynicotine oxidase: pH and solvent isotope effects and edentification of key active site residues. *Biochemistry* **56**, 869–875 (2017).

83. Tang, H. *et al.* Molecular Deceleration Regulates Toxicant Release to Prevent Cell Damage in Pseudomonas putida S16 (DSM 28022). *MBio* **11**, 1–12 (2020).

84. Arai, H. Regulation and function of versatile aerobic and anaerobic respiratory metabolism in pseudomonas aeruginosa. *Front. Microbiol.* **2**, 1–13 (2011).

85. Tribelli, P. M. *et al.* Core regulon of the global anaerobic regulator Anr targets central metabolism functions in pseudomonas species. *Sci. Rep.* **9**, 1–13 (2019).

86. Corpet, F. Multiple sequence alignment with hierarchical clustering. *Nucleic Acids Res.* **16**, (1988).

87. Graves, S. M. *et al.* Dopamine metabolism by a monoamine oxidase mitochondrial shuttle activates the electron transport chain. *Nat. Neurosci.* **23**, 15–20 (2020).

88. Wang, J. & Edmondson, D. E. Topological probes of monoamine oxidases A and B in rat liver mitochondria: Inhibition by TEMPO-substituted pargyline analogues and inactivation by proteolysis. *Biochemistry* **50**, 2499–2505 (2011).

89. Zhuang, Z., Marks, B. & McCauley, R. B. The insertion of monoamine oxidase A into the outer membrane of rat liver mitochondria. *J. Biol. Chem.* **267**, 591–596 (1992).

90. Russell, S. M., Davey, J. & Mayer, R. J. The vectorial orientation of human monoamine oxidase in the mitochondrial outer membrane. *Biochem. J.* **181**, 7–14

(1979).

91. Gaweska, H. & Fitzpatrick, P. F. Structures and mechanism of the monoamine oxidase family. **2**, 365–377 (2012).

92. Londer, Y. Y. Expression of recombinant cytochromes c in e. coli. *Methods Mol. Biol.* **705**, 123–150 (2011).

93. Demeler, B. & Gorbet, G. E. Analytical Ultracentrifugation Data Analysis with UltraScan-III. in *Analytical Ultracentrifugation: Instrumentation, Software, and Applications* (eds. Uchiyama, S., Arisaka, F., Stafford, W. F. & Laue, T.) 119–143 (Springer Japan, 2016). doi:10.1007/978-4-431-55985-6_8.

94. Demeler, B., Brookes, E. & Nagel-Steger, L. B. T.-M. in E. Chapter 4 Analysis of Heterogeneity in Molecular Weight and Shape by Analytical Ultracentrifugation Using Parallel Distributed Computing. in *Computer Methods, Part A* vol. 454 87–113 (Academic Press, 2009).

95. Brookes, E., Cao, W. & Demeler, B. A two-dimensional spectrum analysis for sedimentation velocity experiments of mixtures with heterogeneity in molecular weight and shape. *Eur. Biophys. J.* **39**, 405–414 (2010).

96. Brookes, E. & Demeler, B. Genetic Algorithm Optimization for Obtaining Accurate Molecular Weight Distributions from Sedimentation Velocity Experiments. in *Analytical Ultracentrifugation VIII* 33–40 (Springer-Verlag, 2006).

97. Moran, G. R. Anaerobic methods for the transient-state study of flavoproteins: the use of specialized glassware to define the concentration of dioxygen. *Methods Enzymol.* **620**, 27–49 (2019).

98. Zabinski-Snopko, R. M. & Czerlinski, G. H. Spectrophotometric titrations of

ferricytochrome c with ferrohexacyanide in the pH range 5 to 7. *J. Biol. Phys.* **9**, 155–167 (1981).

99. Gaweska, H. & Fitzpatrick, P. F. Structures and mechanism of the monoamine oxidase family. *Biomol. Concepts* **2**, 365–377 (2011).

100. Bisswanger, H. *Enzyme Kinetics: Principles and Methods*. (John Wiley & Sons, Incorporated, 2017). doi:10.1002/9783527806461.

101. Waterhouse, A. M., Procter, J. B., Martin, D. M. A., Clamp, M. & Barton, G. J. Jalview Version 2--a multiple sequence alignment editor and analysis workbench. *Bioinformatics* **25**, 1189–1191 (2009).

102. Forneris, F., Orru, R., Bonivento, D., Chiarelli, L. R. & Mattevi, A. Thermo FAD, a Thermofluor ® -adapted flavin ad hoc detection system for protein folding and ligand binding. *FEBS J.* **276**, 2833–2840 (2009).

103. Nisthal, A., Wang, C. Y., Ary, M. L. & Mayo, S. L. Protein stability engineering insights revealed by domain-wide comprehensive mutagenesis. *Proc. Natl. Acad. Sci. U. S. A.* **116**, 16367–16377 (2019).

104. Tan, A. K. & Ramsay, R. R. Substrate-specific enhancement of the oxidative half-reaction of monoamine oxidase. *Biochemistry* **32**, 2137–2143 (1993).

105. Chen, L., Lyubimov, A. Y., Brammer, L., Vrielink, A. & Sampson, N. S. The Binding and Release of Oxygen and Hydrogen Peroxide Are Directed by a Hydrophobic Tunnel in Cholesterol Oxidase. *Biochemistry* **47**, 5368–5377 (2008).

106. Eisenmesser, E. Z., Bosco, D. A., Akke, M. & Kern, D. Enzyme Dynamics During Catalysis. *Science (80-.).* **295**, 1520–1523 (2002).

107. Guo, J., Melançon, C. E., Lee, H. S., Groff, D. & Schultz, P. G. Evolution of Amber

Suppressor tRNAs for Efficient Bacterial Production of Proteins Containing Nonnatural Amino Acids. *Angew. Chemie Int. Ed.* **48**, 9148–9151 (2009).

108. Hughes, T. S., Wilson, H. D., de Vera, I. M. S. & Kojetin, D. J. Deconvolution of Complex 1D NMR Spectra Using Objective Model Selection. *PLoS One* **10**, e0134474 (2015).
109. Clore, G. M. & Iwahara, J. Theory, Practice, and Applications of Paramagnetic Relaxation Enhancement for the Characterization of Transient Low-Population States of Biological Macromolecules and Their Complexes. *Chem. Rev.* **109**, 4108–4139 (2009).
110. Choudhary, V. *et al.* The enzyme pseudooxynicotine amine oxidase from Pseudomonas putida S16 is not an oxidase, but a dehydrogenase. *J. Biol. Chem.* 102251 (2022) doi:10.1016/j.jbc.2022.102251.
111. Newman, J. R. & Fuqua, C. Broad-host-range expression vectors that carry the L-arabinose-inducible Escherichia coli araBAD promoter and the araC regulator. *Gene* **227**, 197–203 (1999).
112. Bryksin, A. V. & Matsumura, I. Overlap extension PCR cloning: A simple and reliable way to create recombinant plasmids. *Biotechniques* **48**, 463–465 (2010).
113. Luft, J. R. *et al.* A deliberate approach to screening for initial crystallization conditions of biological macromolecules. *J. Struct. Biol.* **142**, 170–179 (2003).
114. Powell, H. R., Battye, T. G. G., Kontogiannis, L., Johnson, O. & Leslie, A. G. W. Integrating macromolecular X-ray diffraction data with the graphical user interface iMosflm. *Nat. Protoc.* **12**, 1310–1325 (2017).
115. McCoy, A. J. Solving structures of protein complexes by molecular replacement

with Phaser. *Acta Crystallogr. Sect. D Biol. Crystallogr.* **63**, 32–41 (2007).

116. Afonine, P. V. *et al.* Towards automated crystallographic structure refinement with phenix.refine. *Acta Crystallogr. Sect. D Biol. Crystallogr.* **68**, 352–367 (2012).
117. Emsley, P. & Cowtan, K. Coot : model-building tools for molecular graphics. *Acta Crystallogr. Sect. D Biol. Crystallogr.* **60**, 2126–2132 (2004).
118. Groitl, B. *et al.* Protein unfolding as a switch from self-recognition to high-affinity client binding. *Nat. Commun.* **7**, 10357 (2016).
119. Hammill, J. T., Miyake-Stoner, S., Hazen, J. L., Jackson, J. C. & Mehl, R. A. Preparation of site-specifically labeled fluorinated proteins for 19f-nmr structural characterization. *Nat. Protoc.* **2**, 2601–2607 (2007).
120. Saleem-Batcha, R. & Teufel, R. Structural methods for probing the interaction of flavoenzymes with dioxygen and its surrogates. in 349–363 (2019). doi:10.1016/bs.mie.2019.03.016.
121. Kitahara, R., Yoshimura, Y., Xue, M., Kameda, T. & Mulder, F. A. A. Detecting O2 binding sites in protein cavities. *Sci. Rep.* **6**, 20534 (2016).
122. Teng, C.-L. & Bryant, R. G. Mapping Oxygen Accessibility to Ribonuclease A Using High-Resolution NMR Relaxation Spectroscopy. *Biophys. J.* **86**, 1713–1725 (2004).
123. Burgener, S., Schwander, T., Romero, E., Fraaije, M. W. & Erb, T. J. Molecular basis for converting (2S)-Methylsuccinyl-CoA dehydrogenase into an oxidase. *Molecules* **23**, (2018).
124. Rabkin, R. & Dahl, D. C. Renal Uptake and Disposal of Proteins and Peptides. in *Biological Barriers to Protein Delivery* (eds. Audus, K. L. & Raub, T. J.) 299–338

(Springer US, 1993). doi:10.1007/978-1-4615-2898-2_12.

125. Andersen, J. T. *et al.* Extending Serum Half-life of Albumin by Engineering Neonatal Fc Receptor (FcRn) Binding. *J. Biol. Chem.* **289**, 13492–13502 (2014).

126. Jonsson, A., Dogan, J., Herne, N., Abrahmsen, L. & Nygren, P.-A. Engineering of a femtomolar affinity binding protein to human serum albumin. *Protein Eng. Des. Sel.* **21**, 515–527 (2008).

127. Glassman, P. M. *et al.* Vascular drug delivery using carrier red blood cells: Focus on RBC surface loading and pharmacokinetics. *Pharmaceutics* **12**, 1–21 (2020).

128. Muzykantov, V. R. Drug delivery by red blood cells: vascular carriers designed by mother nature. *Expert Opin. Drug Deliv.* **7**, 403–427 (2010).

129. Hammel, P. *et al.* Erythrocyte-encapsulated asparaginase (eryaspase) combined with chemotherapy in second-line treatment of advanced pancreatic cancer: An open-label, randomized Phase IIb trial. *Eur. J. Cancer* **124**, 91–101 (2020).

130. Sauna, Z. E., Lagassé, D., Pedras-Vasconcelos, J., Golding, B. & Rosenberg, A. S. Evaluating and Mitigating the Immunogenicity of Therapeutic Proteins. *Trends Biotechnol.* **36**, 1068–1084 (2018).

131. Gupta, V. *et al.* Protein PEGylation for cancer therapy: bench to bedside. *J. Cell Commun. Signal.* **13**, 319–330 (2019).

132. Harris, J. M. & Chess, R. B. Effect of pegylation on pharmaceuticals. *Nat. Rev. Drug Discov.* **2**, 214–221 (2003).

133. Veronese, F. M. & Pasut, G. PEGylation, successful approach to drug delivery. *Drug Discov. Today* **10**, 1451–1458 (2005).

134. Mahajan, S. D., Homish, G. G. & Quisenberry, A. Multifactorial Etiology of

Adolescent Nicotine Addiction: A Review of the Neurobiology of Nicotine Addiction and Its Implications for Smoking Cessation Pharmacotherapy. *Front. Public Heal.* **9**, (2021).

135. Subramaniyan, M. & Dani, J. A. Dopaminergic and cholinergic learning mechanisms in nicotine addiction. *Ann. N. Y. Acad. Sci.* **1349**, 46–63 (2015).
136. Lessov-Schlaggar, C. N., Pergadia, M. L., Khroyan, T. V. & Swan, G. E. Genetics of nicotine dependence and pharmacotherapy. *Biochem. Pharmacol.* **75**, 178–195 (2008).
137. Bechara, A. *et al.* A Neurobehavioral Approach to Addiction: Implications for the Opioid Epidemic and the Psychology of Addiction. *Psychol. Sci. Public Interes.* **20**, 96–127 (2019).
138. Mirkin, N., Jaconcic, J., Stojanoff, V. & Moreno, A. High resolution X-ray crystallographic structure of bovine heart cytochrome c and its application to the design of an electron transfer biosensor. *Proteins Struct. Funct. Bioinforma.* **70**, 83–92 (2007).
139. Winn, M. D. *et al.* Overview of the CCP 4 suite and current developments. *Acta Crystallogr. Sect. D Biol. Crystallogr.* **67**, 235–242 (2011).
140. Sanishvili, R., Volz, K., Westbrook, E. & Margoliash, E. The low ionic strength crystal structure of horse cytochrome c at 2.1 å resolution and comparison with its high ionic strength counterpart. *Structure* **3**, 707–716 (1995).